UNIVERSITA' DEGLI STUDI DI PADOVA

Sede Amministrativa: Università degli Studi di Padova
Dipartimento di Scienze Farmaceutiche

SCUOLA DI DOTTORATO DI RICERCA IN SCIENZE MOLECOLARI
INDIRIZZO IN SCIENZE FARMACEUTICHE
CICLO XX

INVESTIGATION ABOUT THE MECHANISM OF ACTION OF NEW ANTIPROLIFERATIVE COMPOUNDS

Direttore della Scuola: Ch.mo Prof. Maurizio Casarin
Supervisore: Ch.ma Prof.ssa Daniela Ester Vedaldi

Dottoranda: Alessia Salvador

31 gennaio 2008

INDEX

RIASSUNTO V

ABSTRACT VII

1. INTRODUCTION 1

1.1 CANCER 3

1.2 CHEMOTHERAPY 4
1.2.a CHEMOTHERAPEUTICS AND CELL CYCLE 5
1.2.b CLASSIFICATION OF CHEMOTHERAPEUTICS 6

1.3 CELL DEATH: NECROSIS AND APOPTOSIS 9
1.3.a MORPHOLOGICAL AND BIOCHEMICAL CHANGES IN APOPTOSIS 10

1.4 PHOTOMEDICINE 14

1.5 MECHANISM OF PHOTOSENSITIZER-LIGHT INTERACTION 16

1.6 PUVA THERAPY AND PSORALES 18
1.6.a PSORALEN PHOTOPHYSICS AND PHOTOCHEMESTRY 20
1.6.b PSORALEN MOLECULAR MECHANISM 22
1.6.c PUVA AND APOPTOSIS 24

2. AIM OF THE PROJECT 25

2.1 3-METHOXY-5H-ISOINDOLO[2,1-*a*]QUINOXALIN-6-ONE 27

2.2 ANGELICIN ANALOGUES 30
2.2.a THIOPYRANO[2,3-*e*]INDOL-2-ONES 31
2.2.b PYRROLO[3,4-*h*]QUINOLIN-2-ONES 31

3. 3-METHOXY-5H-ISOINDOL[2,1-*a*]QUINOXALIN-6-ONE 35

3.1 CELLULAR CYTOTOXICITY 37

3.2 DETERMINATION OF MECHANISM OF CELLULAR DEATH 38

3.3 INVOLVEMENT OF MITOCHONDRIA IN CELL DEATH 40
3.3.a DETERMINATION OF MITOCHONDRIAL MEMBRANE POTENTIAL 40
3.3.b DETERMINATION OF REACTIVE OXYGEN SPECIES (ROS) PRODUCTION 42
3.3.c DETERMINATION OF CARDIOLIPIN PEROXIDATION 44

3.4 CASPASE ACTIVATION 45

3.5 CELL CYCLE 47

3.6 MITOTIC INDEX 50

3.7 EVALUATION OF MICROTUBULE NETWORK AS A POSSIBLE TARGET 52
3.7.a IMMUNOFLUORESCENCE DETENTION OF MICROTUBULE PERTURBATION 52
3.7.b TUBULIN POLYMERIZATION 54

3.8 INTERACTION WITH DNA... 55
3.8.a SPECTROSCOPIC AND SPECTROFLUORIMETRIC TITRATIONS............. 57
3.8.b LINEAR DICHROISM... 58
3.8.c CIRCULAR DICHROISM... 60

3.9 TOPOISOMERASE INTERACTION... 61

3.10 TOPOISOMERASE I ASSAY... 62
3.10.a PLASMID DNA RELAXATION BY HUMAN TOPOISOMERASE I.............. 62
3.10.b TOPOISOMERASE I CLEAVABLE-COMPLEX ASSAY................................ 63

3.11 TOPOISOMERASE II ASSAY.. 64
3.11.a PLASMID DNA RELAXATION BY HUMAN TOPOISOMERASE II............ 64
3.11.b TOPOISOMERASE II CLEAVABLE-COMPLEX ASSAY............................... 65

3.12 EFFECT OF **ISQ3** IN ANTICANCER DRUG RESISTANT CELL LINES........... 65

3.13 CONCLUSION.. 66

4. THIOPYRANO[2,3-*e*]INDOL-2-ONES.. 69

4.1 PHYSICOCHEMICAL PROPERTIES.. 71

4.2 CELLULAR CYTOTOXICITY AND PHOTOTOXICITY..................................... 72

4.3 DETERMINATION OF MECHANISM OF CELLULAR DEATH......................... 73

4.4 INVOLVEMENT OF MITOCHONDRIA IN CELL DEATH................................. 74
4.4.a DETERMINATION OF MITOCHONDRIAL MEMBRANE POTENTIAL....... 74
4.4.b DETERMINATION OF REACTIVE OXYGEN SPECIES (ROS) PRODUCTION.. 75
4.4.c DETERMINATION OF CARDIOLIPIN PEROXIDATION.............................. 76

4.5 DETERMINATION OF REDUCED GLUTATHIONE CONTENT........................ 77

4.6 INVOLVEMENT OF LYSOSOMES IN CELL DEATH.. 78

4.7 CASPASE ACTIVATION ASSAY.. 79

4.8 PHOTOREACTION WITH THE MAIN BIOMOLECULES.................................. 80

4.9 CONCLUSIONS... 80

5. PYRROLO[3,4-*h*]QUINOLIN-2-ONES... 83

5.1 PHYSICOCHEMICAL PROPERTIES.. 85

5.2 PHOTOSTABILITY... 86

5.3 CELLULAR CYTOTOXICITY AND PHOTOTOXICITY..................................... 89

5.4 INTRACELLULAR LOCALIZATION OF THE PHOTOSENSITIZER................. 93

5.5 DETERMINATION OF MECHANISM OF CELLULAR DEATH......................... 95

5.6 CELL CYCLE.. 96

5.7 DETERMINATION OF MITOCHONDRIAL MEMBRANE POTENTIAL........... 98

5.8 INVOLVEMENT OF LYSOSOMES IN CELL DEATH.. 99
5.9 CASPASE ACTIVATION ASSAY.. 100
5.10 DNA INTERACTION.. 101
5.10.a DNA BINDING.. 101
5.10.b DNA PHOTODAMAGE... 102
5.11 LIPID PEROXIDATION.. 106
5.12 CONCLUSIONS.. 107

6. MATERIALS AND METHODS... 109

6.1 MATERIALS.. 111
6.2 METHODS... 113
6.2.a SPECTROPHOTOMETRIC DETERMINATIONS.. 113
6.2.b SPECTROFLUORIMETRIC DETERMINATIONS.. 113
6.2.c IRRADIATION PROCEDURES.. 114
6.2.d CELL CULTURES.. 114
6.2.e CELLULAR CYTOTOXICITY AND PHOTOTOXICITY............................... 115
6.2.f INTRACELLULAR LOCALIZATION OF THE PHOTOSENSITIZER............ 116
6.2.f.1 CONFOCAL MICROSCOPY.. 117
6.2.f.2 EPIFLUORESCENCE MICROSCOPY.. 117
6.2.g FLOW CYTOMETER.. 117
6.2.h ANALYSIS OF CELL CYCLE.. 119
6.2.i DETERMINATION OF MECHANISM OF CELLULAR DEATH.................... 120
6.2.j INVOLVEMENT OF MITOCHONDRIA IN CELL DEATH............................ 121
6.2.j.1 DETERMINATION OF MITOCHONDRIAL MEMBRANE POTENTIAL. 121
6.2.j.2 DETERMINATION OF ROS PRODUCTION... 121
6.2.k INVOLVEMENT OF LYSOSOMES IN CELL DEATH.................................. 123
6.2.l DETERMINATION OF REDUCED GLUTATHIONE CONTENT................... 123
6.2.m CASPASE ACTIVATION ASSAY.. 124
6.2.n MITOTIC INDEX DETERMINATION... 125
6.2.o IMMUNOFLUORESCENCE DETENTION OF MICROTUBULE PERTURBATION... 125
6.2.p TUBULIN POLYMERIZATION.. 125
6.2.q INTERACTION WITH DNA.. 126
6.2.q.1 SPECTROPHOTOMETRIC AND SPECTROFLUORIMETRIC TITRATIONS.. 126
6.2.q.2 CIRCULAR DICHROISM SPECTROSCOPY.. 128
6.2.q.3 LINEAR DICHROISM SPECTROSCOPY... 128
6.2.r DNA PHOTOCLEAVAGE... 129
6.2.s TOPOISOMERASE I ASSAY.. 131
6.2.s.1 TOPOISOMERASE I RELAXATION ASSAY.. 131
6.2.s.2 TOPOISOMERASE I CLEAVABLE-COMPLEX ASSAY........................... 131
6.2.t TOPOISOMERASE II ASSAY.. 131
6.2.t.1 TOPOISOMERASE II RELAXATION ASSAY... 131
6.2.t.2 TOPOISOMERASE CLEAVABLE-COMPLEX ASSAY.............................. 132
6.2.u EVALUATION OF LIPID PEROXIDATION... 132

7. REFERENCES.. 133

8. ACKNOWLEDGEMENTS... 145

RIASSUNTO

L'attività di ricerca che ho svolto riguarda lo studio del meccanismo d'azione di nuovi composti a potenziale azione antineoplastica. Ho valutato molecole che dimostrano attività antiproliferativa sia come tali sia in seguito ad attivazione con la luce UV-A (fotochemioterapici).

STUDIO DI NUOVI POTENZIALI AGENTI ANTITUMORALI:

Le chinossaline e i chinossalinoni rappresentano un'importante classe di composti con interessante attività antiproliferativa. E' stato valutato il meccanismo d'azione del composto più attivo, **ISQ3**[1], di una serie di derivati dell'isoindolo[2,1-*a*]chinossalinone, sintetizzati presso il Dipartimento Farmacochimico, Biologico e Tossicologico dell'Università degli Studi di Palermo. **ISQ3** ha dimostrato un'interessante attività antineoplastica, con valori di IC_{50} dell'ordine del nanomolare in varie linee cellulari umane tumorali.

Attraverso citometria a flusso, si è valutata la tipologia di morte cellulare, andando a ricercare caratteristiche tipiche del processo apoptotico come la perdita dell'asimmetria della membrana plasmatica con l'esposizione di fosfolipidi utili al riconoscimento della cellula da parte dei macrofagi. Si è sono analizzate eventuali modifiche nel ciclo cellulare di cellule trattate con **ISQ3**. Successivamente, si è ricercato un coinvolgimento del mitocondrio nell'induzione di morte cellulare rilevando un'eventuale disfunzione mitocondriale. Per identificare i potenziali targets a livello cellulare, si è partiti dalle caratteristiche del composto.

STUDIO DI NUOVI POTENZIALI AGENTI FOTOCHEMIOTERAPICI:

La terapia PUVA combina l'azione degli psoraleni e la luce UV-A nella cura di patologie dermatologiche a carattere iperproliferativo e/o autoimmune, quali psoriasi, vitiligine e micosi fungoide. Questo trattamento presenta alcuni effetti collaterali a lungo termine, tra cui mutagenesi e aumentata insorgenza di tumore cutaneo, a causa della formazione di legami crociati al DNA. Quindi, si ricercano dei nuovi derivati con stessa efficacia ma privi della capacità di provocare cross-links al DNA. In particolare, sono state valutate le proprietà fotochimiche e fotobiologiche di alcuni analoghi delle angelicine, ossia delle furocumarine angolari, in cui sono stati sostituiti gli ossigeni con altri eteroatomi. Infatti, la sintesi dei tiopirano[2,3-*e*]indol-2-oni (serie L) e dei pirrolo[3,4-*h*]chinolin-2-oni (serie BV) è stata effettuata presso l'Università di Palermo proprio perché si supponeva che essi per geometria non potessero formare legami crociati.

---

[1] 3-metossi-5H-isoindolo[2,1-*a*]chinossalin-6-one.

Sono state dunque valutate le proprietà di legame e di fotodanno al DNA, l’attività antiproliferativa e fototossica, il meccanismo di morte cellulare per i composti più attivi.

ABSTRACT

My research activity deals with the evaluation of the mechanism of action of new compounds with potential anticancer action. I studied molecules that demonstrated their antiproliferative activity without or after UV-A irradiation (photochemotherapics).

EVALUATION OF NEW POTENTIAL ANTICANCER AGENTS:

Quinoxalines and structure-related quinoxalinones represent an important class of molecules with antiproliferative activity. A series of new isoindolo[2,1-*a*]quinoxalin-6-ones derivatives was synthesized in Palermo University (Dipartimento Farmaco-Chimico, Tossicologico and Biologico) and the mechanism of action of the most active compound, **ISQ3**[1], was evaluated. In fact, **ISQ3** showed a very interesting antineoplastic activity reaching nanomolar IC_{50} values in many human tumor cell lines.

Cell death mode was checked through flow cytometry, searching for such typical apoptotic features as the loss of plasmatic membrane asymmetry after the exposure of phospholipids. This translocation is needed for the recognition of apoptotic cells by macrophages. Potential modifications in cell cycle were examined after the treatment with **ISQ3**. Then, the involvement of mitochondria in cell death was studied searching signals of a possible mitochondrial dysfunction. We started from the compound characteristics to find potential cellular targets.

EVALUATION OF NEW POTENTIAL PHOTOCHEMOTHERAPIC AGENTS:

PUVA therapy combines the action of psoralens with UV-A radiation for the cure of dermatological diseases with a hyperproliferative/ autoimmune character, for instance psoriasis, vitiligo and mycosis fungoides. This treatment presents some long-term adverse effects, such as mutagenesis and increased onset of cutaneous tumors, as a consequence of the formation of cross-links with DNA. Thus, there is an enhanced research of new derivatives with the same potency but devoid of the capability to induce DNA cross-links. In particular, the photochemical and photobiological properties of new angelicin, or angular furocoumarin, analogues, in which both oxygens were substituted with other heteroatoms, were studied. In fact, the synthesis of thiopyrano[2,3-*e*]indol-2-ones (L series) and pyrrolo[3,4-*h*]quinolin-2-ones (BV series) was conducted in Palermo University because the incapability of inducing DNA cross-links for geometry problems was supposed. Thus, DNA binding and photodamage

---

[1] 3-methoxy-5H-isoindolo[2,1-*a*]quinoxalin-6-one.

properties, antiproliferative and phototoxic activity, the mechanism of cell death were evaluated for the most active compounds.

1. INTRODUCTION

1.1 CANCER

Cancer is a generic term for a group of more than 100 diseases that can affect any part of the body [1]. One defining feature of cancer is the rapid creation of abnormal cells which grow beyond their usual boundaries, and which can invade adjoining parts of the body and spread to other organs, a process referred to as metastasis.

Cancer is a leading cause of death. From a total of 58 million deaths worldwide in 2005, cancer accounts for 7,6 million (or 13%) of all deaths. The main types of cancer leading to overall cancer mortality are: lung (1,3 million deaths/year); stomach (almost 1 million deaths/year); liver (662000 deaths/year); colon (655000 deaths/year) and breast (502000 deaths/year). More than 70% of all cancer deaths in 2005 occurred in low and middle income countries. Deaths from cancer in the world are projected to continue rising, with an estimated 9 million people dying in 2015 and 11,4 million dying in 2030 [2].

Cancer derives from modifications of the genes responsible for cell growth and repair. These changes are the result of the interaction between genetic host factors and external agents which can be categorized as: *physical carcinogens*, such as ultraviolet (UV) and ionizing radiation, *chemical carcinogens*, such as asbestos and tobacco smoke, *biological carcinogens*, such as infections by virus (Hepatitis B Virus and liver cancer, Human Papilloma Virus (HPV) and cervical cancer) and bacteria (Helicobacter pylori and gastric cancer) and parasites (schistosomiasis and bladder cancer), contamination of food by mycotoxins, such as aflatoxins (products of Aspergillus fungi) causing liver cancer [3].

Cancer arises from one single cell. The transformation from a normal into a tumour cell is a multistage process, typically a progression from a pre-cancerous lesion to malignant tumours. The development of cancer may be initiated by external agents and inherited genetic factors. Ageing is another fundamental factor for the development of cancer. The incidence of cancer increases dramatically with age, most likely due to risk accumulation over the life course combined with the tendency for cellular repair mechanisms to be less effective as a person grows older. Cancer cell genotypes is a manifestation of six essential alterations in cell physiology that collectively lead to malignant growth: self-sufficient in growth signals, insensitivity to growth-inhibitory signals, evasion of programmed cell death, limitless replicative potential, sustained angiogenesis, and tissue invasion and metastasis [1].

Treatment of tumour is aimed at curing, prolonging life and improving the quality of life of patients with cancer. Some of the most common tumour types such as breast cancer, cervical cancer and colon-rectal cancer have a high cure rate when detected early and treated according to best evidence. The principal methods of treatment are surgery, radiotherapy and chemotherapy. Fundamental for adequate treatment is an accurate diagnosis by means of investigations involving imaging technology (ultrasound, endoscopy, radiography) and laboratory (pathology).

1.2 CHEMOTHERAPY

The word "chemotherapy" was created by *Herlich* at the beginning of the 20th century and it meant a medical therapy which uses synthetic chemical compounds as antimicrobials [4]. Now, this word indicates drugs for anticancer therapy with the aim of slowing or blocking neoplastic cellular proliferation through cytotoxic mechanisms. The success possibility for a chemotherapeutic agent is as greater as the differences between target cells and healthy ones. If these differences are few, as in the case of a neoplastic cellular population and the original healthy cellular population, an anticancer agent can not eliminate tumour cells without giving toxic effects to the patient. In fact, tissues or organs with a high proliferative index, such as bone marrow, epithelia of the gastro-intestinal tract, skin, are chemotherapy target like cancerous cells. This unwanted damage causes hair loss, nausea, infections and much other side effects.

Another important problem of chemotherapy is the onset of resistance for antineoplastic drugs in tumour cells. Cellular mechanisms of chemotherapy resistance are different: from the reduced net intracellular drug accumulation resulting from the over-expression of cell surface efflux proteins, such as P-glycoprotein or Multidrug Resistance-associated Protein, to the increase of the cellular inactivation of drug, from the alteration of the drug target to the enhance of the repair cellular mechanisms of drug damage [5]. Various strategies are studied to bypass this problem: synthesis of new compounds similar to a cytotoxic drug but with a better cellular uptake [6], chemotherapy and association with compounds that inhibit drug detoxification or inactivation mechanisms (for example compounds that inhibit P-gP and so expulsion of chemotherapics, [7]) and changes in molecular target compared to the classical anticancer drugs.

1.2.a CHEMOTHERAPEUTICS AND CELL CYCLE

As chemotherapeutics are antiproliferative drugs, there is often a relationship between cell cycle and their cytotoxic action. All cells in proliferation must pass through a series of metabolic steps prior to cell division.

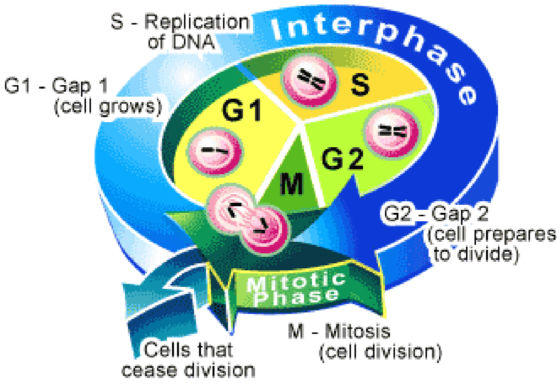
S - Replication of DNA
Interphase
G1 - Gap 1 (cell grows)
S
G1
G2
M
G2 - Gap 2 (cell prepares to divide)
Mitotic Phase
M - Mitosis (cell division)
Cells that cease division

***FIG 1**: cell cycle.*

Cell cycle begins with G1 phase, in which the synthesis of enzymes for the functioning and production of new DNA occurs. During S phase, there are the synthesis of DNA and the duplication of genome. G2 is associated with the metabolic activity for the production of all needed components for mitosis, which is the M phase. Mitosis is marked by the generation of bipolar mitotic spindles, the segregation of sister chromatids and cell division. There are also cells in G0 phase or in quiescence state. External stimuli (mitogens or growth factors) induce them to move out of G0 and through the early part of G1 [8]. These external stimuli are communicated through a cascade of intracellular phosphorylations, by upregulating expression of the cyclins, which associate with the cyclin-dependent kinases (CDKs). In fact, the cell cycle is propelled by a series of protein kinases; these CDKs complex with their respective cyclin and, subsequently, are phosphorylated by an activating kinase. Cyclin is the regulatory unit and CDK is its catalytic partner. The level of each cyclin independently increases or decreases within the phases of the cycle. Cyclin/CDK complexes phosphorylate specific protein substrates to move the cell through the cycle with activation of DNA synthesis (in late G1 and S), and formation of the structural components associated with mitosis (in late G2 and M). The periodicity of the cyclins, mediated by their synthesis and subsequent proteolytic degradation, ensures the well-delineated transitions between cell cycle stages [9].

Anticancer drugs can be divided into three categories considering their relationship with cell cycle: *cycle non-specific*, which demonstrate their antiproliferative activity independently of the presence of cells in cycle, that is also for cells in G0 phase; *phase-specific*, which kill cells when they are in a specific phase of the cycle; *phase non-specific*, which are active towards proliferating cells but independently of cell cycle phase. This classification is important for the operative meaning. For example, in a big tumour mass, there are often a lot of quiescent cells and so the therapeutic approach should begin with radiotherapy, surgery but also with the use of cycle non-specific drugs [10].

1.2.b CLASSIFICATION OF CHEMOTHERAPEUTICS

Chemotherapeutic agents can be classified by their different mechanism of action:

- **antimetabolites**: these drugs prevent the reproduction of tumour cells altering metabolic view such as the synthesis of folate, purines, pyrimidines and nucleosides, and so the synthesis of nucleic acids. These compounds present similar structures to endogenous metabolites; and this structural analogy causes the block of an enzymatic system or the synthesis of an inactive product. In this group, we can find *methotrexate*, which inhibits the formation of tetrahydrofolic acid, a coenzyme of DNA synthesis, acting as an anti-folic; *purine analogues*, such as 6-mercaptopurine or 6-thioguanine, which are able not only to inhibit purine synthesis but also to incorporate into DNA or RNA, damaging them; *pyrimidine analogues*, such as ara-c, which inhibits DNA-polymerase, or 5-fluorouracile, which blocks DNA synthesis through the binding to timidilate synthetase and, when incorporated into RNA, causes errors during transcription [11]. Antimetabolites are phase-specific drugs as they inhibit DNA synthesis during S phase [10].
- **Alkylators**: they show the ability to alkylate nucleophilic sites in cellular macromolecules. Although these agents damage virtually all components of the cell, their biological effects are attributable to their direct interaction with DNA through the formation of a covalent bound between the activated form of the drug (electrophilic carbocation) and the nucleophilic nitrogen bases. Alkylating agents react with DNA either directly or via intermediaries, which are formed by metabolic activation or spontaneous chemical degradation. Oxygen and nitrogen atoms in the bases of DNA and in phosphodiester bonds between the bases are targets for attack, and 12 different products have been identified [12]. Damage to base residues can result in further

chemical modifications such as loss of a base and interstrand or intrastrand DNA crosslinking.

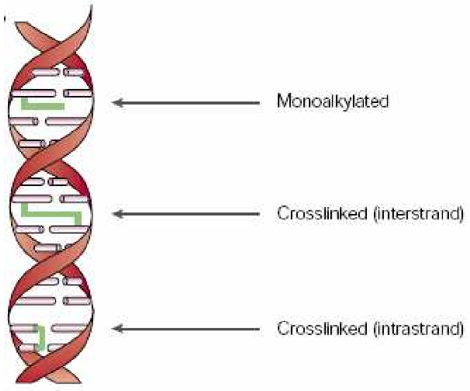

FIG 2*: interaction between alkylators and DNA*

Nitrogen mustards, nitrosoureas, mitomycins, tetrazines, platinum coordination complex[1] belong to this group of drugs. Alkylators are cytotoxic in cells independently of cell cycle and so also in quiescent cells. However, they are more efficacious towards highly proliferating tissues, in which G1 and S phases are very vulnerable. After DNA alkylation, cells accumulate and dead in G2-phase [10].

- **Topoisomerase inhibitors**: Topoisomerases are enzymes that can change the topological state of DNA through the breaking and rejoining of DNA strands. Cells encode two classes of topoisomerases that are distinguished by their catalytic mechanisms. Type I topoisomerases act by generating a transient single-stranded break in the double helix, followed by either a single-stranded DNA passage event or controlled rotation about the break. As a result, these enzymes are able to alleviate torsional stress (i.e., remove superhelical twists) in duplex DNA [13]. Type II topoisomerases act by generating a transient double-stranded DNA break, followed by a double-stranded DNA passage event. Consequently, these enzymes are able to remove superhelical twists from DNA and resolve knotted or tangled duplex molecules [14]. Topoisomerases are valuable targets for cancer chemotherapeutic agents . Several classes of topo inhibitors have been introduced into cancer clinics as potent anticancer drugs, including camptothecins (Irinotecan, Topotecan) inhibiting topo I and anthracyclines (Doxorubicin, Daunorubicin), epipodophyllotoxins (etoposide, teniposide), aminoacridines (amsacrine) and ellipticines, targeting topo II. The activity of these agents is thought to derive from stabilization of DNA/topo cleavable complex, an intermediate in the catalytic cycle of the enzymes , resulting ultimately in apoptosis. As cells in S and G2 phase present the highest levels of topoisomerase, inhibitors are more cytototoxic during these phases [10].

---

[1] The chemical reaction of platinum coordination complex involved in cytotoxic mechanism is not an alkylation but “platination” of DNA. As the effects (covalent bound to DNA, intra and interstrand cross-links) are the same, these compounds are often classified as alkylators.

- **Antimitotic agents**: these agents interfere with microtubules, which are essential components of the cytoskeleton, that help regulate diverse processes such as cell migration, cell growth, organelle transport and correct segregation of chromosomes during mitosis [15]. Microtubule system is an high dynamic structure, constantly growing and shortening, and antimitotic drugs affect this dynamics by interacting with tubulin. The most clinically useful classes of antimitotic drugs are the *Vinca* alkaloids and the taxanes [16]. The strategy of using tubulin as a target for cancer chemotherapy is based on the increased growth and division of cancer cells and the fact that drugs that interfere with mitosis such as the *Vinca* alkaloids, which shift the equilibrium to the depolymerised form of tubulin, have proven effective in the treatment of cancer. Taxanes target tubulin but, unlike the *Vinca* alkaloids and colchicine, shift the equilibrium to the polymerized form, thus stabilizing microtubules. Antimitotic agents prevent the normal formation and above all the dynamics of mitotic spindle, stopping cellular division in metaphase. Nevertheless, as microtubules take part in many cellular functions (intracellular transport, signal transduction, receptor mechanisms), antimitotic agents can damage cells not only in mitosis but also during interphase [17].
- **Hormones or their antagonists**: Tumours originated by hormone-sensitive tissues can retain their hormone-dependency, which can be used for the inhibition of their growth. Hormones with opposite activity to the ones that induce tumour development or hormone antagonists can be used. For example antiestrogens, such as tamoxifene, or antiandrogens, such as cyproterone, can be implied for hormone-dependent breast or prostate carcinoma, respectively [10].

A new generation of cancer drugs ('targeted therapy') was designed to interfere with a specific molecular target (typically a protein) that is believed to have a critical role in tumour growth or progression. The identification of appropriate targets is based on a detailed understanding of the molecular changes underlying cancer [18]. This approach presents some advantages, such as the reduction of side effects thanks to the improvement of tumour specificity and the choice of the therapy after the identification of the molecular target alteration in the specific neoplasm. Among these new drugs, we can find inhibitors of kinases, which have so far proved to be a promising class of targets for cancer therapy. Kinases play key roles in cancer as they are directly or indirectly involved in most signalling pathway.

Aberrant kinase activity has been associated with this disease. All these enzymes make use of ATP for phosphorylation of a specific Ser/Thr/Tyr residue(s) on protein substrates. The success of small-molecule ATP-competitive inhibitors such as, imatinib (Gleevec) for the treatment of chronic myeloid leukaemia (CML) and gastrointestinal stromal tumors (GIST), and gefitinib (Iressa) and erlotinib (Tarceva) for the treatment of non-small-cell lung cancer (NSCLC), confirms that this strategy is indeed effective [19].

However, classical chemotherapy and radiotherapy approaches remain the mainstay of cancer treatment for tumours that cannot be cured solely by surgical excision. For example, because of the recent success in defining the biochemical details of cell's responses to DNA-damaging agents, these conventional cancer therapies may be combined with targeted agents that disrupt the DNA-repair response; hopefully a more catastrophic cell kill in tumours will result [18].

1.3 CELL DEATH: NECROSIS AND APOPTOSIS

Cell death is the aim of chemotherapy and it is usually classified into two broad categories: apoptosis and necrosis [20]. Necrosis is a passive, catabolic process, which represents a cell's response to acute injury such as hypoxia, hyperthermia, viral invasion, exposure to various exogenous toxins. Necrosis is characterized by early mitochondrial swelling and failure, dysfunction of the plasma membrane with loss of homeostasis, cell swelling, and rupture. The loss of cell membrane integrity with the outflow of cell contents, including proteases and lysozymes, induces an inflammatory response with cytokine release by the surrounding macrophages as they mop up the damaged cells and begin the process of repair [21].

The major physiological mechanism of cell removal is apoptosis—a Greek descriptive term for falling leaves or petals. Apoptosis indicates the process by which cells are "silently" removed under normal conditions when they reach the end of their life span, are damaged, or superfluous. It is a general tissue phenomenon necessary for development and homeostasis: elimination of redundant cells during embryogenesis, cell atrophy upon endocrine withdrawal or loss of essential growth factors or cytokines, tissue remodelling and repair, and removal of cells that have sustained genotoxic damage [22]. Apoptosis is an active process regulated by molecular mechanisms that set in motion or modify a stereotyped program of effector events.

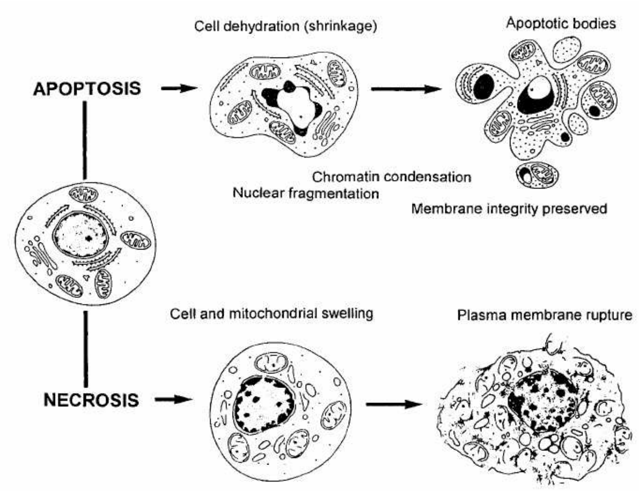

FIG 3*: necrosis and apoptosis.*

1.3.a MORPHOLOGICAL AND BIOCHEMICAL CHANGES IN APOPTOSIS

A cell triggered to undergo apoptosis activates a cascade of molecular events which lead to its total disintegration. One of the early events is cell dehydration. Loss of intracellular water causes condensation of the cytoplasm followed by a change in cell shape and size: generally, cells may become elongated and smaller [21]. The most characteristic feature of apoptosis is the condensation of nuclear chromatin, which starts at the nuclear periphery. The condensed chromatin often presents a concave shape resembling a half-moon, horseshoe, or sickle. The nuclear envelope disintegrates, lamin proteins undergo proteolytic degradation, followed by nuclear fragmentation, a stepwise degradation of nuclear DNA, first into subchromosomal fragments of 50-300 kbp, then into mono- or oligonucleosomal DNA fragments [23]. Activation of endonuclease(s), which preferentially cleaves DNA at the internucleosomal sections, is another characteristic event of apoptosis. The nuclear fragments, together with constituents of the cytoplasm (including intact organelles), are then packaged and enveloped by fragments of the plasma membrane, the so called ‘‘apoptotic bodies’’. When apoptosis occurs *in vivo,* apoptotic bodies are phagocytized by neighbouring cells, including those of epithelial or fibroblast origin (i.e., not necessarily by ‘‘professional’’ macrophages), without triggering an inflammatory reaction in the tissue [24]. Another feature of apoptosis is the maintenance, at least during the initial phase of cell death, of the structural integrity and most of the plasma membrane function. Also, cellular organelles, including mitochondria and lysosomes, remain preserved during apoptosis, although the dying cell manifests subtle biochemical alterations, in particular partial proteolysis and the permeabilization of membranes (ex: the mitochondrial transmembrane potential is markedly decreased) [25].

Other features of apoptosis include the mobilization of intracellular ionized calcium [26], the loss of asymmetry of the phospholipids on the plasma membrane leading to exposure of phosphatidylserine on the outer surface [27], and other plasma membrane changes needed to apoptotic cell to become a target for phagocytizing cells [28].

A family of cysteine proteases, called caspases, plays a central role in the initiation and execution phases of apoptosis. Upon activation, these enzymes cleave specific substrates and thereby mediate many of the typical biochemical and morphological changes in apoptotic cells. Evidence for the sequential activation of caspases has led to the concept of a caspase cascade [29]. This cascade begins with autocatalytic activation of initiator caspases which, in turn, transmit the signal by cleaving and thus activating the downstream effector caspases. More than 100 caspase substrates have been identified so far and this list includes proteins with very different functions: structural proteins, signalling proteins, regulators of transcription and translation, regulators of replication and cell cycle, regulators of DNA repair and cleavage, regulators of RNA metabolism, regulators of apoptosis, regulators of cell-cell interaction [30].

Two main pathways of procaspase[2] activation during apoptosis have been proposed: first, *extrinsic* activation, triggered by formation of a receptosome complex; second, *intrinsic* activation, after the formation of an apoptosome complex [31].

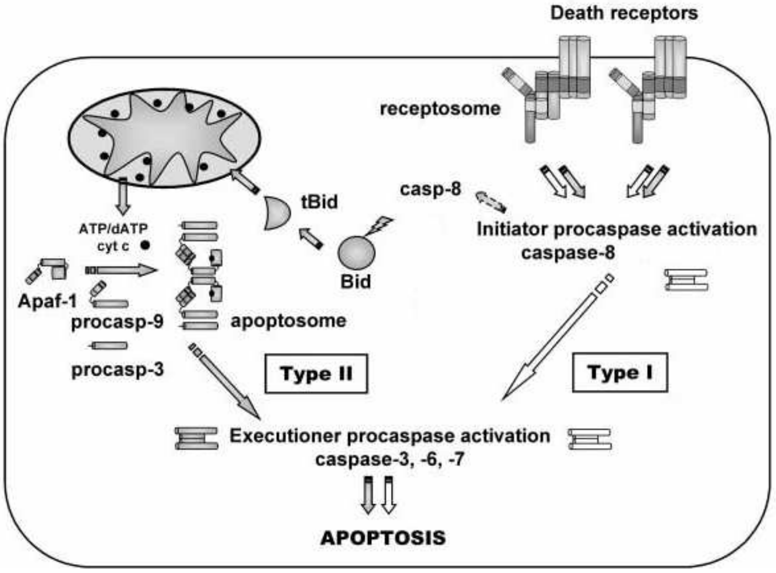
Death receptors
receptosome
casp-8
tBid
Bid
Initiator procaspase activation
caspase-8
ATP/dATP
cyt c
Apaf-1
procasp-9
procasp-3
apoptosome
Type II
Type I
Executioner procaspase activation
caspase-3, -6, -7
APOPTOSIS

***FIG 4**: Activation of caspase cascade*

---

[2] Procaspase = non activated caspase.

Extrinsic activation is initiated by the binding of ligands to death receptors, such as tumor necrosis factor (TNF)-RI or Fas. For example, upon binding of Fas ligand, Fas receptor forms microaggregates at the cell surface, allowing the adaptor molecule FADD (Fas-Associated protein with Death Domain) to be recruited to its cytosolic tail by a multi-step mechanism. FADD recruits caspase-8 zymogens by virtue of homophilic interaction with their N-terminal Death Effector Domains (DEDs). It is within this Death-Inducing Signaling Complex (DISC) that the initiator caspase-8 is activated [31].

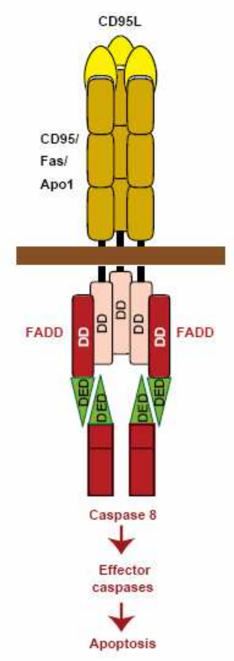

***FIG 5**: Receptosome.*

Two types of cell death induced by Fas ligation have recently been described. In type I cell death, a large amount of active caspase-8 is generated within seconds at the DISC, leading to an efficient and direct activation of downstream effector procaspases (-3, -6 and -7). In type II cells, DISC formation is strongly reduced, resulting in lowered and delayed procaspase- 8 and -3 activation. In this cell type, propagation and amplification of the apoptotic signal require mitochondrial factors. A molecular link connecting DISC activation and mitochondria is caspase-8-mediated cleavage of Bid, a proapoptotic member of the Bcl-2 family. The C-terminal part of Bid (tBid) translocates to the mitochondria, where it induces the release of cytochrome c. The latter activates downstream effector procaspases through apoptosome formation [32].

Intrinsic activation of procaspases involves release of cytochrome c from the mitochondrial intermembrane space to the cytosol. Cytochrome c together with dATP/ATP binds to Apaf-1 (Apoptotic protease activating factor-1), which initiates the formation of the apoptosome complex. Subsequently, Apaf-1 undergoes a conformational change and recruits procaspase-9 via its N-terminal Caspase-Activation Recruitment Domain (CARD). Mature caspase-9 proteolytically activates the executioner procaspase-3, which is also recruited to the apoptosome complex [31]. Although the exact mechanism for induction of cytochrome c release during intrinsically induced activation of procaspases has not yet been elucidated, the proapoptotic Bcl-2 family members Bax, Bak, Bad, Bik, and Noxa are implicated [22]. So, numerous pro-apoptotic signal transduction and damage pathways converge on mitochondrial membranes to induce their permeabilization and mitochondria are recognized to be important in the control of cell survival and death.

Accumulating evidences suggest that other organelles, including the endoplasmic reticulum (ER), lysosomes and the Golgi apparatus, are also major points of integration of pro-apoptotic signalling or damage sensing. Each organelle possesses sensors that detect specific alterations, locally activates signal transduction pathways and emits signals that ensure inter-organelle cross-talk. For example, upon membrane destabilization, lysosomes release cathepsins, which can trigger mitochondrial membrane permeabilization [25].

1.4 PHOTOMEDICINE

Photomedicine is used to cure various cutaneous and neoplastic diseases and includes phototherapy and photochemotherapy [33].

Phototherapy and photochemotherapy are treatments in which the light with an appropriate wavelength is used to induce a therapeutic response, in the absence or in presence of a photosensitizer drug, respectively.

To be effective, light has to be adsorbed by an endogenous chromophore (phototherapy) or by a photosensitizer agent (photochemotherapy), which can be administered by topical or systemic way. With the absorption of a photon, chromophore passes to the excited state and then it can provoke reaction that leads to biological responses.

Phototherapy consists in the use of light in different wavelength (UV-vis) mainly for treatment of skin diseases. The photon energy causes the excitation of particular chromophore electron, provoking specific chemical reactions.

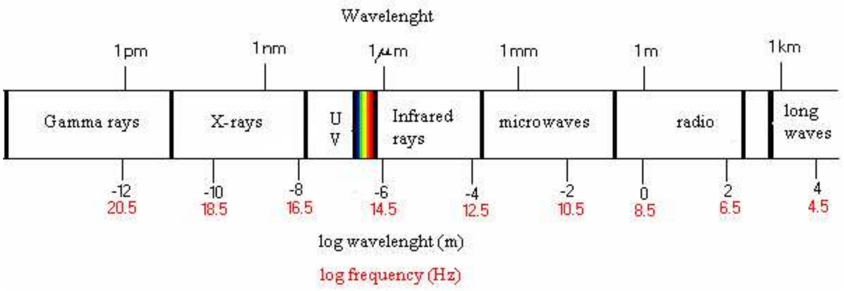

FIG 6:*Classification of electromagnetic radiations.*

The UV spectrum includes the range between 380 and 180 nm; from a biological point of view, it is divided into 3 groups: UV-A (380-320 nm), UV-B (320-290 nm) and UV-C (290-190 nm) [34].

The shorter wavelength end of UV-C (190 nm) represents the region where air and water become transparent. The longer-wavelength limit (290 nm) of the UV-C region can be defined as the shortest UV wavelength easily measured at the earth’s surface. UV-C radiations are too dangerous to be applied in therapy but, as they show a germicide activity, they find application in environment, surface and instruments disinfection.

The longer-wavelength limit of UV-B (320 nm) can be defined as that wavelength at which ozone becomes transparent. UV-B therapy is still the most frequently used phototherapeutic modality for the treatment of a variety of skin diseases, including psoriasis, parapsoriasis, pityriasis lichenoides, polymorphic light eruption, atopic dermatitis and many others [35].

Unfortunately, the utilization of UV-B rays presents two limitations: the possibility of cutaneous tumours and phototoxicity as they are responsible for sun bursts. The narrowband UV-B lamp with an emission spectrum peaking at 311-313 nm was developed as an alternative to broadband UV-B (290-320 nm) for the phototherapy of psoriasis to reduce erythemogenicity and the risk of skin carcinogenesis [36].

The longer-wavelength UV-A limit (380 nm) is where human vision begins and the UV ends. UV-A beams, which reach earth surface in a greater rate, are implicated in photosensitization reactions and in skin aging. UV-A1 phototherapy utilizes long wave UV-A radiation (340-380 nm) while filtering out the erythematogenic UV-A and UV-B wavelengths (290-340 nm). It has been shown to be very effective in the treatment of several inflammatory skin diseases such as atopic dermatitis, localized scleroderma, urticaria pigmentosa, disseminated granuloma annulare and in some cases in systemic sclerosis, lichen sclerosus et atrophicans, graft-*versus*-host disease (GvHD), cutaneous T cell lymphoma and psoriasis in HIV-infected individuals [36].

In photochemotherapy, first a drug-photosensitiser is administered to the patient. The photosensitiser alone is harmless and has no effect on either healthy or abnormal tissue. However, when radiation is directed into tissue containing the drug, the drug becomes activated. Thus, by careful application of the light beam, the technique can be targeted selectively to the ill tissue.

There are two different kinds of photochemotherapy: photodynamic therapy (PDT), which combines porphyrin derivatives and red visible light (600-630 nm), and PUVA therapy, which combines psoralens and UV-A radiations.

PDT is used above all in oncology field: in fact, its applications are the treatment of localized solid tumours of bladder, lung, head, neck, prostate, gastrointestinal tract, pancreas, brain, breast, skin and oesophagus [37]. It can also be used in the treatment of such dermatological diseases as psoriasis and scleroderma, of age-related macular degeneration and other eye diseases, of arthritis and finally of infections by drug-resistant microorganisms.

PUVA is extensively employed in various skin diseases such as psoriasis, vitiligo, mycosis fungoides, atopic dermatitis, alopecia areata, scleroderma [33, 38]. Extracorporeal photochemotherapy (photopheresis) has been recently introduced in the treatment of autoimmune diseases such as T-cell lymphoma [38-43].

1.5 MECHANISM OF PHOTOSENSITIZER-LIGHT INTERACTION

Light absorption in UV-visible spectrum by an organic molecule triggers the shift of one of its electron from an orbital in the ground-state S_0 to one with more energy ^1S, which represents the singlet excited state of the molecule. The excited molecule can be considered as a radical species with a very short life time and it can react with various substrates. Moreover, the singlet state can be converted into an other excited state, the triplet, through an intersystem crossing (ISC). Triplet is characterized by a smaller energy and a longer life time, so photosensization is more probable.

$$S_0 \xrightarrow{h\nu} {}^1S \xrightarrow{ISC} {}^3S$$

Triplet is the excited species that provokes reactions with biological substrates. These can occur through two different mechanisms:

- **oxygen-dependent mechanism** (photodynamic mechanism), which can be divided into type I and II reactions.
- **oxygen-independent mechanism** or type III reaction.

Molecular oxygen, which in the ground-state is a triplet ($^3O_2$), represents an excellent substrate for excited photosensitizers and thus it is the most important mediator for indirect modifications of biological target.

Type I mechanism includes the formation of such radical species as superoxide anion and hydroxyl radical, which are able to damage various biological substrates: nucleic acids, proteins and fat acids.

$$\text{Sens}\ (T_1) + D \longrightarrow \text{Sens}^{-\cdot} + D^{+\cdot}$$

$$\text{Sens}^{-\cdot} + {}^3O_2 \longrightarrow \text{Sens}\ (S_0) + O_2^{-\cdot}$$

D = electron donor

Addition of a second electron to $O_2^{-\cdot}$ gives the peroxide ion, O_2^{2-}, which has no unpaired electrons and is not a radical. Any O_2^{2-} formed at physiological pH will immediately protonate to give hydrogen peroxide (H_2O_2) since the pKA of H_2O_2 is very high. In aqueous solution, O_2^{2-} undergoes the so-called dismutation reaction to form H_2O_2 and O_2. The overall reaction can be written:

$$2\ O_2^{-\cdot} + 2H^+ \longrightarrow H_2O_2 + O_2$$

Homolytic fission of the O-O bond in H_2O_2 produces two hydroxyl radicals, $^{\cdot}OH$. Homolysis can be achieved by heat or ionising radiation. A simple mixture of H_2O_2 and an iron (II) salt also forms the $^{\cdot}OH$ radical, as was first observed by Fenton in 1894:

$$Fe^{2+} + H_2O_2 \longrightarrow Fe^{3+} + {\cdot}OH + OH^-$$

So superoxide anion ($O_2^{-\cdot}$) can lead to the spontaneous or enzymatic production of hydrogen peroxide that can react in catalytic quantity with transition metals inside the organism (Cu^{2+}, Mn^{2+}, Fe^{2+}, Ni^{2+}, etc). From this metal-catalysed reaction there is the production of hydroxyl radicals:

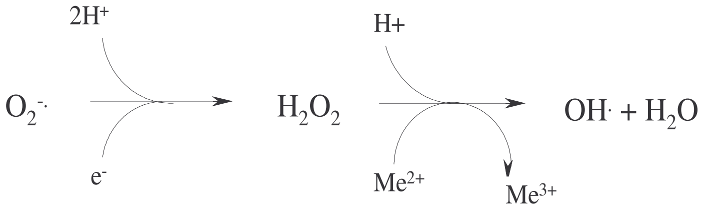

The reactivity of hydroxyl radicals versus DNA and other biological substrates is greater than singlet oxygen and moreover there is not an intracellular detoxification system for them. Luckily, its short time life prevents its diffusion from a cellular compartment to another.

Type II mechanism is characterized by direct energy transfer from an excited triplet molecule to molecular oxygen leading to the formation of singlet oxygen.

$$Sens(T_1) + {}^3O_2 \longrightarrow Sens(S_0) + {}^1O_2$$

$$Biomolecule + {}^1O_2 \longrightarrow \text{Products, membrane damage, cell death.}$$

As the singlet state energy for oxygen is just 22 Kcal/mol higher than the ground-state one, even Vis-absorbing molecules can give sufficient energy to produce singlet oxygen. Singlet oxygen is able to induce modification in DNA, proteins and lipids.

In **type III** reactions, oxygen is not involved and in fact the excited state of photosensitizer reacts directly with substrates. Type III reactions can involve three different mechanisms:

- **Energy transfer**, by which the substrate goes to the excited state while the photosensitizer returns to ground-state. In this process, the total spin of this system is always conserved:

$$Sens(S_0) + h\nu \xrightarrow{ISC} Sens(T_1)$$

$$Sens(T_1) + Sub(S_0) \longrightarrow Sens(S_0) + Sub(T_1)$$

- **One electron or hydrogen transfer**, by which substrate is reduced or oxidised by photosensitizer. Usually, radicals are formed from both substrate and photosensitizer. The inverse reaction between the two radicals often occurs, and in this case no reaction is observed:

$$\mathrm{Sens}(S_0) + h\nu \xrightarrow{\mathrm{ISC}} \mathrm{Sens}(T_1)$$

$$\mathrm{Sens}(T_1) + \mathrm{Sub}(S_0) \longrightarrow \mathrm{Sens}^{+\cdot} + \mathrm{Sub}^{-\cdot}$$

$$\mathrm{Sens}(T_1) + \mathrm{Sub}(S_0) \longrightarrow \mathrm{Sens}^{-\cdot} + \mathrm{Sub}^{+\cdot}$$

- **Photobinding**, by which the excited photosensitizer reacts with substrate to form a covalent product:

$$\mathrm{Sens}(S_0) + h\nu \xrightarrow{\mathrm{ISC}} \mathrm{Sens}(T_1)$$

$$\mathrm{Sens}(T_1) + \mathrm{Sub}(S_0) \longrightarrow \text{formation of covalent binding}$$

The covalent binding between photosensitizer and substrate is called photoinducted. The most known photobinding reactions are the ones that involve furocoumarins.

1.6 PUVA THERAPY AND PSORALENS

Psoralens are naturally occurring or synthetic trycicling aromatic compounds, deriving from the condensation of a coumarin nucleus with a furan ring. Their related angular isomers, angelicins, are also present in nature, for example in *Angelica archangelica*.

They show interesting photobiological and phototherapeutic properties such as skin photosensitization characterized by the onset of erythema followed by dark pigmentation [38].

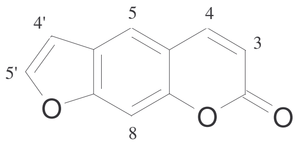

Psoralen

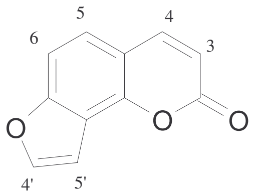

Angelicin

The introduction of photochemotherapy of generalized psoriasis, utilizing an orally administrated photoactive drug, 8-methoxypsoralen (8-MOP) and exposure of the skin to UV-A, was performed in the early 1970s by a group of dermatologists and pharmacologists at

Harvard Medical School and Massachusetts General Hospital [33]. Although this new pharmacological concept (photochemotherapy) was first reported in 1974, it has been used in Egypt and India since 1200-2000 BC [39]. In fact, photochemotherapy for vitiligo was practised in the ancient world by physicians and herbalists who used boiled extracts of leaves, seeds or roots of certain umbelliferous plants, e.g. *Amni majus* Linnaeus in Egypt or the leguminous plant, *Psoralea corylifolia* L. in India. These preparations were either applied to the skin or ingested as an infusion, the patient then exposed the skin to the intense Egyptian or Indian sunlight. In the Ayurvetic system of Indian medicine, the importance of exposure to solar radiation in the form of sun-worshipping prayer was found.

The modern history of photochemotherapy began with the study of the chemistry of psoralens (1930-60): extraction, identification of their structure, synthesis and the relationship between chemical structure and their photoreactivity. Then, there was a period during which basic science studies and clinical investigations into various properties of psoralens were developed. The initial studies for vitiligo led to further development of this therapy for the treatment of psoriasis. In recent years, there has been a new found interest in the basic aspects of psoralen photobiology and molecular mechanistic events contributing to therapeutic responses as well as to the development of skin cancers in PUVA patients [40].

Today, PUVA is one of the most common procedures performed in dermatology: diseases responsive to it are vitiligo, psoriasis, palmoplantar pustolosis, mycosis fungoides, atopic dermatitis, generalized lichen planus, urticaria pigmentosa, alopecia aerata.

In 1982, an extracorporeal form of 8-MOP photochemotherapy (photopheresis) was developed by *Edelson et al.* for the treatment of T-cell lymphoma, a CD4-positive T-cell malignancy [41]. Extracorporeal photopheresis (ECP) involves the reinfusion of peripheral blood leucocytes, following apheresis-isolation and exposure to 8-methoxypsoralen (8-MOP) and UV-A light. Photopheresis was also found to be effective in a number of other T-cell mediated diseases. Clinical trials demonstrated beneficial effects in pemphigo vulgaris, severe atopic dermatitis, AIDS-related complex, rheumatoid arthritis and systemic lupus erythematosus and chronic graft-versus-host disease [41]. It is accepted that the action of ECP is based on damaging pathological lymphocytes but the mechanism of action is still not fully understood. Some events such as induction of apoptosis in lymphocytes, changes to cytokine secretion patterns, induction of a clonal cytotoxic response which targets the malignant T-cell population, but also down-regulation of pro-inflammatory cytokines and enhanced anti-inflammatory responses have been reported following ECP treatment [42, 43].

Some psoralens are also used in the photosterilization of blood products, in particular, platelet concentrate because of their ability of target DNA [44].

1.6.a PSORALEN PHOTOPHYSICS AND PHOTOCHEMESTRY

Furocoumarins are tricyclic aromatic compounds that are able to intercalate into DNA thanks to their planar structure. Upon irradiation activation, they can photobind covalently DNA bases.

The important photophysical processes of psoralens are photoabsorption (excitation), radiative transitions (fluorescence and phosphorescence), and non-radiative deactivation (e.g., energy and electron transfer) [45, 46]. Kinetic parameters on the electronically excited states[3] have been determined. There may be two different types of electronic transitions for coumarins and psoralens, in the ultraviolet and near-ultraviolet (200–400 nm) regions of the spectrum:

- the transition from the non-bonding electron in the C_2 carbonyl group to the antibonding π* orbital.
- the transition from the electron in the bonding π orbital to the antibonding π* orbital.

These transitions produce n–π* and π–π* excited states. The fluorescent and phosphorescent states (S_1 and T_1) have been assigned to the π–π* excited state on account of their polarization spectra, lifetimes, theoretical transition energies, and transition moments. Both the spectroscopic and quantum chemical calculations of the electronic structures of coumarin's excited states indicate that excitation is substantially localized in the pyrone moiety [47].

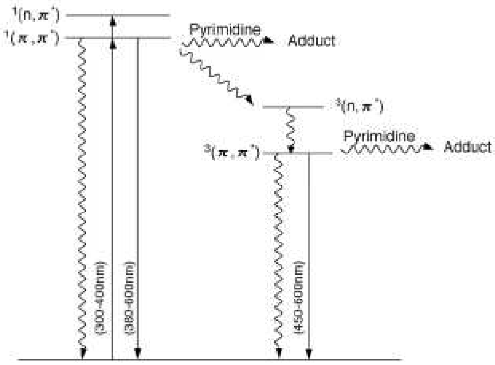

FIG 7: *Jablonski diagram for the relative orientations of energy levels in the excited states.*

---

[3] Fluorescence quantum yields (small: from 0,01 to 0,02) and lifetimes (short: from 1 to 5 ns), phosphorescence lifetimes and quantum yields (from 1 μs to 1s), quantum yields of intersystem crossing (0,45 for psoralen in water) and singlet oxygen generation [47].

Psoralens and coumarins fluoresce weakly, while they phosphoresce relatively strongly. Fluorescence emission can be observed from ca. 380 to 600 nm, depending upon the nature of substitutions and that of the solvent. Phosphorescence can usually be observed from ca. 450 to 600 nm. Phosphorescence intensity of psoralens is significantly stronger than that of the fluorescence because of the efficient intersystem crossing.

The photosensitizing effects of psoralens may involve oxygen-dependent and oxygen-independent mechanisms. The following scheme summarizes several different reactions that are induced by the photoexcitation of psoralens with UV-A light [45]:

(i) Excited States Formation:

$\mathrm{Ps}(S_0) \xrightarrow{h\nu} \mathrm{Ps}(S_1)$ (Photoexcitation)

$\mathrm{Ps}(S_1) \longrightarrow \mathrm{Ps}(T_1)$ (Intersystem Crossing)

(ii) Photosensitizations Pathways:

Type Ⅰ. Electron Transfer :

Photosensitizer Triplet State Reacts with an Electron Donor D.

$\mathrm{Ps}(T_1) + D \longrightarrow \mathrm{Ps}^{\bullet -} + D^{\bullet +}$ (Reduction)

$\mathrm{Ps}^{\bullet -} + {}^3O_2 \longrightarrow \mathrm{Ps} + O_2^{\bullet -}$ (Electron Transfer)

$D^{\bullet +} + O_2^{\bullet -} \longrightarrow D(O_2)$ (Back Electron Transfer)

Type Ⅱ. Energy Transfer

$\mathrm{Ps}(T_1) + {}^3O_2\,({}^3\Sigma_g) \longrightarrow \mathrm{Ps}(S_0) + {}^1O_2\,({}^1\Delta_g)$

(iii) Photobinding.

$\mathrm{Ps}(S_1) + \mathrm{DNA}(S_0) \longrightarrow \mathrm{Ps}\underset{\vee}{\overset{\wedge}{\;}}\mathrm{DNA}$ (Cyclobutane Formation)

(iv) Direct Electron Transfer (Charge Separation)

$\mathrm{Ps}(S_0) + {}^3O_2 \xrightarrow{h\nu} \mathrm{Ps}^{\bullet +} + O_2^{\bullet -}$

(v) Autoionzation

$\mathrm{Ps}(T_1) + \mathrm{Ps}(S_0) \longrightarrow \mathrm{Ps}^{\bullet -} + \mathrm{Ps}^{\bullet +}$

$\mathrm{Ps}(T_1) + \mathrm{Ps}(T_1) \longrightarrow \mathrm{Ps}^{\bullet -} + \mathrm{Ps}^{\bullet +}$

After UV absorption, psoralens are first pumped from the ground state (S_0) to the lowest excited singlet state (S_1). The short-lived S_1 state then undergoes intersystem crossing to create a relatively long-lived lowest excited triplet state (T_1).

In oxygen-dependent type I sensitization, an electron donor, such as one of the DNA bases, may readily reduce the psoralens in the excited triplet state. A subsequent electron transfer from the reduced photosensitizer to molecular oxygen results in the formation of reactive superoxide anions and fragmentation of the substrate cations.

In oxygen-dependent type II sensitization, the excitation energy of the first excited triplet state of the psoralens is transferred to molecular oxygen. The excited singlet molecular oxygen can then react rapidly and rather indiscriminately with a wide variety of biomaterials (e.g., nucleic acids, proteins, and unsaturated lipids), causing severe damage.

In the oxygen-independent photoreaction, the excited psoralen reacts with such biomolecules as DNA or unsaturated fatty acids. In fact, structures with olefinic double bonds can easily form C_4-cycloaddition with one or both of the photoreactive sites of furocoumarins (furan-site, i.e. $C_{4'}$-$C_{5'}$ double bond and pyrone-side, i.e. C_3-C_4 double bond) [48].

Other possible furocoumarin compound reactions are direct electron transfer and autoionization reactions. In the former process, a direct photo-induced charge separation takes place between psoralen and molecular oxygen ("direct electron transfer"). In the latter process, one sensitizer in the T_1 or S_0 state can reduce another sensitizer that is in the excited triplet state, thus forming a pair that consists of a radical anion and a radical cation. The term of autoionization refers to the process of charge-separation between the two identical molecules. The psoralen may finally become ionized, either directly or through an excited state, and may possibly react with the target compound in the form of a radical cation [49].

1.6.b PSORALEN MOLECULAR MECHANISM

The photochemical reactions with DNA are well characterized and develop in two steps:

1. Formation of a molecular complex in the ground state, in which psoralen intercalates between base pairs, thanks to hydrophobic interactions.
2. After photoactivation, the excited intercalated psoralen reacts with the 5,6-double bond of thymine (and to a lesser extend with those of cytosine), forming C_4-cycloadducts.

The psoralen adducts with DNA are formed primarily by a [2+2] photocycloaddition reaction between the 4',5' furan double bond and the 5,6-double bond of thymine. Monoadducts involving the 3,4 pyrone site can also be formed. After the absorption of another photon, psoralen can generate an inter-strand cross-link with another thymine in the adjacent base pairs [38, 49]. The formation of cross-links to DNA is the main cause of the long-term side effects of PUVA such as mutagenesis and the risk of skin tumours.

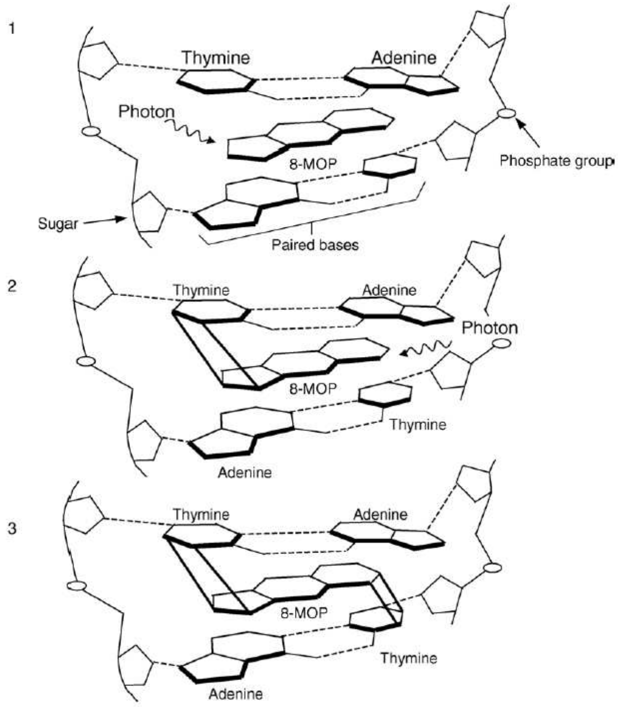

FIG 8: *The photochemical reactions of psoralens with DNA*

For years, the photobinding to DNA was considered the main molecular mechanism of PUVA, which was ,in fact, applied for treatment of diseases that would be expected to profit from DNA-alkylating agents: psoriasis was the first choice because of its hyperproliferative character. More recently, some evidence showed that psoriasis is an immune disorder, and its clearing by PUVA is not only due to the antiproliferative effect on skin cells, as the effect on circulating cells that trigger the immune response may also be involved.

Simple DNA photobinding is not sufficient to explain all these different activities, and other targets have been hypothesised and studied. For example, unsaturated lipids undergo photobinding by psoralens. Cyclobutane-like adducts are formed—similar to those between psoralens and thymine—between one of the reactive double bonds of psoralen (mainly the 3,4) and one or more of the double bonds of the fatty acid residue. It has been suggested that the products may be involved in the enzymatic pathway leading to skin melanization [50].

Proteins have also been considered; photobinding occurs, but details of the molecular events are still unknown.

Furthermore, oxidative processes cannot be ruled out. As a consequence of the photosensitizing properties of psoralens, the production of activated species of oxygen affects all biological substrates: lipids (peroxidation), nucleic acids (oxidation of guanine, strand breaks), and proteins (oxidation of amino acids, inactivation of enzymes) [48, 50].

On the other hand, upon UV-A irradiation, psoralen photoproducts (POPs) are generated, which are likely to contribute to PUVA cytotoxicity. In fact, POPs were reported to elicit a wide variety of effects, such as oxidation of proteins and unsaturated lipids, modulation of the immunologic response, inhibition of the growth and induction of apoptosis by mitochondrial involvement in tumour cell lines *in vitro* [51].

1.6.c PUVA AND APOPTOSIS

Many authors demonstrated that apoptosis was the main way of cellular death in PUVA and psoralen photopheresis treatments. Few information is available concerning the mechanisms underlying apoptotic cell death effected by PUVA. Some authors suggested a possible correlation between DNA photodamage and apoptosis: in fact the involvement of p53 pathway was demonstrated both *in vitro* and *in vivo* [52]. It is well known that agents that damage DNA induce high levels of p53 and accumulation of p53 in the nucleus. Moreover, it has been shown that PUVA treatment of Jurkat T lymphoblastoid cells causes caspase activation and mitochondrial dysfunction resulting in the opening of the permeability transition pore and a decrease in mitochondrial transmembrane potential ($\Delta\Psi_M$) [53, 54].

2. AIM OF THE PROJECT

The present project focused on the evaluation of the mechanism of action of new antiproliferative compounds. Despite the different oncological therapeutic approaches, which increased the survival for many kinds of tumors, and the recent improvement in the understanding of neoplastic transformation mechanisms, cancer still represents one of the most common causes of death. It is important to discover new drugs to introduce in therapy. In particular, two kinds of molecules were analyzed:

- an isoindoloquinoxalinone derivative.
- angelicin analogues, which were tested for their phototoxicity.

2.1 3-METHOXY-5H-ISOINDOLO[2,1-*a*]QUINOXALIN-6-ONE

Quinoxalines and the structurally related quinoxalinones represent an important class of biologically and medicinally useful agents: in fact, in function of their substitutions and condensations, they can demonstrate antiviral, antibacterial or antiprotozoan activity [55-57].
Furthermore, a large number of synthetic quinoxalines and quinoxalinones showed an interesting antineoplastic activity [58, 59]. For instance, the design of a novel series of cyclin-dependent kinase (CDK) inhibitors was conducted condensing the structure of quinoxalin-2-one with a macrocycle. These new compounds demonstrated a potent inhibition activity towards CDK1,2,4,6, which represent an attractive targets for new anticancer drugs [60].
Quinoxaline ring was condensed with pyridine moiety with the aim of synthesizing new intercalating polycyclic agents and led to benzo[*f*]pyrido[4,3-*b*] and pyrido[3,4-*b*]quinoxalines derivatives. Results demonstrated that appropriately substituted benzo[*f*]pyrido[4,3-*b*]quinoxalines were inhibitors of topoisomease I and II and had significant anticancer properties in various experimental models [61].
The incorporation of an indolo ring afforded 5-substituted 2-bromoindolo[3,2-*b*]quinoxalines that showed a broad spectrum of antitumor activity with two biochemical mechanism-based screens (cdc2 kinase and cdc25 phosphatase) [62].
We analysed the most active compound of a series of isoindolo[2,1-*a*]quinoxalin-6-one derivatives with the aim of evaluating their antiproliferative activity and their targets at cellular and molecular level. These molecules were synthesized by Cirrincione's group in "Dipartimento Farmaco-Chimico Tossicologico e Biologico" of Palermo University and they were evaluated for their antineoplastic activity by the National Cancer Institute (NCI, Bethesda, USA). The molecular structures are reported below in Fig 1.

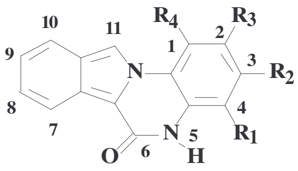

***FIG 1**: Isoindolo[2,1-a]quinoxal-6-ones.*

COMPOUNDS	R_1	R_2	R_3	R_4
ISQ1	H	H	H	H
ISQ2	Me	H	H	H
ISQ3	H	OMe	H	H
ISQ4	H	Me	Me	H
ISQ5	H	Cl	Cl	H

All these compounds were submitted to the NCI *in vitro* anticancer drug discovery screen. It consisted of a panel of approximately 60 human cancer cell lines against which compounds were tested over a defined range of concentrations to determine the relative degree of growth inhibition or cytotoxicity. Cell lines were grouped in disease sub-panels including leukemia, non-small-cell lung, colon, central nervous system, melanoma, ovarian, renal, prostate and breast tumors cell lines [63].

The mean of –log GI_{50} (pGI_{50}) was reported in figure 2 for each compound and each sub-panel.

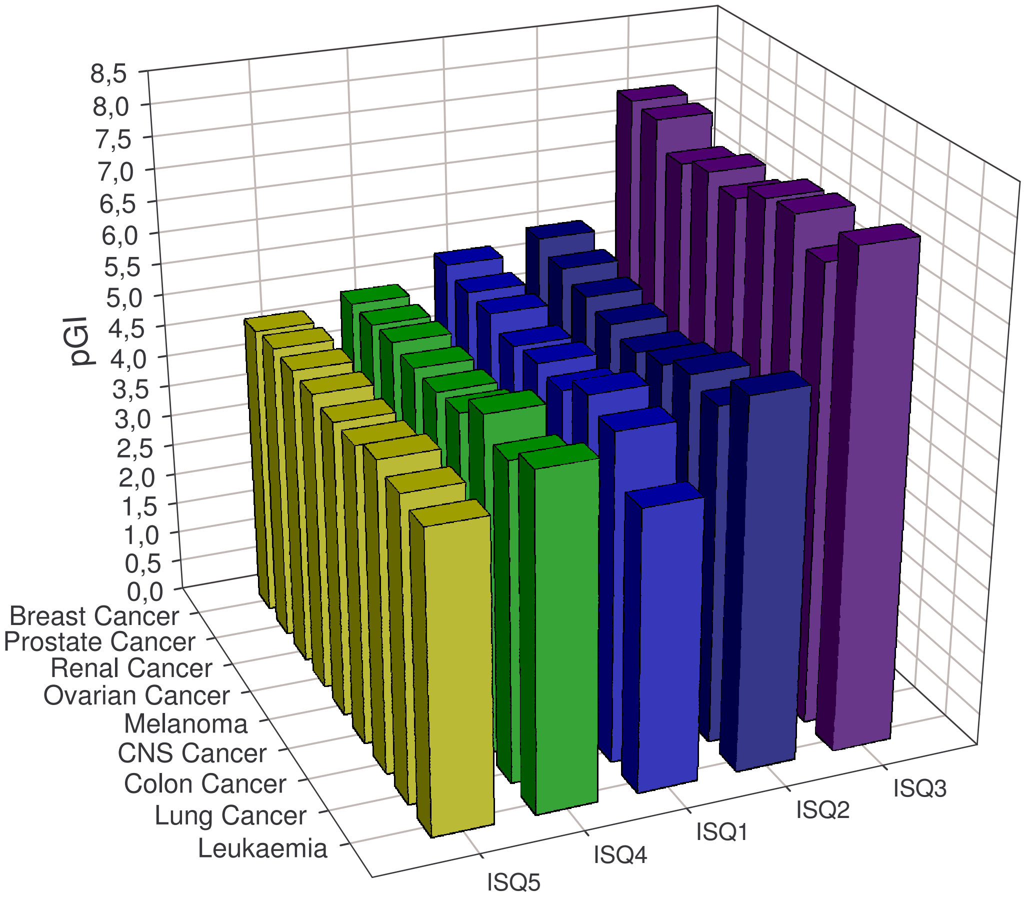

FIG 2*: Data obtained from the NCI's in vitro disease-oriented human tumor cells screen:* pGI_{50}

The first step was the investigation of the way of induced cell death through a series of flow cytofluorimetric experiments. Some typical apoptotic characteristics were researched in treated human tumor cells. It is important to identify the process of cell death: in fact, for a possible therapeutic use, it is better that cellular death involves apoptosis as it does not cause an inflammatory response *in vivo* as necrosis does.

To understand the mechanism of action of a new anticancer compound, several information can be obtained from the analysis of cell cycle in treated cells. It is well known that many antineoplastic drugs provoke deep modifications in cell cycle [10]. Thus, it is possible to compare the obtained data with the profile of cell cycle after the treatment with classical anticancer drugs.

As isoindolo[2,1-*a*]quinoxal-6-ones showed a policyclic planar structure, DNA affinity was studied. Actually, DNA represents one of the most important targets for several chemotherapeutic drugs [64]; so polycyclic nitrogen heterocycles with planar structure can be good pharmacophores for classes of antitumor drugs since they can intercalate between the base pairs of double-stranded DNA.

The investigation about the possible cellular target was carried out starting from the characteristics of the most active compound:

- the kind of cell cycle modifications.
- policyclic nitrogen heterocycle with planar structure.

2.2 ANGELICIN ANALOGUES

PUVA therapy is efficacious for the treatment of dermatological and oncological diseases but it demonstrates some adverse effects which limit its employment. These unwanted side effects can be divided into short-time risks, as nausea, skin phototoxicity reactions, immune system depression, and long-term risks, as premature cutaneous ageing, degeneration of dermal collagen and elastic tissues, cataract formation but also mutagenicity and neoplastic changes [65].

Because of the increasing interest in photochemotherapy, many groups are working to find out new derivatives which maintain the same efficacy of psoralens but lack the long-term adverse effects [66-71]. In particular, the risk of skin cancer development can be avoided using compounds that are not able to provoke DNA inter-strand cross-links. For example, angular furocoumarins, or angelicins, do not induce cross links because of their geometric structure but only monofunctional photoaddiction to DNA [66].

Another approach is the reduction of the reactivity of the photoreactive bonds through the introduction of electron-accepting or electron-donating groups. For example, 3-carbethoxypsoralen photoreacts with DNA only with its 4',5'-double bond. It exhibits low mutagenesis, an absence of cancerogenicity but therapeutic properties for psoriasis [67].

Many references are based on the evaluation of the photochemical and photobiological properties of furocoumarin analogues in which one or both oxygens were substituted with a heteroatom [68-70].

Another evaluated possibility is the protection of one of the psoralen photoreactive sites through the condensation of a new ring. One example is the synthesis of benzopsoralens, in which the condensation of a benzene ring was carried out in the furan reactive site. Nevertheless, these compounds showed an inspected activity in the dark with a possible topoisomerase inhibition, as well as a discrete DNA photoreactivity [71].

Cirrincione's group synthesized new psoralen analogues with the aim of finding compounds with better phototherapeutic profile. In particular, the synthesis was conducted combining two of the most employed strategies: the use of angular furocoumarin and the oxygen substitution with other heteroatoms. We analysed the photochemical and , above all, the photobiological properties of these angelicin derivatives: thiopyrano[2,3-*e*]indol-2-ones, in which the pyrone oxygen was replaced by a sulphur and the furan oxygen by a nitrogen, and pyrrolo[3,4-*h*]quinolin-2-ones, in which both oxygens were substituted by nitrogen atoms.

2.2.a THIOPYRANO[2,3-*e*]INDOL-2-ONES

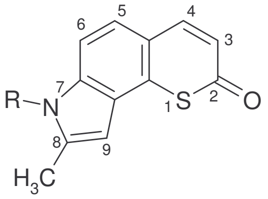
6
5
4
3
R
N
7
1
S
2
O
8
9
H3C

FIG 3a: *structure a*

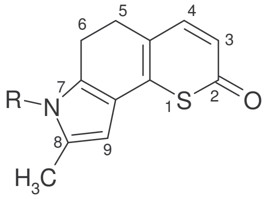
6
5
4
3
R
N
7
1
S
2
O
8
9
H3C

FIG 3b: *structure b*

COMPOUNDS	**STRUCTURE**	**R**
L1	b	Phe
L2	a	Phe
L3	a	Me
L4	b	Benzyl
L5	b	SO_2Phe
L6	b	Me

2.2.b PYRROLO[3,4-*h*]QUINOLIN-2-ONES

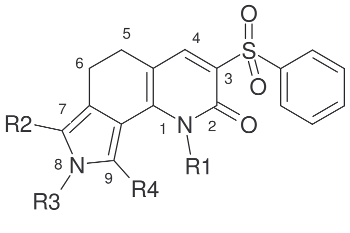
O
S
O
5
4
6
3
R2
7
1
N
2
O
8
N
R1
9
R3
R4

FIG 4a*: structure a*

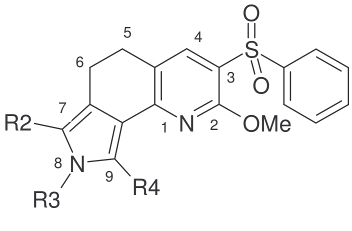
O
S
O
5
4
6
3
R2
7
1
N
2
OMe
8
N
9
R3
R4

FIG 4b*: structure b*

COMPOUNDS	**STRUCTURE**	**R1**	**R2**	**R3**	**R4**
BV1	a	H	H	Me	H
BV2	a	H	COOEt	Me	Me
BV3	a	H	H	Me	Me
BV4	a	H	H	Phe	H
BV5	a	H	COOEt	Benzyl	Me
BV6	a	H	H	Benzyl	Me
BV7	a	H	H	Benzyl	H
BV8	a	H	COOEt	H	Me
BV9	a	Me	COOEt	H	Me
BV10	a	Me	COOEt	Me	Me
BV11	a	Me	COOEt	Benzyl	Me
BV12	a	Me	H	Benzyl	H
BV13	a	Me	H	Me	H
BV14	a	Me	H	Phe	H
BV15	b	/	H	Benzyl	H
BV16	b	/	H	Me	H
BV18	a	H	COOH	H	Me
BV19	a	H	COOH	Me	Me
BV20	a	H	COOH	Benzyl	Me

The phototoxicity of these derivatives was checked and a relationship between structure and photobiological properties was hypothesized. We performed some experiments with the most active compounds to better understand the mechanism of cell death and the biological targets involved in photosensitization reactions. Flow cytofluorimetric analysis were conducted to find the way of cell death, apoptosis or necrosis. Moreover, other cytofluorimetric tests were carried out to evaluate which organelles were mostly implicated in inducing cell death.

As it is well known that the main psoralen mechanism for antiproliferative activity is the DNA photobinding, the interaction with this macromolecule was tested. We performed experiments to check the affinity of our compounds for DNA but also a potential photocleavage.

As these compounds showed a high liposolubility, a phospholipid photodamage was also investigated.

Aim____

3. 3-METHOXY-5H-ISOINDOLO[2,1-*a*] QUINOXALIN-6-ONE

3.1 CELLULAR CYTOTOXICITY

The evaluation of cytotoxic activity of the most active compound, **ISQ3**, was carried out in various human tumour cell lines: Jurkat (lymphoblastic leukaemia), K-562 (myelogenous leukemia), HL-60 (promyelocytic leukaemia), CEM (lymphoblastoid leukaemia), LoVo (colon adenocarcinoma) and MCF-7 (breast adenocarcinoma).

The cytotoxicity was checked with MTT test [72] after 72 hours from the incubation with **ISQ3**, as described in material and methods section. Moreover, the same experiments were performed in the presence of some common anticancer drugs, as reference.

In table 1, IC_{50}[1] (μM) in suspension cell lines were reported.

DRUGS	JURKAT	K-562	HL-60	CEM
ISQ3	0,00485±0,0002	0,0257±0,0026	0,025±0,003	0,0201±0,002
CAMPTOTHECINE	0,0125±0,003	0,0062±0,0007	0,0073±0,0009	0,012±0,008
ETOPOSIDE	0,250±0,030	0,137±0,016	0,464±0,043	0,0485±0,005
AMSACRINE	0,0653±0,0112	0,0876±0,011	0,0492±0,0042	0,104±0,012
DOXORUBICINE	0,0066±0,0012	0,0112±0,0007	0,0168±0,002	0,0095±0,001
PACLITAXEL	0,0001±0,00002	n.d	n.d.	n.d.
COLCHICINE	0,0056±0,0001	n.d.	n.d.	n.d

***TAB 1**: IC_{50} (μM) in some human leukaemia cell lines after 72 h of exposure as determined by MTT assay. Data are expressed as means ± SEM for at least three independent experiments. n.d. not determined.*

ISQ3 showed a very interesting cytotoxic activity in leukemia lines, reaching a IC_{50} lower than 5 nM in jurkat cells. Only paclitaxel presented a higher toxic power, in fact **ISQ3** IC_{50} values were comparable with the ones of the most drugs (colchicine, doxorubucine and camptothecine) or even they were lower than the ones of amsacrine and etoposide.

In table 2, IC_{50} (μM) in human solid tumor cell lines were presented.

---

[1] Concentration of compound required to inhibit the cell growth by 50%.

DRUGS	LoVo	MCF-7
ISQ3	0,128±0,015	0,175±0,023
CAMPTOTHECINE	0,036±0,004	0,135±0,018
ETOPOSIDE	1,25±0,20	2,50±0,59
AMSACRINE	0,300±0,027	3,80±0,60
DOXORUBICINE	0,0687±0,009	0,134±0,015
PACLITAXEL	n.d.	0,006±0,0006
COLCHICINE	n.d.	0,175±0,025

***TAB 2**: IC_{50} (μM) in some human solid tumor cell lines after 72 h of exposure as determined by MTT assay. Data are expressed as means ± SEM for at least three independent experiments. n.d. not determined.*

The antiproliferative activity of **ISQ3** was maintained in solid tumor cell lines with submicromolar IC_{50}. In adenocarcinoma cells, the same considerations of suspension cells can be valid. For all compounds, we can note a reduction of the antiproliferative effect passing from leukemia to solid cell lines but **ISQ3** resulted less cytotoxic than paclitaxel, as active as camptothecin and doxorubicin, and finally more toxic than etoposide and amsacrine.

As jurkat was found to be the more sensitive cells, further studies were conducted using this cell line.

3.2 DETERMINATION OF MECHANISM OF CELLULAR DEATH

For the evaluation of new antiproliferative compounds, it is important to understand the mechanism of induced cellular death. Fundamentally, two different forms of cell death, apoptosis and necrosis, have been defined [20, 24]. Necrosis is an accidental passive process resulting in an early disruption of the cell membrane and in the progressive breakdown of cell structures and organelle swelling. In contrast, apoptosis involves the activation of an energy-requiring intracellular machinery and occurs typically without provoking inflammatory changes. Thus, for a potential therapeutic purpose, it is preferable an anticancer drug induces apoptosis to avoid the inflammatory side effects.

We looked for some apoptotic characteristics in jurkat after the treatment with **ISQ3**.

Apoptotic cells were first identified by a series of typical morphological changes. Initially, cell membrane integrity is preserved while subtle changes, such as exposure of phosphatidylserine, occur. These membrane modification are recognition signals for the subsequent phagocytosis [27]. Other characteristics of apoptotic cells include cellular shrinkage, membrane blebbing, nuclear chromatin condensation and fragmentation. Eventually, cell breaks into membrane-surrounded fragments (apoptotic bodies) which are engulfed *in vivo* by professional phagocytes (macrophages and dendritic cells) [20]. In cell cultures, apoptotic bodies will lose the integrity of the plasma membrane during the late stages of apoptosis, followed by complete cell disintegration, also called secondary necrosis [24].

The apoptotic loss of plasmatic membrane asymmetry with the exposure of phosphatidylserine (PS) was used to evaluate cell death. In fact, this early event of apoptosis was monitored by flow cytometry, using a PS-binding protein, Annexin-V, conjugated with fluorescein isothiocyanate (FITC). Another probe, propidium iodide (PI), was added during the analysis for detecting the integrity of plasmatic membrane. PI penetrated the cell only with a collapsed plasmatic membrane, intercalated into DNA and gave the typical red fluorescence. Thus, the cytofluorimetic measure discriminated between intact (FITC$^-$/PI$^-$), early apoptotic (FITC$^+$/PI$^-$) and late apoptotic or necrotic cells (FITC$^+$/PI$^+$) [73].

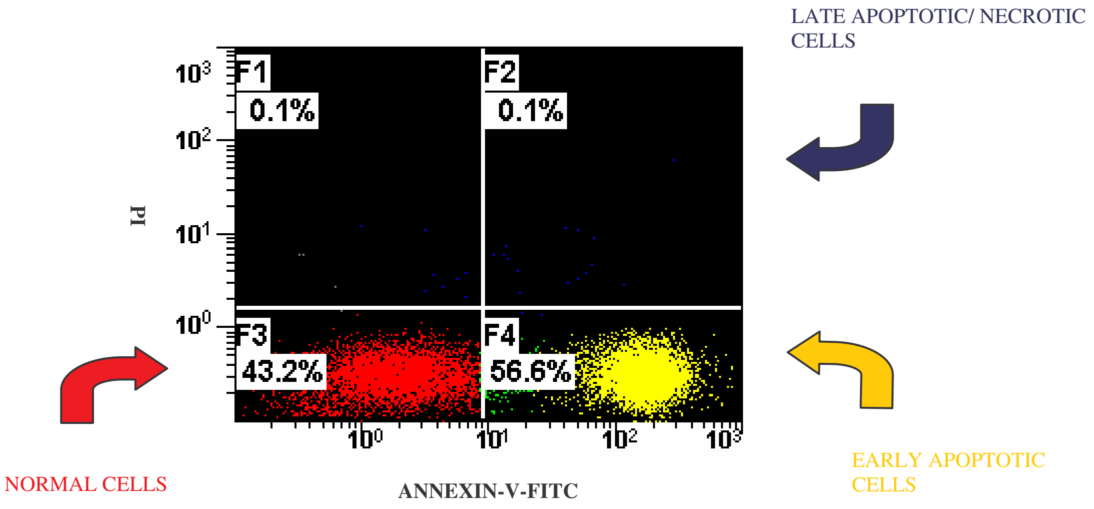

FIG 1*: Example of flow cytometry analysis after staining with Annexin-V-FITC and PI.*

The exposure of PS was evaluated in jurkat cells after 24 hours of the incubation with various concentrations of **ISQ3** and results were presented in fig 2.

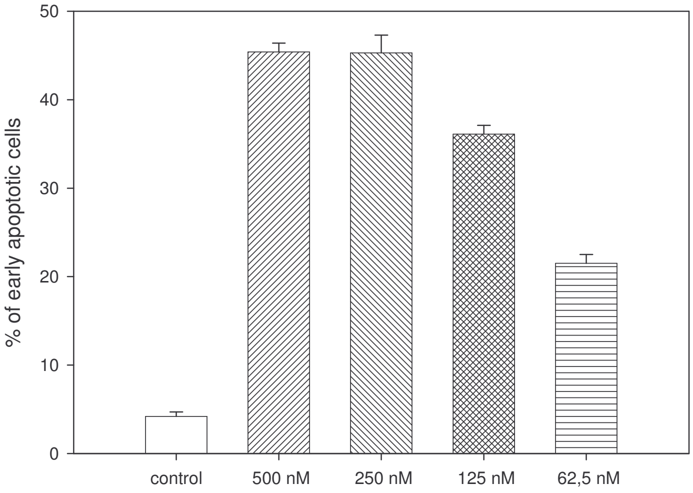

FIG 2*: Percentage of early apoptotic cells (FITC$^+$/PI$^-$) after 24 hours of treatment with* ***ISQ3*** *at various concentrations. Data were expressed as Mean ± SEM of three independent experiments.*

After 24 hours from the treatment, **ISQ3** was able to induce a significant PS translocation to outer membrane layer, compared to the control. The exposure of this phospholipid was not accompanied by a loss of membrane integrity (negative fluorescence of PI) and so necrosis was not detected. From these data, we can hypothesize **ISQ3** induced cell death by apoptosis.

3.3 INVOLVEMENT OF MITOCHONDRIA IN CELL DEATH

Mitochondria are central to many forms of cell death. In fact, a variety of key events in apoptosis focuses on mitochondria, including the release of caspase activators (such as cytochrome c), changes in electron transport, loss of mitochondrial transmembrane potential, altered cellular oxidation-reduction and participation of pro- and antiapoptotic Bcl-2 family proteins [74, 75]. The different signals that converge on mitochondria to trigger or inhibit these events and their downstream effects delineate several major pathways in cell death [25]. Thus, mitochondria operate not only as power stations required for aerobic life but also as amplifiers or sometimes even as sources of signals for apoptosis.

A potential involvement of mitochondria in **ISQ3** inducted apoptosis was detected through the research of some characteristic signals of mitochondrial dysfunction.

3.3.a DETERMINATION OF MITOCHONDRIAL MEMBRANE POTENTIAL

An early and irreversible event in apoptotic mitochondrial dysfunction can be the collapse of mitochondrial membrane potential: in normal conditions, it reaches a value of -220/-180 mV for the effect of the electron transport in respiratory chain and of the function of proton pump. After mitochondrial damage, a depolarization of the inner mitochondrial membrane can occur and the potential increases [76].

The detection of a possible mitochondrial potential collapse was conducted through a flow cytometric analysis, as described in materials and methods.

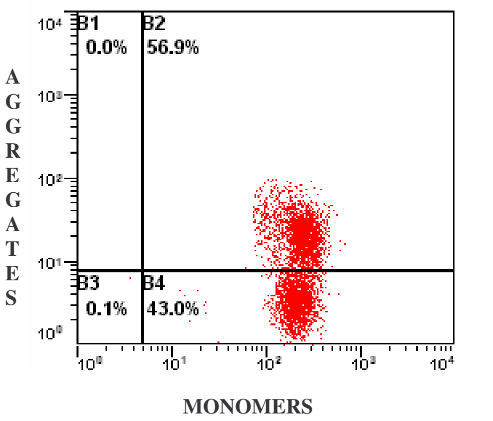

FIG 3*: Example of flow cytometry analysis after cellular staining with JC-1.*

Briefly, after 24 hours from the treatment with **ISQ3** at different concentrations, jurkat cells were stained with a membrane permeable cation, JC-1. JC-1 was able of entering selectively mitochondria and presented different fluorescence properties according to the membrane potential. This property was due to the reversible formation of JC-1 aggregates upon membrane polarization that caused shifts in emitted light from 530 nm (i.e., emission of JC-1 monomeric form) to 590 nm (i.e., emission of J-aggregate), when excited at 490 nm. The changes of the ratio of orange/green fluorescence reflected the $\Delta\psi_{mt}$ variation independently of the mitochondrial mass [74].

The percentage of cells with low mitochondrial potential for **ISQ3** treatment is depicted in Figure 4.

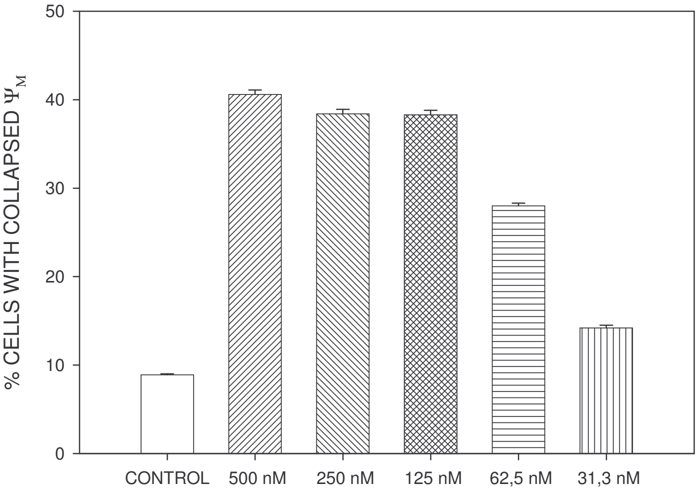

FIG 4*: Percentage of jurkat with collapsed* $\Delta\psi_M$ *(fluorescence of the JC-1 monomeric form) after 24 hours from the treatment with different concentrations of* ***ISQ3****. Data were expressed as Mean ± SEM of three independent experiments.*

Treated Jurkat cells in the presence of **ISQ3** exhibited a dramatic shift in fluorescence from orange to green, compared to the control cells. This fact was indicative of depolarization of mitochondrial membrane potential. Interestingly, the disruption of $\Delta\psi_{mt}$ was associated with the appearance of Annexin-V-FITC fluorescence in the treated cells. In fact, the dissipation of $\Delta\psi_{mt}$ is characteristic of apoptosis and has commonly been observed with a variety of anticancer drugs irrespective of the cell type.

3.3.b DETERMINATION OF REACTIVE OXYGEN SPECIES (ROS) PRODUCTION

During apoptosis, mitochondria suffer specific damages that result in loss of their function. For example, release of cytochrome c can potentially arrest the electron transfer, leading to failure in maintaining the mitochondrial membrane potential and ATP synthesis. Moreover, as cytochrome c carries electrons from cytochrome c reductase (complex III) to cytochrome c oxidase (complex IV), by which oxygen molecules are reduced to water, a blockade at this step would increase the production of reactive oxygen species [75].

The primary ROS generated in this organelle is superoxide ($O_2^{-\cdot}$), which is then converted to hydrogen peroxide (H_2O_2) by spontaneous dismutation or by superoxide dismutase (SOD). ROS can act as inducers or secondary messengers of apoptosis.

The production of ROS was monitored through a flow cytometric analysis using hydroethidine (HE) and 2’,7’-dichorofluorescin-diacetate ($DCFH_2$-DA), as probes. HE permeated the cell membrane easily and, in the presence of superoxide anion, was directly oxidized to red fluorescent ethidium bromide, which was trapped in the nucleus by intercalation into DNA, leading to enhancement of red fluorescence. DCFH$_2$-DA was capable of crossing the plasma membrane and in the cytosol, cellular esterases hydrolyzed its acetyl moieties to produce 2’-7’-dichlorofluorescin. The deacetylated form of the probe was then susceptible to oxidation by peroxides, generating the green fluorescent product, 2’-7’dichlorofluorescein (DCF) [77]. In conclusion, the production of ROS led to the appearance of the oxidised probe fluorescence in both experiments.

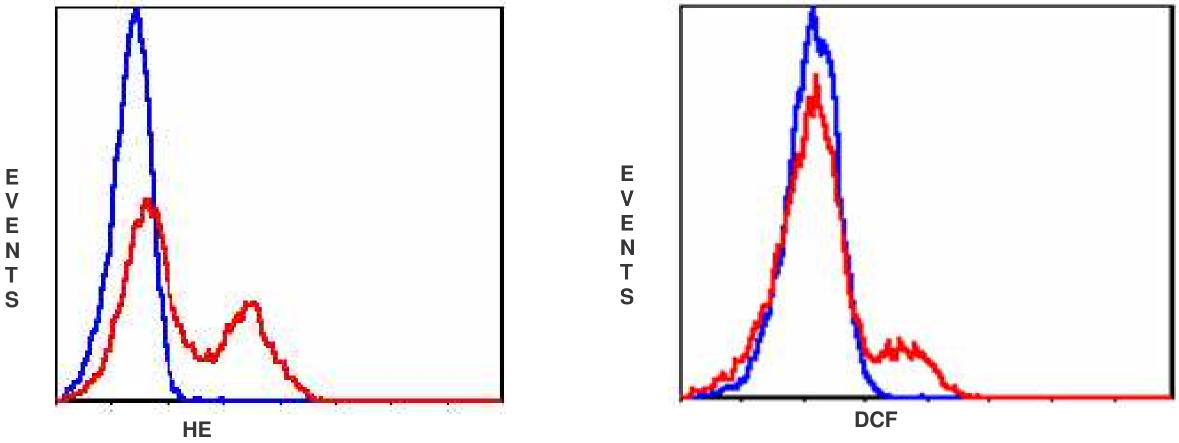

FIG 5*: Example of flow cytometric analysis after cellular staining with HE (right panel) or DCF (left panel). In both cases, control was presented in blue (no fluorescence) and treated cells in red (a percentage of cells demonstrated probe fluorescence).*

A possible ROS production was investigated after 24 hours from the incubation of jurkat cells with different concentration of **ISQ3**.

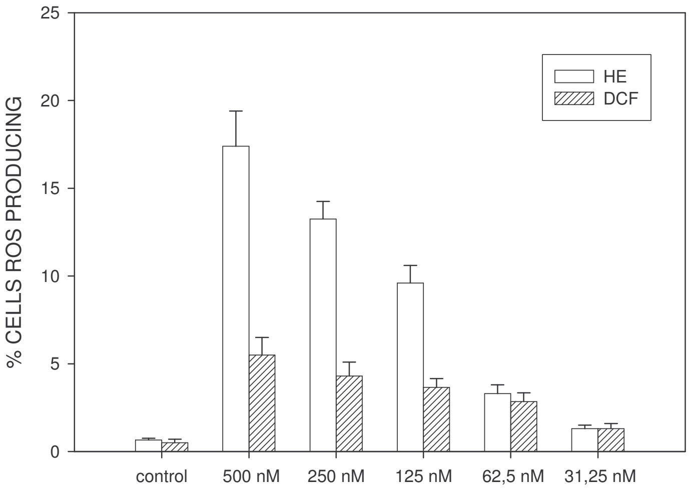

FIG 6*:Percentage of ROS producing jurkat after 24 hours from the treatment with various concentrations of* ***ISQ3****. Data were expressed as Mean ± SEM of three independent experiments.*

ISQ3 was able to induce reactive oxygen species in a concentration-dependent manner as a consequence of mitochondrial dysfunction: these last data were in accord with the ones of mitochondrial membrane potential collapse.

3.3.c DETERMINATION OF CARDIOLIPIN PEROXIDATION

Cardiolipin (CL) is a unique phospholipid with dimeric structure, carrying four unsaturated fatty acids and two negative charges. CL is exclusively found in the inner membrane of mitochondria. CL has particular properties, which include the organization into surface head group microdomains, asymmetry in bilayer membranes, and moreover, CL is essential as the boundary lipid for the normal functions of various mitochondrial proteins such as NADH: ubiquinone oxidoreductase, cytochrome c oxidase, F0F1 ATPase, adenine nucleotide transporter, and cytochrome c, as well as for the function of cytosolic proteins such as tBid. CL oxidation, as a consequence of mitochondrial ROS production, clearly enhances apoptotic mitochondrial dysfunction and, for example, facilitates the cytochrome c release in the cytosol [78].

We evaluated the damage produced by ROS in mitochondria by assessing the oxidation state of cardiolipin. This analysis was conducted through flow cytometry using 10-N-nonyl acridine orange (NAO), as a probe. NAO interacted stoichiometrically with non-oxidized CL. The increase of CL peroxidation led to a reduction of green fluorescence as NAO lost its affinity for oxidized CL [79].

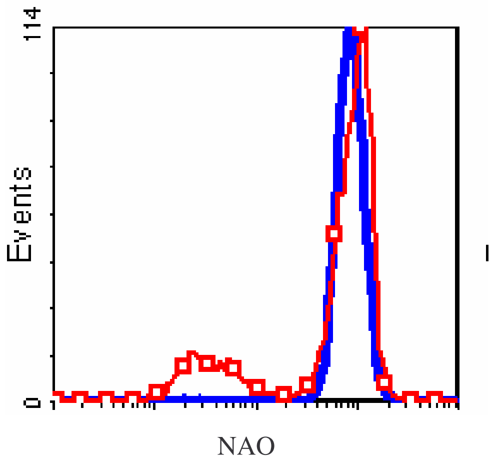

***FIG 7**: Example of flow cytometric analysis after cellular staining with NAO. Control was presented in blue (NAO fluorescence) and treated cells in red (a percentage of cells demonstrated no probe fluorescence).*

The degree of CL oxidation was monitored after 24 hours from the incubation with different concentrations of **ISQ3** and was represented in fig 8.

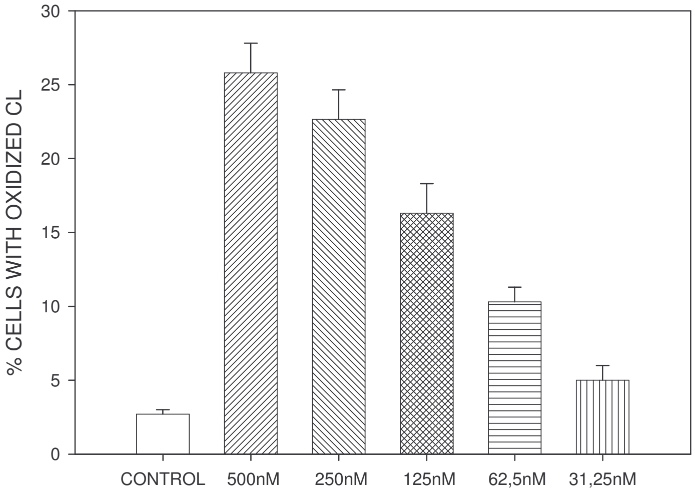

***FIG 8**: Percentage of jurkat with oxidized CL after 24 hours from the treatment with various concentrations of **ISQ3**. Data were expressed as Mean ± SEM of three independent experiments.*

Treatment with **ISQ3** caused an increase of the percentage of cells with oxidised CL; these data were well in agreement with all the previous mitochondrial investigations.

We demonstrated a mitochondrial dysfunction with three different tests and so that these organelles were deeply involved in **ISQ3** apoptosis induction in jurkat cells.

3.4 CASPASE ACTIVATION

Continuing our studies about cell death induced by **ISQ3**, we performed some flow cytometric experiments to find a possible involvement of caspase cascade.

Caspases constitute a family of cysteine proteases — peptidases that use a cysteine residue as the catalytic nucleophile — that share specificity for cleaving target proteins at sites next to aspartic acid residues. In addition to their participation in propagate apoptosis events, a subgroup of the caspase family is involved in inflammation, where they act as pro-cytokine activators [29].

The apoptotic caspases are classified into initiators or executioners, depending on their point of entry into the apoptotic cascade. The initiator caspases are the first to be activated in a particular death pathway and they initiate a cascade which ends by activating the executioner caspases. Unregulated caspase activity would be lethal for a cell, so to prevent this, the cell stores caspases as latent precursors — zymogens. These “procaspases” require an activating event, which consists in a proteolitic cleavage of the prodomain and dimerization [31].

Recognition of at least four amino acids NH_2-terminal to the cleavage site is a necessary requirement for efficient catalysis. The preferred tetrapeptide recognition motif differs significantly among caspases and explains the diversity of their biological functions. The strict specificity of caspases is consistent with the observation that apoptosis is not accompanied by indiscriminate protein digestion; rather, a select set of proteins is cleaved by executioner caspases in a coordinated manner, usually at a single site, resulting in a loss or change in function [29].

We investigated the activation of three key caspases: first of all, the one of caspase-3, an executioner, and then the one of caspase-8 and -9, which are initiators associated with extrinsic and intrinsic pathways, respectively.

The analysis was conducted through flow cytometry after the incubation of treated cells with FITC-conjugated and cell-permeable substrates of caspase-3 (FITC-DEVD-fmk), caspase-8 (FITC-IETD-fmk) and caspase-9 (FITC-LEDH-fmk) [30].

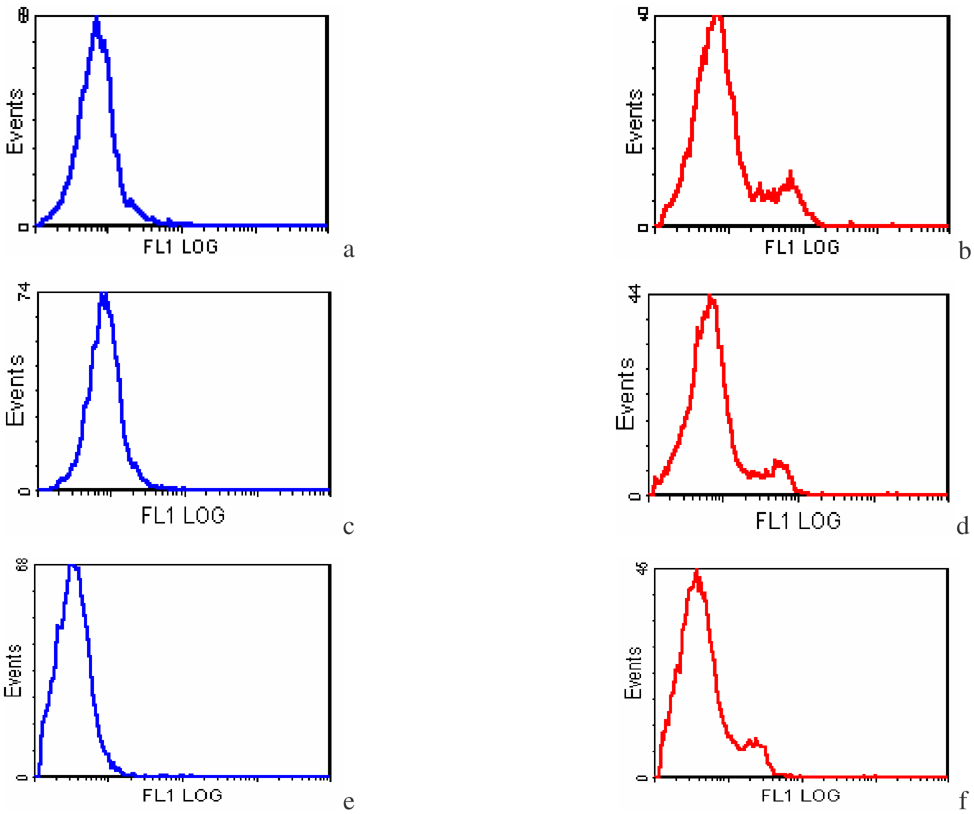

FIG 9: *Flow cytometric determination of caspase activation after 24 hours from the treatment of 500 nM* ***ISQ3***. *Blue distribution: control; Red distribution: jurkat treated with 500 nM* ***ISQ3***. *Panel a and b: activation of caspase-3; panel c and d: activation of caspase-8; panel e and f: activation of caspase-9.*

Fig 10 represented the summary of the results obtained for caspase activation.

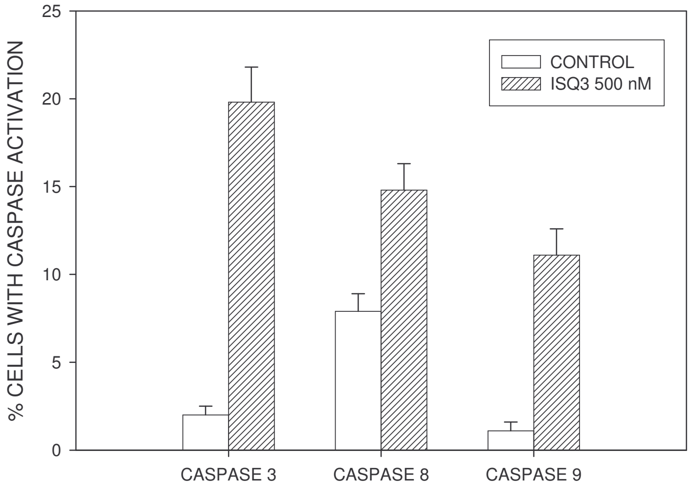

FIG 10*: Percentage of jurkat with caspase-3, -8 and -9 activation after 24 hours from the treatment of 500 nM* ***ISQ3****. Data were expressed as Mean ± SEM of three independent experiments.*

In this test, we observed a clear activation of caspases in jurkat treated with **ISQ3** and the participation of this cascade in cell death resulted another prove for apoptotic pathway. The activation of caspase-9 was well in agreement with all the data of mitochondrial dysfunction and confirmed the important role of mitochondria in provoking cell death. A certain activation of caspase-8 could indicate a contribution of extrinsic pathway.

3.5 CELL CYCLE

With the purpose to clarify the mechanism(s) of action of these compounds, the effects ISQ3 on cell cycle progression of Jurkat cells were studied after 24, 48 and 72 h of drug exposure. In fact, it is well known many antiproliferative drugs are able to induce remarkable changes in cell cycle of treated cells [10]. This analysis was performed through flow cytometry, after fixing cells in ethanol, treating with RNAse and staining them with PI. This test used the fact that DNA content was different in each phase of cell cycle. The obtained diagrams presented in the x- axis the DNA content and in the y-axis the number of cells [21]. A diagram of a control (fig 11) showed a first peak, which corresponded to the G1 phase, a second peak, which corresponded to the G2-M phase, and finally a part between those two peaks, which represented the S phase.

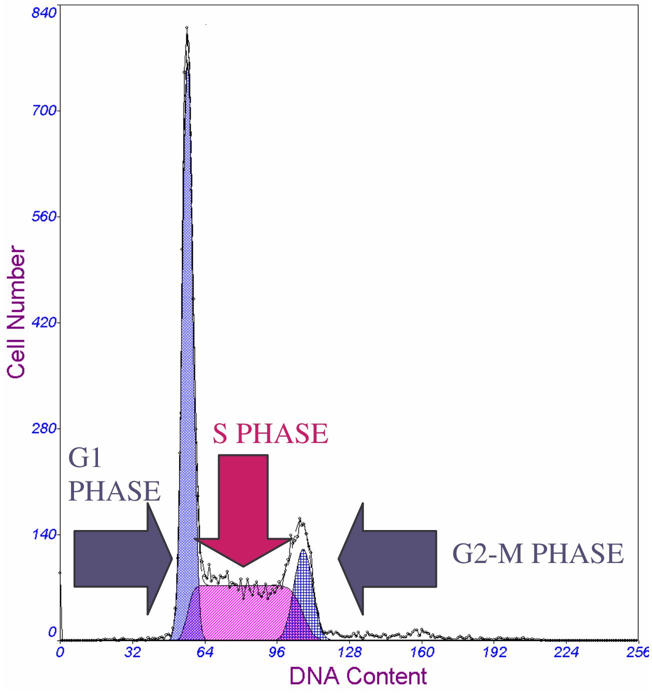

FIG 11: *Diagram of cell cycle of non treated jurkat.*

In fig 12, diagrams of cell cycle were represented after the treatment of 24, 48 and 72 hours of **ISQ3** at the concentration of 500 nM.

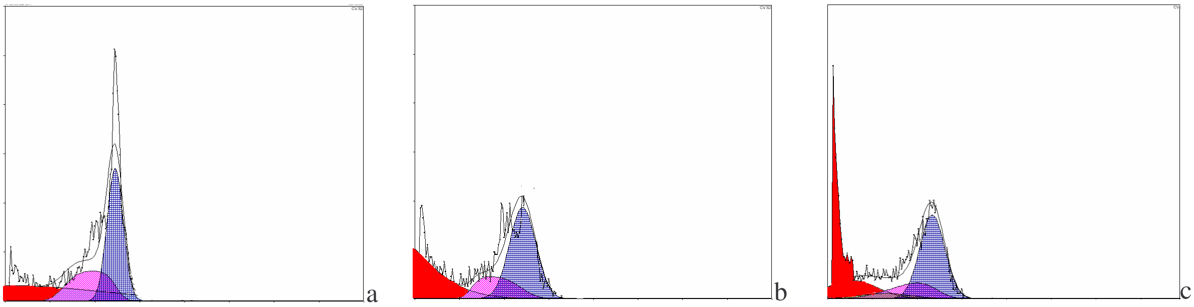

FIG 12: *Histograms of cell cycle of jurkat after 24 (panel a), 48 (panel b) and 72 hours (panel c) from the treatment of 500 nM* ***ISQ3****.*

Histograms in figure 12 showed **ISQ3** was able to induce a block of cell cycle in G2-M phase and, at the same time, the appearance of a hypodiploid cells (sub-G1 peak). The sub-G1 peak represented a distribution of cells with a low content in DNA: this characteristic is typical of apoptotic cells in which a nuclear DNA fragmentation occurs. The amount of these cells with low content in DNA increased with the duration of the treatment.

After this first screening, we decided to study changes at lower concentrations of **ISQ3** too.

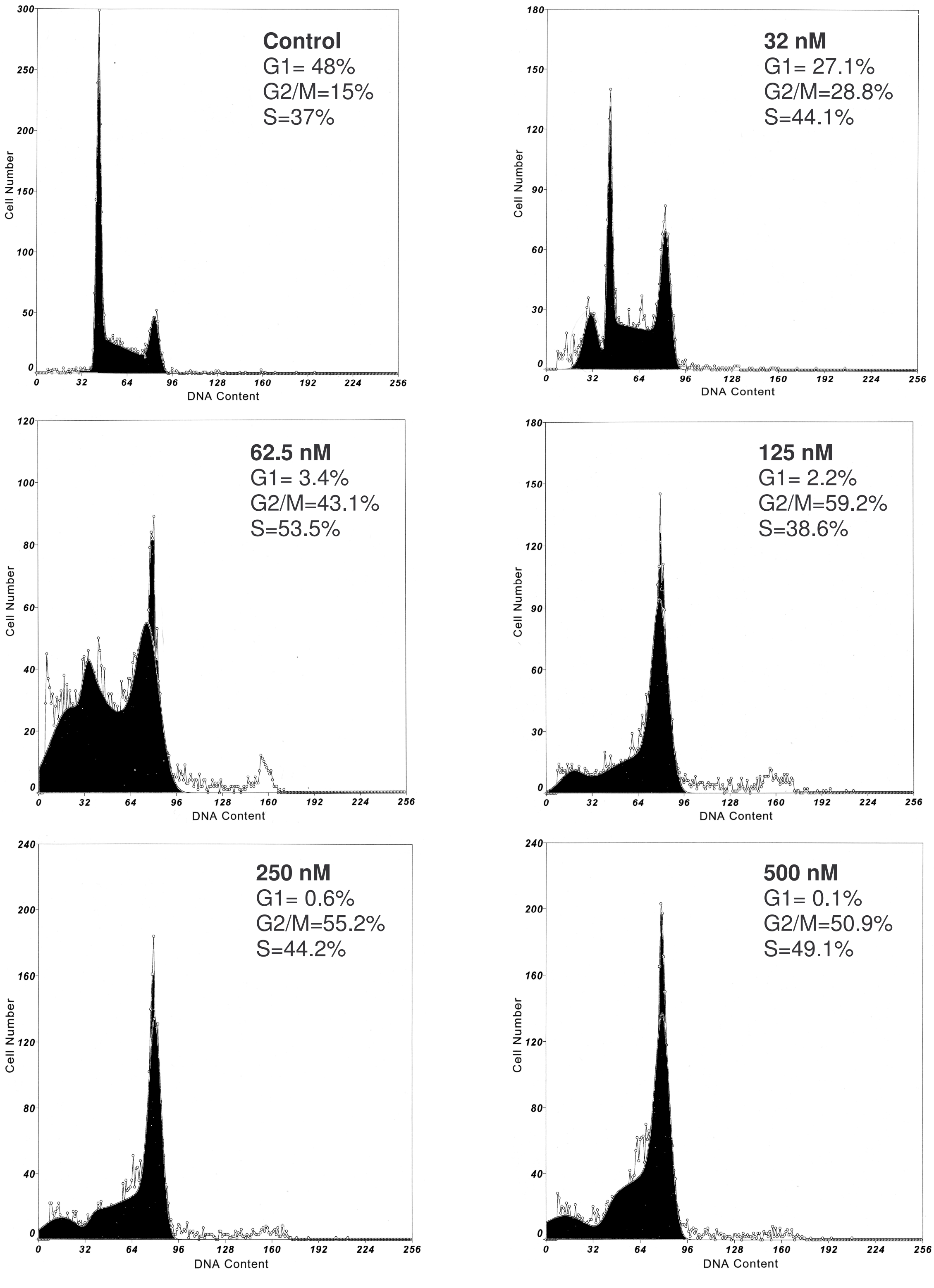

*FIG 13: Histograms of cell cycle of jurkat after 24 hours from the treatment of 0, 32, 62,5, 125, 250 and 500 nM **ISQ3**.*

The cell cycle histograms based on flow cytometric analysis of **ISQ3** at different concentrations, were illustrated in fig 13. It can be noted that treatment of Jurkat cells with **ISQ3** led to deep changes of the cell cycle profile. Untreated cells showed a classical pattern of proliferating cells proportionally distributed in G1 (48%), S (37%) and G2/M (15%)

phases. On the contrary, a clear and rapid G2/M arrest pattern was observed with a concomitant decrease of the G1 phase, even at the lowest concentration. It is also interesting to note the appearance of a hypodiploid peak (sub-G1), indicative of apoptosis.

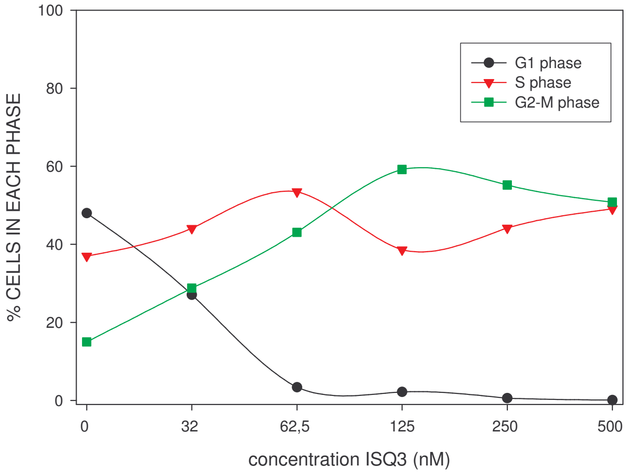

FIG 14*: Percentage of cells in each cell cycle phase after 24 hours from the treatment with different concentrations of* ***ISQ3****.*

The effects of **ISQ3** on cell cycle were summarized in fig 14, which showed the percentage of non-apoptotic cells in each phase of the cycle in function of **ISQ3** concentration.

3.6 MITOTIC INDEX

Since many anticancer drugs induced a block in G2-M phase, we decided to study if the accumulation of cells occurred during G2 phase or mitosis. The appearance of mitotic cells was recognized by optical microscopy, observing the amount of dispersed chromosomes in the cytoplasm and the disappearance of the nuclear membrane, which are typical of mitotic metaphase. After 24 hours from the incubation with 0,25, 0,5 and 1 µM of **ISQ3**, jurkat cells were treated with an ipotonic solution to eliminate plasmatic membrane and make metaphases more visible. Then, after fixation and coloration with 4% Giemsa, cells were counted distinguishing between integer nuclei and metaphasic nuclei.

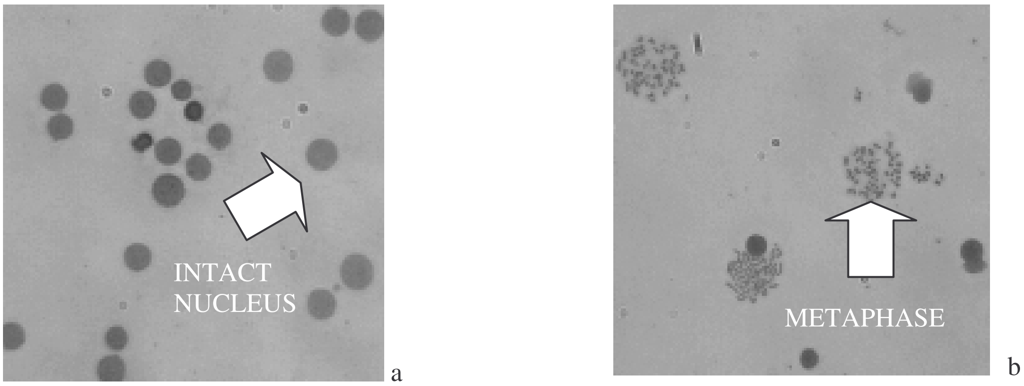

FIG 15*: Control jurkat (panel a) and treated jurkat with* ***ISQ3*** *(panel b). These images were taken by a contrast phase microscope (40X).*

In the picture corresponding to the treated cells, there was a significant increase of dispersed chromosomes. The same experiments were conducted in the presence of the same concentrations of the antimitotic colchicine, as reference drug.

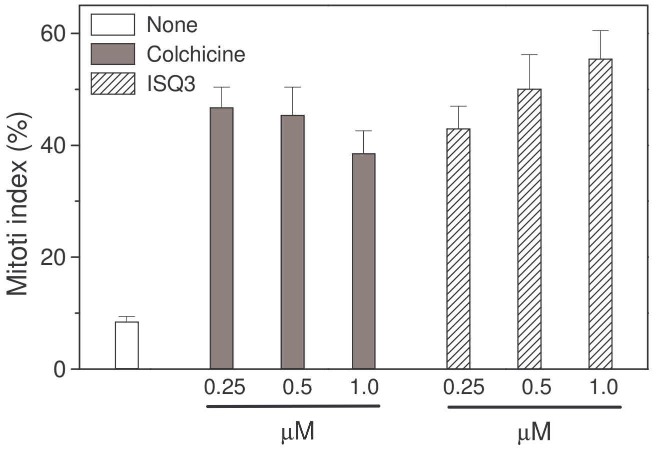

FIG 16*:Mitotic index in jurkat cells in the absence or presence of 0,25, 0,5 and 1 μM colchicine or* ***ISQ3****.*

Mitotic index of **ISQ3** treated jurkat increased in a concentration-dependent manner and it was significantly higher than control and comparable to that of the reference compound. Moreover, the values of mitotic index were well in agreement with the cellular percentage of G2-M phase in cell cycle analysis. Thus, the G2-M block was represented by an accumulation of cells in mitotic phase.

3.7 EVALUATION OF MICROTUBULE NETWORK AS A POSSIBLE TARGET

The block of cell cycle in mitotic phase is a typical characteristic of microtubule-targeting drugs [10]. Thus, we hypothesized **ISQ3** was able to induce a possible interference with microtubule network.

The microtubule or tubulin-based cytoskeleton arises from the polymerization of α- and β-tubulin monomers in a GTP-dependent manner. Although appearing as a definite structure, each microtubule fibre exists in the state of dynamic equilibrium, which determines its growth and degradation by the reversible non-covalent association and dissociation of α-β-tubulin heterodimers at its two ends. Generally, the tubulin-based cytoskeleton performs two distinct functions in the cell: during interphase, it promotes the transport of vesicles between individual cell compartments and it is implicated in cell locomotion, then, at the onset of mitosis, it forms the mitotic spindle apparatus controlling over accurate cell division [17].

Chemical compounds targeting microtubules exert their inhibitory effects on cell proliferation primarily by blocking mitosis, which requires an fine control of microtubule dynamics [16].

3.7.a IMMUNOFLUORESCENCE DETENTION OF MICROTUBULE PERTURBATION

To evaluate tubulin as probable **ISQ3** molecular target, treated cells were checked by immunofluorescence microscopy. For these experiments, a non-small cell lung carcinoma (A-549) cell line was used. After 18 hours from the treatment with different concentrations of **ISQ3**, A-549 were incubated with an anti-β-tubulin antibody and then with a TRITC-conjugated secondary antibody. Pictures were examined by confocal microscopy.

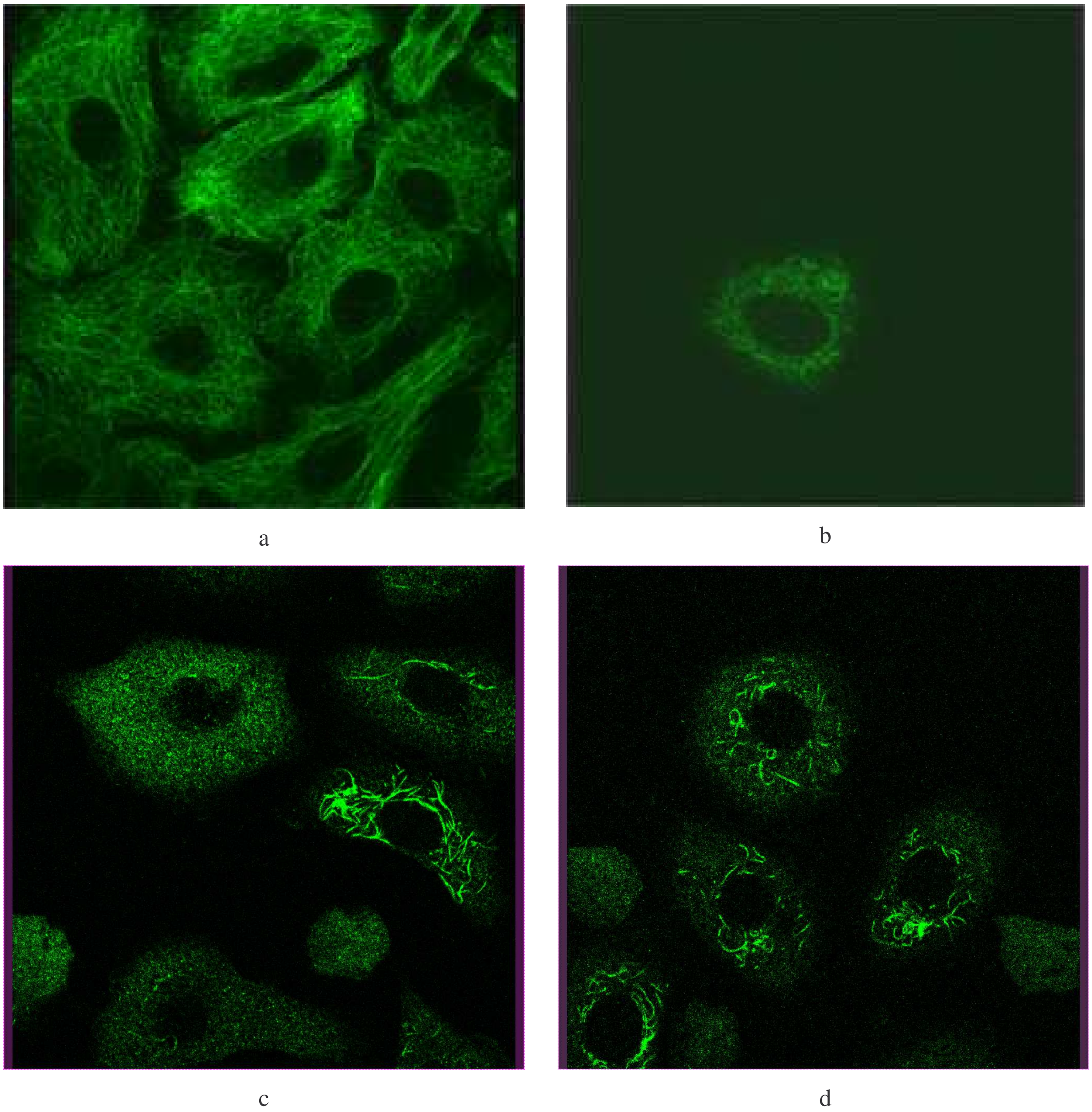

FIG 17: *Immunofluorescence images of A-549 cells treated with anti-β-tubulin antibody and with a secondary antibody TRITC-conjugated and then observed by confocal microscopy. Cells were exposed to the concentration of 5 μM (panel d) and 2.5 μM (panel c) of compound* ***ISQ3*** *for 18 h. Control was represented in panel a. As reference compound, 1 μM vinblastine (panel b) was used.*

As shown in fig. 17 (panel a), the microtubule network exhibited normal organization and arrangement in control cells. On the contrary, compound **ISQ3** completely disrupted the tubulin network. Cells showed an evident characteristic "rounded up" morphology caused by disaggregation of microtubule in both interphase and mitotic phases after 18 h of treatment. These effects resembled those of vinblastine, chosen as reference compound (panel b).

3.7.b TUBULIN POLYMERIZATION

As the immunofluorescence studies suggested that **ISQ3** impaired the formation or the stability of microtubules in the cells, we examined the effects of this compound on the polymerization of tubulin protein isolated from porcine brain.

In fig 18, the scheme of *in vitro* tubulin polymerization was illustrated. In this representation, the three typical phases of this process can be observed: nucleation, elongation and finally the steady state. When tubulin polymerizes, it initially forms proto-filaments, microtubules consist of 13 protofilaments and are 25 nm in diameter [17]. Tubulin can polymerize from both ends *in vitro*, however, the rate of polymerization is not equal: the rapidly polymerizing end is called plus-end while the slowly polymerizing end, the minus end. *In vivo* the plus end of a microtubule is distal to the microtubule organizing center.

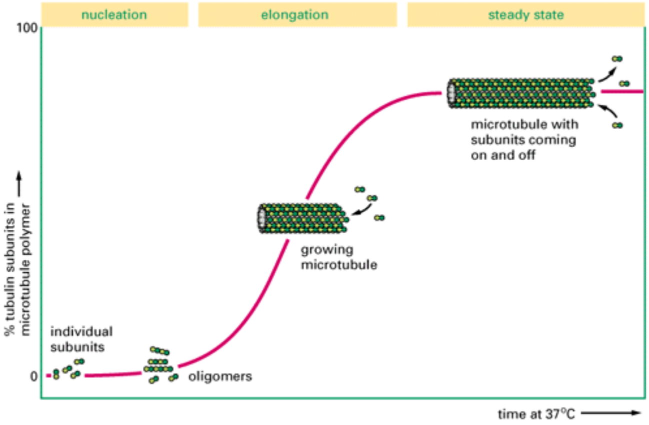
nucleation
elongation
steady state
100
0
% tubulin subunits in microtubule polymer
individual subunits
oligomers
growing microtubule
microtubule with subunits coming on and off
time at 37°C

FIG 18: *Scheme of in vitro tubulin polymerization.*

The assay utilized a fluorescent compound, DAPI (4’-6-Diamidino-2-phenylindole), which bound to tubulin and microtubules. Polymerization was followed by fluorescent enhancement due to incorporation of the fluorescent reporter into microtubules as polymerization occurred [80]. Compounds that interact with tubulin often alter one or more characteristic phases of polymerization.

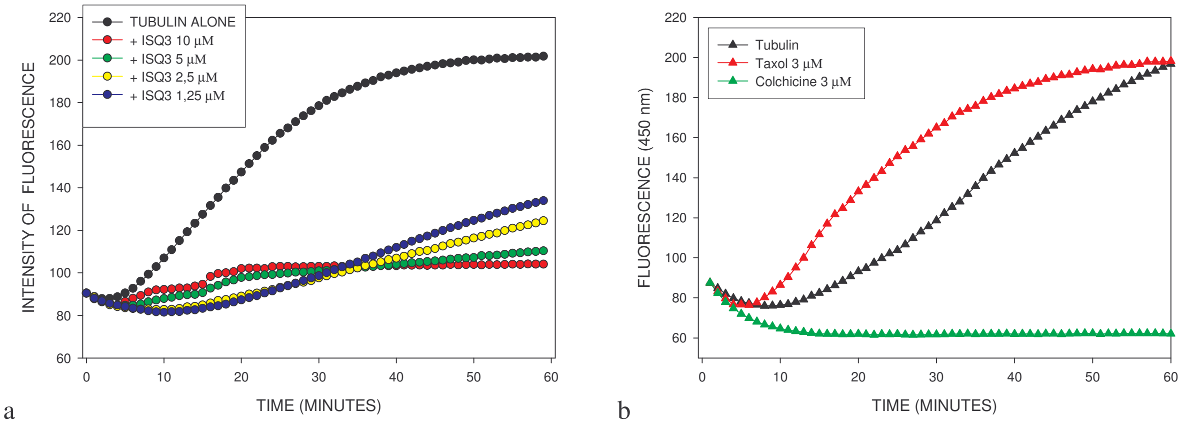

***FIG 19**: Effect of compound **ISQ3** (panel a) and of taxol and colchicine (panel b) on microtubule assembly. Purified tubulin was incubated in the absence or in the presence of the compound at the indicated concentrations. Fluorescence measurement (λ_{ex} 355 nm; λ_{em} 450 nm) was determined every 1 min for 60 min at 37 °C. Polymerization was initiated by the addition of tubulin.*

Fig 19 showed that in the control sample (tubulin alone without addition of any test agent) the fluorescence increased with time, after the period of nucleation. On the contrary, compound **ISQ3** clearly induced a concentration-dependent inhibition of tubulin polymerization. A complete inhibition of microtubule assembly was observed for **ISQ3** at the concentration of 5 µM. As reference drug, colchicine completely inhibited the tubulin polymerization at the concentration of 3 µM while at the same concentration taxol significantly promoted tubulin polymerization (panel b).

ISQ3 was able to interfere with microtubule network as demonstrated by the immunofluorescence and mitotic index experiments and moreover it was able to inhibit *in vitro* tubulin polymerization. **ISQ3** was a tubulin-interfering agent.

3.8 INTERACTION WITH DNA

As polycyclic nitrogen heterocylcles with planar structure can be good pharmacophores for classes of anticancer drugs since they demonstrate a good affinity for DNA [81], we analyzed an possible interaction of **ISQ3** with this macromolecule.

DNA represents one of the most important targets for several chemotherapeutic drugs [10, 64], as described in introduction section. The association of an external molecule with DNA leads to significant modifications in its structure and can provoke cell death as a consequence of suppression of its replication and gene transcription [82].

Interactions between a compound and DNA can be either covalent or non-covalent. A covalent bond generally induces DNA base modifications. Unrepaired DNA base damage can lead to potentially mutagenic and lethal consequences, such as by mismatch or production of apurinic/apirymidinic sites. In addition, covalent bulky adducts are able to cause DNA backbone distortion, which in turn can affect both transcription and replication, such as by disrupting protein complex recruitment [83].

Interactions between DNA and non-covalent agents occur through Van der Waals forces, hydrogen bonding, hydrophobic, and/or charge transfer forces and as such they are reversible. In principle, there are three modes for reversible binding of molecules with double-helical DNA: external binding, as a consequence of electrostatic attractions with the anionic sugar-phosphate backbone of DNA; groove-binding interactions, which involve direct interactions of the bound molecule with the edges of base-pairs in minor or major grooves; intercalation mode [82].

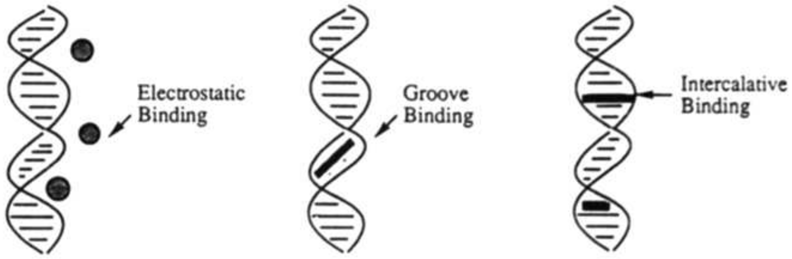

***FIG 20**: Binding modes of small molecules with DNA*

The binding pocket of the DNA groove consists of two regions, “the walls”, which are formed by the deoxyribose-phosphate backbone of the DNA and the “bottom”, formed by the edges of nucleic bases that face into the groove. Groove binders usually contain several small aromatic ring systems linked with torsional freedom to allow a twist complementary to that of the DNA groove and so a perfect fitting into the helical groove with displacement of water. Groove binders can block DNA protein interactions; e.g. groove binding agents, such as diamidine-2-phenylindole (DAPI), can act as catalytic topoisomerase inhibitors by blocking the docking site on DNA for topoisomerase II [83].

Intercalators are planar aromatic molecules that insert between bases; important driving forces for this binding mode are dipole-dipole interactions and π-stacking of the guest molecule with the aromatic nucleic bases. They can cause DNA backbone distortion and frameshift mutations during DNA replication. By their winding/unwinding effects on supercoiled DNA, intercalators can change the normal torsional strain in cellular DNA. Some can act as topoisomerases poisons, with resultant strand breaks, and this is probably a major cause for their genotoxicity in mammalian cells [84].

3.8.a SPECTROSCOPIC AND SPECTROFLUORIMETRIC TITRATIONS

In a complex with DNA, the guest molecule is positioned in a different environment from that of the free molecule in solution. Thus, the interaction of compounds with DNA can be studied with spectroscopic methods as their absorption and emission properties change significantly on complex formation [85].

The binding of **ISQ3** to DNA in buffered aqueous solution was monitored by absorption and fluorescence spectroscopy.

The absorption of the compound was recorded in the absence and in the presence crescent aliquots of salmon testes DNA (st-DNA). Absorption spectrum of **ISQ3** exhibited absorption bands in the 300-400 nm region.

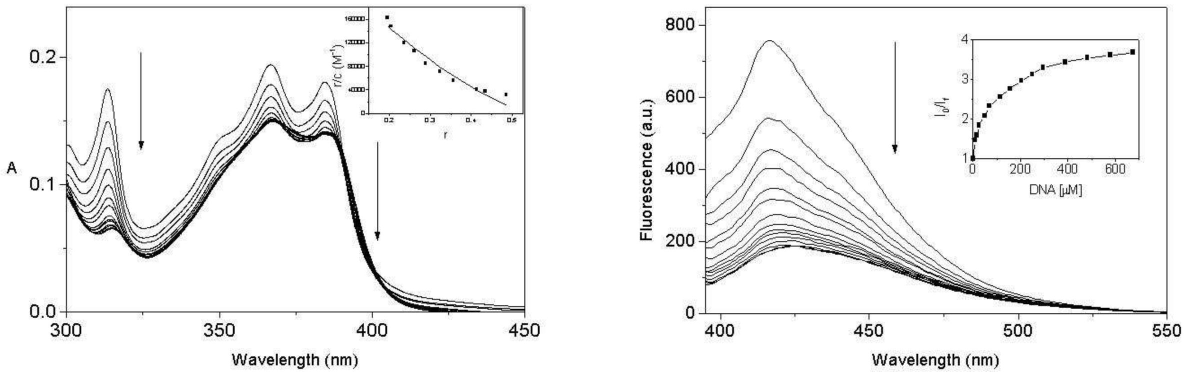

FIG 21*: Spectrophotometric titration (left panel) of st-DNA to* ***ISQ3*** *in phosphate buffer. In the inset, was represented the Scatchard plot of the spectrophotometric titration. The line represented the best fit of the experimental data to the McGhee and von Hippel equation. Fluorometric titration (right panel) of st-DNA to* ***ISQ3*** *in phosphate buffer. In the inset was represented the Stern Vomer plot.*

The absorption maxima of compound **ISQ3** exhibited a weak batochromic shift of about 2 nm in the presence of nucleic acid relative to the free drug (fig 21, left panel), along with a hypochromism of the signal intensity suggesting the association of the drug with DNA. Most notably, isosbestic points appeared in the titration, which indicated that one type of drug-DNA complex was formed almost exclusively. The spectrophotometric titration data for **ISQ3** bound to the DNA were used to estimate the binding constant as well as binding site size according to McGhee and von Hippel [86]. The corresponding binding isotherm, represented as Scatchard plot [87], was given in the inset of fig 21 (left panel). The binding constants K revealed a high binding affinity of **ISQ3** ($K = 2.7 \times 10^5$ M^{-1}) and the binding-site size n is 3.6 (in bases), which was in agreement with an intercalative binding mode, according to the neighbor-exclusion model.

Spectrofluorometric titrations of st-DNA to compound **ISQ3** were also performed (fig 21, right panel). The fluorescence spectrum of **ISQ3** exhibited a broad emission peak in the 400-500 nm range. The emission intensity of the free drug was strongly quenched upon addition of st-DNA without any shift of the emission maximum.

A Stern-Volmer plot derived from the fluorimetric titration of st-DNA exhibited linear behavior of the titration curve up to concentrations 40 μM (fig 21, right panel). From these data, quenching efficiency was estimated by the Stern-Volmer constant K_{SV} (**ISQ3**: $K_{SV} = 3{,}17 \times 10^{5}\ M^{-1}$) [88].

3.8.b LINEAR DICHROISM

This technique permits to obtain interesting information about the nature of the binding between DNA and a compound. We used flow linear dichroism, which allowed the alignment of macromolecule along a flow field, generated by a rotating couette. Molecular alignment ensures that the electronic transitions that would normally interact with the incident light are aligned and hence can coherently interact with the polarised light [82].

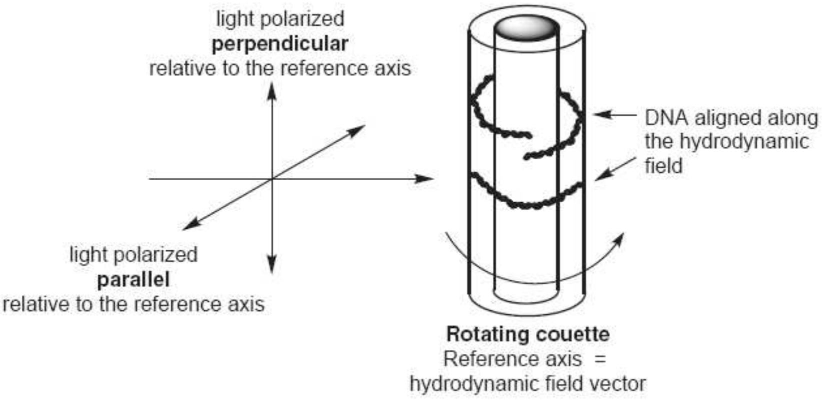
light polarized
perpendicular
relative to the reference axis
DNA aligned along the hydrodynamic field
light polarized
parallel
relative to the reference axis
Rotating couette
Reference axis = hydrodynamic field vector

***FIG 22**: Schematic illustration of the orientation of a cylindrical Couette flow cell relative to the linearly polarized light.*

In an hydrodynamic field, most of the DNA molecule are partially arranged along flow lines, and as the transition moment of nucleic bases is perpendicular to the reference axis (hydrodynamic field vector), the DNA bases afford a clear negative LD signal. In fact, if the angle α between the reference axis and the light-absorbing transition dipole is major to 55°, a negative LD signal is observed, while with a $\alpha < 55°$, a positive signal appears in the spectrum. Small molecules are not able to align along the flow lines of the field, but the existence of LD in the region where they absorb is indicative of an interaction with DNA and of a consequent orientation. As its transition moment is coplanar to that of DNA bases, a intercalator gives a clear negative LD signal (α ≈ 90°). A groove binder demonstrates an angle α ≈ 45° to the helix axis and so gives a positive signal, which is also relatively weaker to that of an intercalator [89].

LD spectra of solutions of 2,27 mM st-DNA in the presence of incrementing concentrations of **ISQ3** were recorded.

Fig 23 showed absorbance, LD and reduced LD (LDr) spectra for **ISQ3** at different [Drug]/[DNA] ratios.

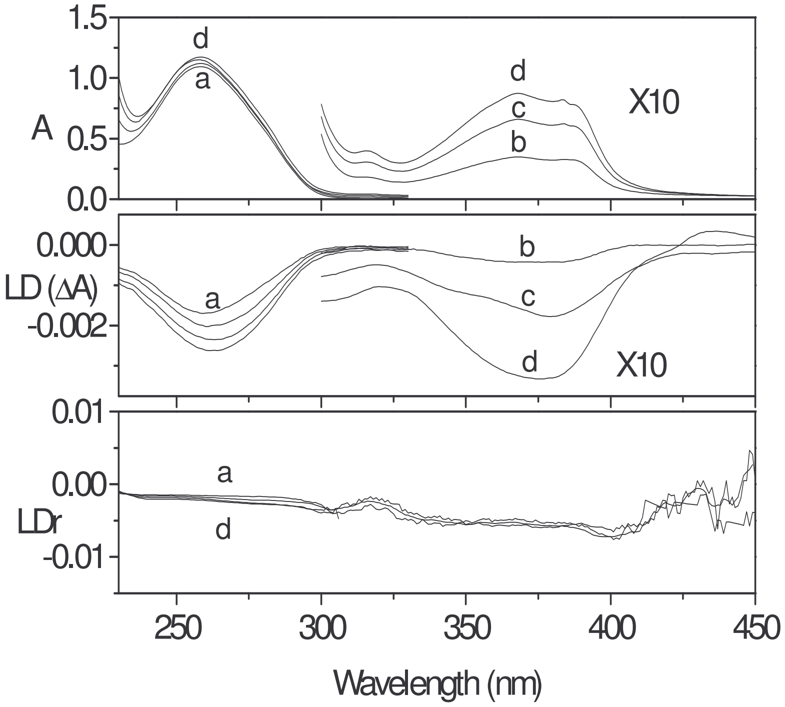

***FIG 23**: Absorbance A (upper panel), linear dichroism LD (medium panel), and reduced linear dichroism LD_r spectra (lower panel) of mixtures of st-DNA and **ISQ3** at different [drug]/[DNA] ratios (a = 0,00, b = 0,02, c = 0,06, d = 0,08,) in phoshate buffer pH = 7,2.*

Examination of the figures revealed that the LD spectra of **ISQ3** complexed with DNA were negative in the 230-300 nm region where the DNA absorbed. A significant increase of the values of LD of the DNA band at 260 nm for these drug–DNA complexes was observed, indicating that the DNA became better oriented due to a stiffening of the helix upon binding of the drug. The negative LD signals in the long-wavelength absorption (300–550 nm) of **ISQ3** revealed that it was oriented perpendicularly to the flow field. This orientation was usually caused by an intercalation into the DNA helix. This assumption was further supported by the observation that the intensity of the DNA signal increased on addition of the drug.

The reduced LD spectrum (LD$_r$) provided additional information on the average orientation of the transition moment of the dye relative to those of the DNA bases and allowed to distinguish between homogeneous and heterogeneous binding. A nearly constant value of LD$_r$ over the range 310–400 nm was observed (fig 23) and it unambiguously proved an almost exclusive intercalation of **ISQ3** into the DNA.

3.8.c CIRCULAR DICHROISM

Circular dichroism was used to further study DNA affinity of **ISQ3**. In fact, although circular dichroism is not observed for an achiral molecule, if it is placed in a chiral environment, it can give an inducted circular dichroic (ICD) signal, derived from non-degenerative coupling between the transitions of the compound and the DNA bases. This technique can provide information about the position of a compound in its complex with DNA. An intercalator usually has a weak and negative ICD signal, when its transitions are polarised along the long axis of the intecalation pocket, or positive ICD, for transitions in the intercalator plane that are perpendicular to the intercalator-pocket long axis. The induced CD of groove binders has generally a stronger positive signal [82].

Circular dichroism (CD) spectra of st-DNA in the presence of increasing concentration of **ISQ3** were recorded.

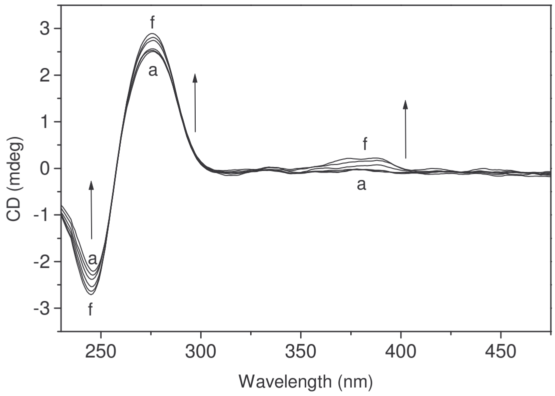

FIG 24: *Circular dichroism spectra of* ***ISQ3*** *complexed to st-DNA, at different [Dye]/[DNA] ratios from a to f (a=0.00, b= 0.02, c=0.04, d=0.08, e=0.2, f=0.4) in phosphate buffer, pH = 7,2, T = 25 °C*

The st-DNA, which was a B-DNA, showed a negative band at 240 nm and a positive band at 275 nm in its CD spectrum. The CD spectra of DNA in the presence of **ISQ3** revealed a perturbation of the DNA signal since the positive CD band of the DNA at 275 nm increased upon successive addition of the compound. Positive induced CD (ICD) signals were also observed in the chromophore absorption region of **ISQ3** (300–400 nm), indicating an orientation of the transition dipole of the molecule perpendicular to the long axis of the binding pocket.

Altogether these results were consistent to a intercalative mode binding.

3.9 TOPOISOMERASE INTERACTION

As many intercalators demonstrated inhibition activity towards topoisomerases, we decided to analyze a possible interaction between **ISQ3** and these enzymes.

Topoisomerases are essential enzymes that modify DNA topology, a process required during a lot of nuclear events (replication, transcription, chromatin remodeling, recombination and repair). As described in introduction section, topoisomerase represent a suitable target for anticancer drugs, which can interfere with the activity of topo I or topo II but also with both of them. Human topoisomerase I is a monomeric protein of 765 amino acids that binds to double-stranded DNA in a “clamp”-like manner [13].

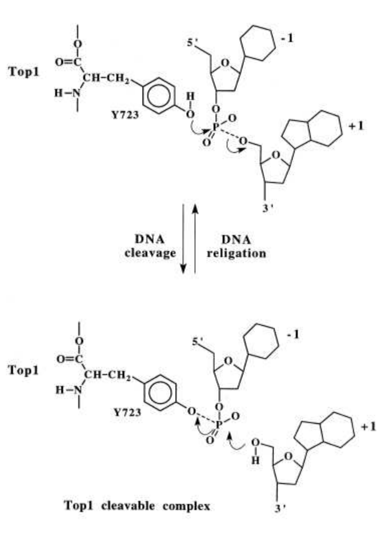

The reaction involves nucleophilic attack of Tyr723 on a phosphodiester bond in the DNA, resulting in temporary breakage of one DNA strand and covalent attachment of the active site tyrosine to the 3-phosphate at the nick. Relaxation likely takes place by a rotational mechanism. Religation occurs with the 5-hydroxyl at the nick acting as the nucleophile to religate the DNA strand and release the enzyme [90].

FIG 25: *Human topoisomerase I-mediated DNA cleavage and religation.*

Type II topoisomerases cleave both strands of DNA during catalysis. In a reaction coupled to ATP binding and hydrolysis, these proteins cleave one DNA duplex, transport a second duplex through the break, and then religate the cleaved duplex.

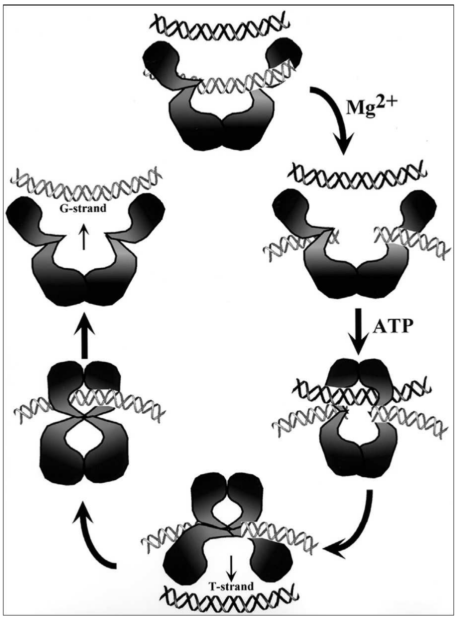

During cleavage, a pair of tyrosines attacks opposite strands of the duplex (G) and becomes covalently attached to the DNA through 5'-phosphotyrosine linkages. ATP binding causes the enzyme to form a closed clamp. The closed clamp may also capture another strand (T strand) that will pass through the break made in the G strand. After passing through the break, the T strand exits the enzyme. ATP hydrolysis allows the clamp to re-open, and allows release of the G strand.

FIG 26: *Catalytic cycle of topoisomerase II.*

Among the drugs that interfere with these enzymes, we can find two different mechanism of actions: there are the *catalytic inhibitors or suppressors*, which avoid the binding of DNA in catalytic site of topoisomerases, and the *poisons*, which bind to the cleavable complex and inhibit the religation of DNA after its nick [90].

3.10 TOPOISOMERASE I ASSAY

3.10.a PLASMID DNA RELAXATION BY HUMAN TOPOISOMERASE I

A relaxation assay was performed, conducing topoisomerase I reaction in the presence of supercoiled plasmidic DNA and **ISQ3** at various concentrations. Thanks to their different hydrodynamic properties, the topoisomers were resolved through a 0,8 % agarose electrophoretic run [91].

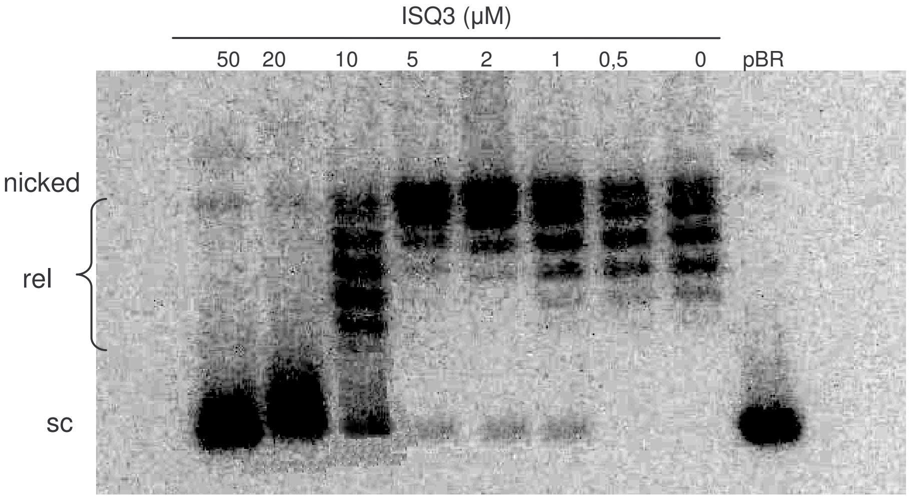

FIG 27: *Effect of* ***ISQ3*** *on topoI-mediated supercoiled DNA relaxation. DNA samples were resolved through agarose electrophoresis and then stained with ethidium bromide.*

ISQ3 was able to interfere with topoisomerase I: in fact, the gel in fig 27 showed that at lowest concentrations the intensity of the slowest migrating band increased significantly while at higher concentrations the relaxation of DNA was completely inhibited. Together with a band corresponding to supercoiled DNA, at 10 μM, changes in the distribution of the relaxed topoisomers were evident, probably as a result of DNA intercalation by **ISQ3** and of a consequent change in the linking number of the topoisomers.

3.10.b TOPOISOMERASE I CLEAVABLE-COMPLEX ASSAY

Ethidium bromide was added to the running buffer and gel for separation of nicked open circles from closed circles. In this case, the relaxed DNA migrated faster than the supercoiled plasmid due to ethidium-induced DNA unwinding effects [92]. This second assay was performed to verify a potential presence of the nicked open circular form, indicating the formation of cleavable complex.

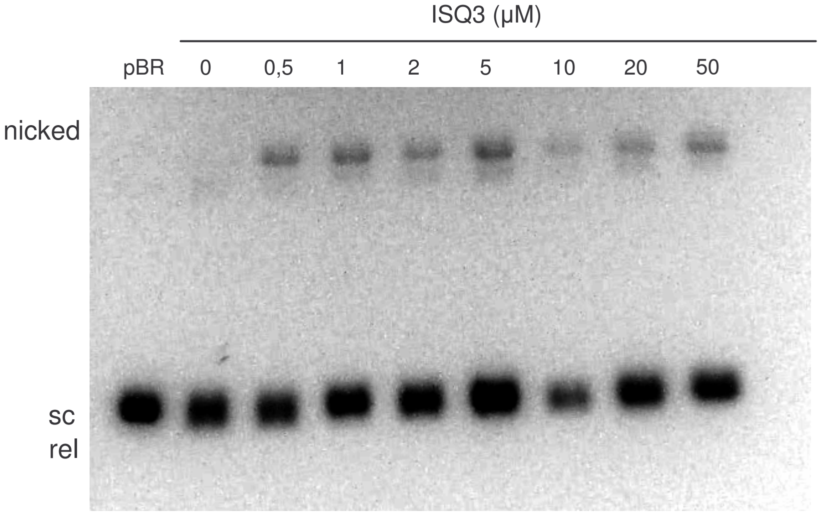

FIG 28: *Topoisomerase I cleavable complex assay in the presence of crescent concentrations of* ***ISQ3.***

ISQ3 stimulated the formation of the nicked open circular form and so the one of the cleavable complex.

ISQ3 was able to inhibit catalytic activity of topoI, as demonstrated in fig 27, but also to stimulate the cleavable complex.

3.11 TOPOISOMERASE II ASSAY

3.11.a PLASMID DNA RELAXATION BY HUMAN TOPOISOMERASE II

The effect of **ISQ3** on DNA relaxation activity of human topoisomerase II was evaluated mixing 2 units of enzyme, 125 ng of supercoiled pBR322 and different concentrations of **ISQ3** at 37°C for 30 min [91].

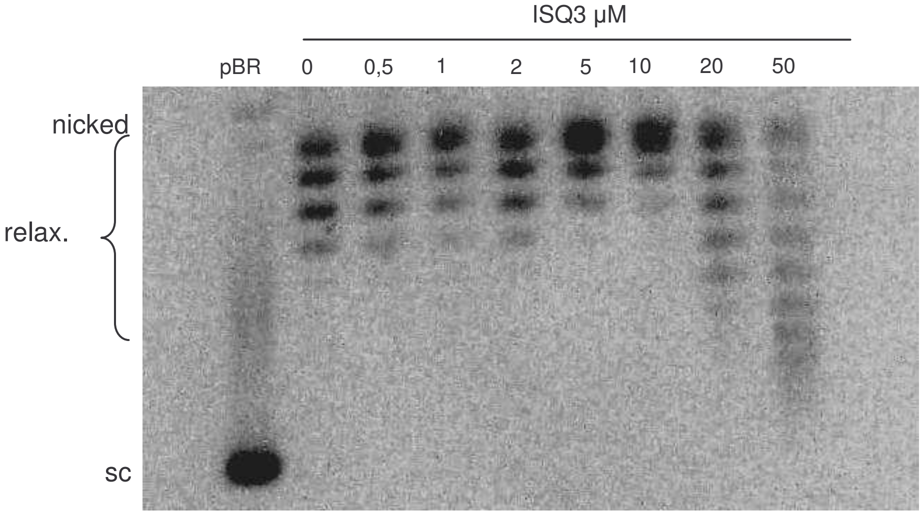

FIG 29: *Effect of* ***ISQ3*** *on topoII-mediated supercoiled DNA relaxation.*

ISQ3 was not able to inhibit relaxation activity of topoisomerase II, as demonstrated in fig 29. At higher concentrations, the modifications of the hydrodynamic properties of the topoisomers were probably due to the intercalative power of the compound.

3.11.b TOPOISOMERASE II CLEAVABLE-COMPLEX ASSAY

In parallel to the relaxation assay, the topoisomerase II cleavable complex test was conducted to verify a possible action of **ISQ3** as an enzyme poison. For this test, 6 units of human topoisomerase II, 100 ng of supercoiled pBR322 and different concentrations of **ISQ3** were incubated at 37° C for 30 min. The electrophoretic run was performed using an ethidium bromide containing gel.

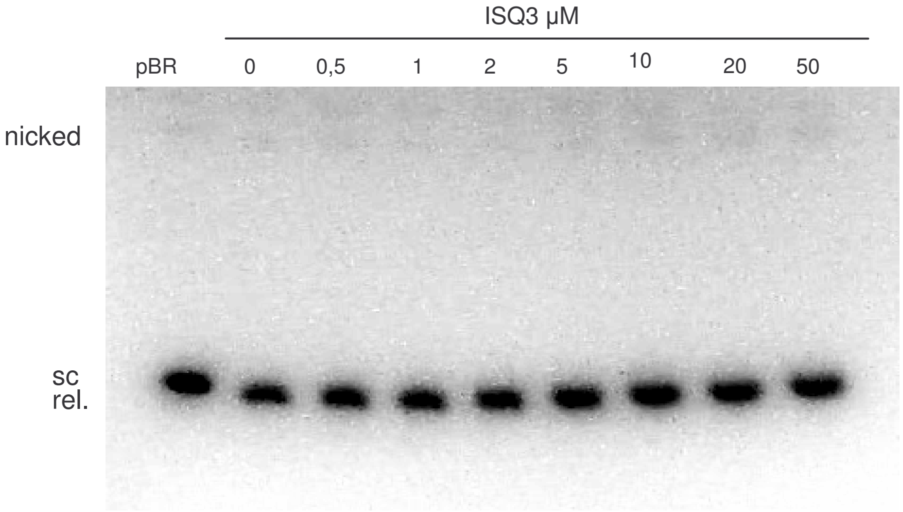

FIG 30: *Topoisomerase II cleavable complex assay in the presence of crescent concentrations of* ***ISQ3****.*

As it can be observed in the fig 30, **ISQ3** was not able to stimulate DNA cleavage mediated by topoisomerase II. These data were in agreement with those of relaxation assay and suggested that topoisomerase II was not a cellular target for **ISQ3** cytotoxicity.

3.12 EFFECT OF **ISQ3** IN ANTICANCER DRUG RESISTANT CELL LINES

Resistance is one of the most important problem of anticancer therapy together with severe adverse effects. The fact that **ISQ3** demonstrated two targets at cellular level can represent an huge advantage to avoid resistance onset. In fact, the possibility of the resistance for modifications in drug target is reduced. We performed a series of cytotoxicity experiments in some human tumor cell lines resistant to common anticancer drugs. Then, we calculated the resistance index (RI), which was the rate between the IC_{50} in resistant line and the IC_{50} in the wild type line. We used some cell lines that developed multidrug resistance through the over-expression of high molecular weight glycoproteins on their cell surface and the consequent increase of drug efflux rate. The cellular viability experiments were conducted in CEM^{Vin100}, a multidrug-resistant line selected against vinblastine and expressing the 170-kD-P-glycoprotein [93], $LoVo^{doxo}$, doxorubicin resistant subclone of LoVo cells, and $MCF\text{-}7^{MDR}$, human mammary carcinoma exhibiting multi-drug resistance for Pgp expression [94].

	CEM^{WT} (nM)	CEM^{Vin100} (nM)	RI
ISQ3	20,1±2,0	19,8±2,1	0,985

	$LoVo^{WT}$ (nM)	$LoVo^{Doxo}$ (nM)	RI
ISQ3	128,4±15,0	133,9± 12,8	1,043

	$MCF\text{-}7^{WT}$ (nM)	$MCF\text{-}7^{MDR}$ (nM)	RI
ISQ3	175,0±23,0	154,2± 21,8	0,881

***TAB 3**: IC_{50} (µM) in some human wild type and resistant tumor cell lines after 72 h of exposure as determined by MTT assay and resistant index. Data are expressed as means ± SEM for at least three independent experiments. n.d. not determined.*

The obtained RI resulted more or less near one and thus **ISQ3** was able to bypass drug resistance in these cell lines.

3.13 CONCLUSIONS

The present results showed that the most active compound among a series of new isoindolo[2,1-*a*]quinoxalin-6-one derivatives possessed high cytotoxic activity against a very wide range of human tumor cell lines with IC_{50} values that reached nanomolar concentrations. We demonstrated that **ISQ3** provoked cellular death through apoptosis. The important role of mitochondria was assed through a series of cytofluorimetric tests. The induction of apoptosis was associated with i) dissipation of the mitochondrial transmembrane potential ii) production of reactive oxygen species and cardiolipin oxidation and iii) activation of caspase-3 and –9.

In cell cycle study, cells treated with **ISQ3** accumulated in G2-M phase with concomitant loss of the G1 phase.

The spectrophotometric results indicated that **ISQ3** bound to DNA by intercalation with high affinity and consequently the macromolecule may be considered as a potential target for this class of compounds.

Starting from the characteristics of the compound, we investigated the cellular target/s. As antimitotic drugs induced a cell cycle block in G2-M phase, we decided to verify a possible **ISQ3** interference with microtubule network.

Using *in vitro* tubulin polymerization assay, we found that **ISQ3** inhibited tubulin polymerization in a concentration-dependent manner, indicating that this compounds can be classified as microtubule depolymerising agent. Moreover, the mitotic index determinations and the immunofluorescence studies clearly confirmed the interaction with tubulin. It is interesting to note that, at the best of our knowledge, the structure of isoindolo[2,1-*a*]quinoxalin-6-one derivatives do not resemble any of the known antimitotic drugs.

It is well known that DNA intercalator could be Topoisomerase I and/or Topoisomerase II inhibitors. Using a DNA relaxation assay we determined that **ISQ3** inhibited Topoisomerase I catalytic activity but not Topoisomerase II activity.

In conclusion, these results suggested that **ISQ3** acted on both tubulin and Topoisomerase I. We found that **ISQ3** was able to bypass the resistance in multi-drug resistant cell lines selected against some of the most common anticancer drugs. Considered their interesting biochemical mechanism of action and the reduced risks of resistance onset, these new derivatives deserve further investigations as promising antitumor agents.

4. THIOPYRANO[2,3-*e*]INDOL-2-ONES

Some photobiological properties of 4 compounds (**L1-L4**) among the thiopyrano[2,3-*e*]indol-2-ones were already studied in my master thesis [95] and were published by *Barraja et al.* [96]. Briefly, an interesting photobiological activity was assessed using some human cell lines. The photoreaction with the main biomolecules (protein, DNA and lipids) was evaluated using the most active compound as archetype.

4.1 PHYSICOCHEMICAL PROPERTIES

To have photosensitizing properties these compounds must absorb solar light (280-800 nm). Thiopyrano[2,3-*e*]indol-2-ones were synthesized as analogues of angelicin, which is a tricyclic aromatic system. The absorption and emission spectra of thiopyrano[2,3-*e*]indol-2-ones were collected in DMSO or in phosphate buffer (10 mM, pH = 7,2), as described in Materials and methods section .

	λ_{MAX} **abs.(A)**	$\varepsilon^{(M^{-1}cm^{-1})}$ **(A)**	λ_{MAX} **abs.(B)**	λ_{MAX} **emiss. (B)**	**clogP**
L1	401,3 nm	19262,7	407,8 nm	479,0 nm	+ 4,69
L2	348,6 nm	9692,8	354,3 nm	424, 447, 484	+ 5,48
L3	353,3 nm	7848,9	362,5 nm	477,9 nm	+ 3,26
L4	411,0 nm	15181,9	414,4 nm	477,8 nm	+ 4,33
L5	395,0 nm	13744,2	392,2 nm	417,3 nm	+ 3,88
L6	382,1 nm	11450,0	414,0 nm	458,4 nm	+ 2,82
Ang	299,8 nm	9350,0	303,0 nm	401,0 nm	+ 2,08

TAB 1*: Physicochemical properties of thiopyano[2,3-e]indol-2-ones. Absorption and emission maxima, molar extinction coefficient (ε) in DMSO (A) or in phosphate buffer (B) and clogP.*

Both absorption and emission maxima bands exhibited a remarkable batochromic shift compared to angelicin, as reference compound. Moreover, the partition coefficients of the test compounds were calculated by a computational method, as described by *Ghose and Crippen* [97]. These molecules resulted to be highly hydrophobic in comparison to angelicin. In fact, the nature of the substituents was very hydrophobic.

4.2 CELLULAR CYTOTOXICITY AND PHOTOTOXICITY

The antiproliferative activity of thiopyrano[2,3-*e*]indol-2-ones was evaluated on a panel of cultured human cell lines. No cytotoxic activity was found by MTT test after 72 hours from the incubation with these compounds [72].

The phototoxicity tests were conducted in different human tumour cell lines: HL-60 (promyelocytic leukaemia), Jurkat (lymphoblastoid leukaemia), LoVo (intestinal carcinoma) and HT-1080 (fibrosarcoma). As PUVA finds its application above all in dermatological field, we performed the same tests in an immortalized cell line of human keratinocytes, NCTC-2544. These experiments were conducted as described in Materials and methods section. Briefly, we incubated cells with the test compounds for 30 min prior to the irradiation. We used two UV-A doses: 2,5 and 3,75 J/cm^2 . Then, the irradiated solution was replaced by cellular medium. Table 2 and 3 showed IC$_{50}$ in leukaemic and solid cell lines after 72 hours from irradiation.

	HL-60		**JURKAT**	
	2,5 J/cm^2	3,75 J/cm^2	2,5 J/cm^2	3,75 J/cm^2
L1	6,2±0,6	2,7±0,3	4,2±0,4	3,5±0,4
L2	2,6±0,3	1,3±0,2	2,5±0,3	1,5±0,4
L3	0,6±0,06	0,3±0,1	0,5±0,03	0,2±0,01
L4	4,0±0,4	2,7±0,3	4,0±0,4	2,2±0,3
L5	>10	>10	7.3±0.7	5.0±0.4
L6	>10	>10	>10	>10
8-MOP	1,4±0,2	1,2±0,4	n.d.	n.d.
ANG	1,2±0,1	0,9±0,2	n.d.	n.d.

TAB 2: *IC$_{50}$ (μM) in some human leukaemia cell lines after 72 h from irradiation (2,5 and 3,75 J/cm^2), as determined by MTT assay. Data are expressed as means ± SEM for at least three independent experiments. n.d. not determined.*

Almost all the compounds inhibited the proliferation of leukemic cells at submicromolar/micromolar concentrations. The most interesting compound resulted to be **L3**, whose IC$_{50}$ values were lower than the reference compounds.

	HT-1080		LoVo		NCTC-2544	
	2,5 J/cm^2	3,75 J/cm^2	2,5 J/cm^2	3,75 J/cm^2	2,5 J/cm^2	3,75 J/cm^2
L1	11,0±0,1	10,5±0,1	>20	12,3±0,2	>20	>20
L2	5,4±0,5	2,0±0,2	5,1±0,5	4,2±0,4	17,0±1,7	14,8±1,5
L3	0,9±0,1	0,63±0,03	1,0±0,1	0,8±0,2	2,1±0,2	1,6±0,2
L4	11,2±0,2	9,8±0,7	>20	7,2±0,8	>20	>20
L5	>20	>20	>20	>20	>20	>20
L6	>20	>20	>20	>20	>20	>20
8-MOP	8,0±2,0	2,1±0,2	7,8±0,4	2,7±0,1	5,5±0,6	n.d.
Ang	7,5±1.9	2,6±0,2	4,0±0,4	1,1±0,4	4,2±0,5	n.d.

TAB 3: *IC_{50} (µM) in some human solid tumour cell lines after 72 h from irradiation (2,5 and 3,75 J/cm^2), as determined by MTT assay. Data are expressed as means ± SEM for at least three independent experiments. n.d. not determined.*

In solid tumour cell lines, the most phototoxic compound still remained **L3**, which demonstrated submicromolar-micromolar IC_{50} and lower values than the reference compounds. **L5** and **L6** were not phototoxic at the employed concentrations.

The most active compound, **L3**, was fully aromatic and this characteristic seemed essential for photoactivity since the corresponding dihydro-derivatives, **L6**, was devoid of any effect. Moreover, among the fully aromatic compounds, the presence of a methyl group in the 7 position seemed to be important for the photobiological activity.

Further experiments to understand the mechanism of action were carried out using the most phototoxic compound.

4.3 DETERMINATION OF MECHANISM OF CELLULAR DEATH

We performed a series of experiments by flow cytometry with the purpose to investigate the mode of cell death. In particular, we carried out the Annexin-V/PI test to verify an early apoptotic event such as the externalization of the membrane phospholipid phosphatidylserine (PS). FITC-conjugated Annexin-V was used to check PS translocation to the outer leaflet of plasmatic membrane while PI was employed to test the plasmatic membrane integrity [73].

The biparametric analysis was conducted in jurkat cells after 24 hours from the irradiation in the presence of various concentrations of **L3**. As control, the same tests were performed in non irradiated jurkat or in irradiated cells in the identical conditions of **L3** treated ones.

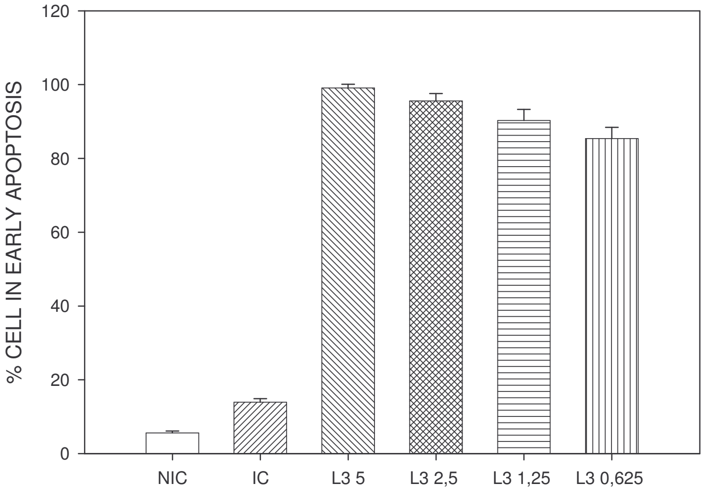

FIG 1: *Percentage of early apoptotic cells (FITC$^+$/PI$^-$) after 24 hours from the irradiation (2,5 J/cm^2) in the presence of **L3** at various concentrations (μM). NIC = non irradiated control; IC= irradiated control. Data were expressed as Mean ± SEM of three independent experiments.*

Figure 1 showed that **L3** induced cell death through apoptosis as a very large amount of cells were found positive to FITC fluorescence but negative to the PI one. A small percentage of necrotic cells (2-3%) was observed only at the highest employed concentrations.

These experiments were in well agreement with the cell cycle tests where we had found the presence of a subG1 peak in **L3** treated cells, corresponding to apoptotic cells with a small content of DNA. Moreover, several studies demonstrated that apoptosis was the main mode of cell death induced by PUVA therapy [52-54].

4.4 INVOLVEMENT OF MITOCHONDRIA IN CELL DEATH

As mitochondrion was found to be a key effector of apoptosis [25, 75] and above all many reports evidenced a mitochondrial dysfunction provoked by PUVA therapy [53-54], we decided to study a possible involvement of this organelle in photoinduced cell death.

4.4.a DETERMINATION OF MITOCHONDRIAL MEMBRANE POTENTIAL

The collapse of mitochondrial membrane potential ($\Delta\psi_{mt}$) is one of the events of mitochondrial dysfunction [75]. The determination of $\Delta\psi_{mt}$ was conducted through a flow cytometric analysis using JC-1, as a probe. In the presence of normal cells (high $\Delta\psi_{mt}$), JC-1 accumulates selectively in mitochondria and, as a consequence of the electrochemical gradient, forms red fluorescence aggregates locally and spontaneously that are associated with emission at 590 nm, whereas when the mitochondrial membrane is depolarized (low $\Delta\psi_{mt}$), JC-1 forms monomers which emits at 530 nm [74].

Cells were irradiated in the presence of 5 µM **L3** or 2,5 µM angelicin, as reference compound, and were analyzed after different times from the irradiation.

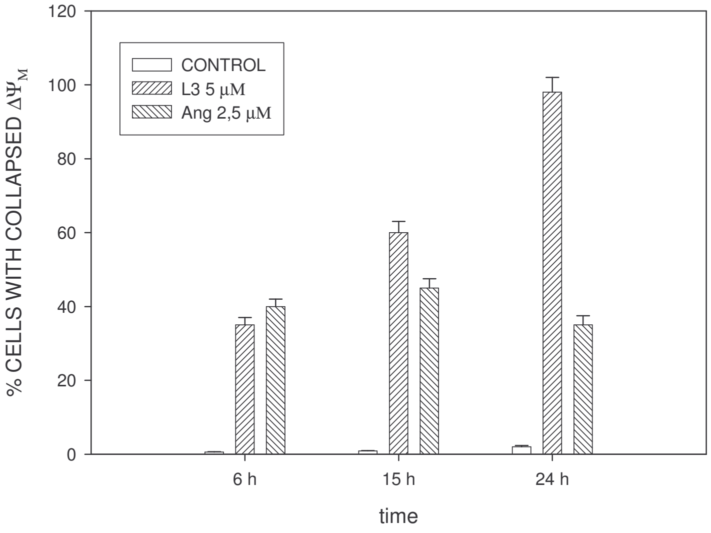

FIG 2: *Percentage of jurkat with collapsed* $\Delta\psi_M$ *(fluorescence of the JC-1 monomeric form) after 6, 15 and 24 hours from the irradiation (2,5 J/cm*^{2}*) with 5 µM* ***L3****, 2,5 µM angelicin (Ang). Data were expressed as Mean ± SEM of three independent experiments.*

These data suggested that **L3** induced a rapid and significant depolarization of mitochondrial potential and this can be indicative of mitochondrial dysfunction. Moreover, these effects were similar to those of the reference compound.

4.4.b DETERMINATION OF REACTIVE OXYGEN SPECIES (ROS) PRODUCTION

The mitochondrial membrane depolarization has been associated with the mitochondrial production of reactive oxygen species (ROS) [75]. In fact, ROS generated from a partially uncoupled respiratory chain can actively participate in the effector phase of apoptosis.

To investigate the effects of thiopyrano[2,3-*e*]indol-2ones on ROS production during apoptosis, we performed some cytofluorimetric analysis using hydroethidine (HE) and dichlorofluorescin-diaceteate ($DCFH_2$-DA), as probes. Fluorescence was detected only if the probes were oxidized by ROS inside the cell [77].

The cytofluorimetric examination was carried out after 24 hours from the irradiation in the presence of **L3** at different concentrations. Data were compared to non irradiated jurkat and irradiated cells without any drug while angelicin was taken as reference compound.

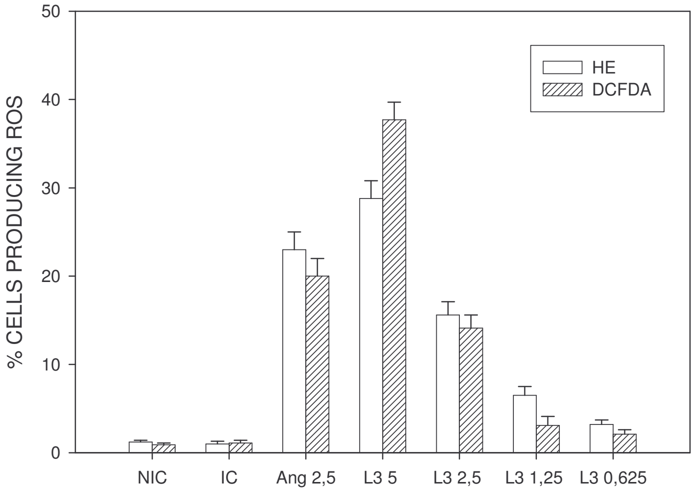

***FIG 3**:Percentage of ROS producing jurkat after 24 hours from irradiation (2,5 J/cm^2) with various concentrations (µM) of **L3** or 2,5 µM angelicin (Ang). NIC = non irradiated control; IC= irradiated control. Data were expressed as Mean ± SEM of three independent experiments.*

There was a remarkable production of ROS, as evidenced by the high percentage of HE- and DCFH$_2$-DA-positive cells, in well agreement with the data of mitochondrial membrane depolarization. This production was **L3** concentration-dependent and was comparable to that of angelicin. After 24 hours from the irradiation, the presence of ROS inside the cell can not be associated to the photosensitization reaction but to other origins such as a mitochondrial dysfunction.

4.4.c DETERMINATION OF CARDIOLIPIN PEROXIDATION

In parallel, we evaluated the damage produced by ROS in mitochondria by assessing the oxidation state of cardiolipin (CL). As already seen before, CL is a phospholipid restricted to the inner mitochondrial membrane and displays important roles for mitochondrial functionality [78].

The oxidation state of CL was examined with 10-N-nonyl acridine orange (NAO) test [79], as described in materials and methods part, and after 24 hours from the jurkat irradiation in the presence of various concentrations of **L3**.

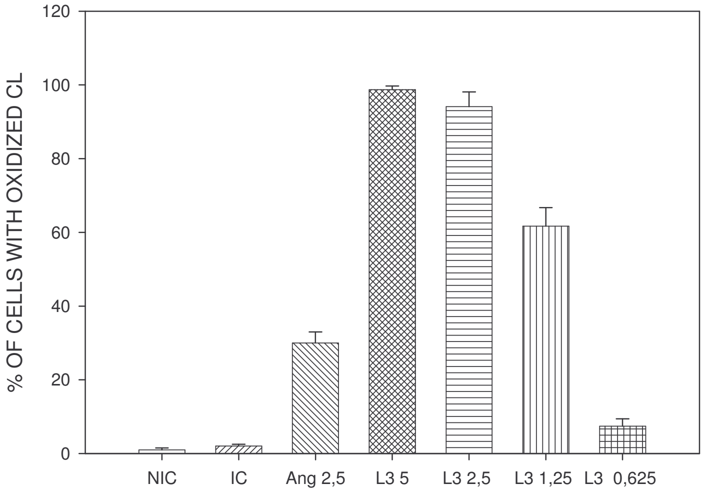

***FIG 4**: Percentage of jurkat with oxidized CL after 24 hours from the irradiation (2,5 J/cm^2) with various concentrations of **L3** or 2,5 µM angelicin (Ang). NIC = non irradiated control; IC= irradiated control. Data were expressed as Mean ± SEM of three independent experiments.*

In well agreement with the production of ROS, treated cells demonstrated a dramatic increase in oxidized CL, which resulted to be higher than the reference compound.

Altogether, these data suggested an important involvement of mitochondria in apoptosis photoinduced by **L3**.

4.5 DETERMINATION OF REDUCED GLUTATHIONE CONTENT

The tripeptide glutathione in its reduced form (GSH; γ-L-glutamyl-L-cysteinyl-glycine) is a key antioxidant in most eukaryotic cells, where it is present at millimolar concentrations as it is the main thiol compound. Reduced glutathione (GSH) is involved in maintaining ascorbic acid in its reduced form. GSH reacts enzymatically (GSH *S*-transferase family) or non-enzymatically with toxic compounds to form GSH conjugates. It also protects against oxidative damage caused by reactive oxygen species (ROS) that may be formed normally in metabolism. GSH may react with ROS non-enzymatically. Hydrogen peroxides and other peroxides are detoxified by GSH peroxidase [98].

With the aim of assessing the effect of ROS accumulation on cellular redox potential, the rate of GSH was measured in Jurkat cells irradiated in the presence of different concentrations of **L3**. For this purpose, flow cytometric analysis was performed using monobromobimane (mBBr), as a probe. The cell permeable mBBr is not fluorescent but forms a fluorescent adduct with GSH (GS-mBBr) in a non-enzymatic manner.

Cellular appearance of GS-mBBr fluorescence was monitored after 24 hours from the irradiation.

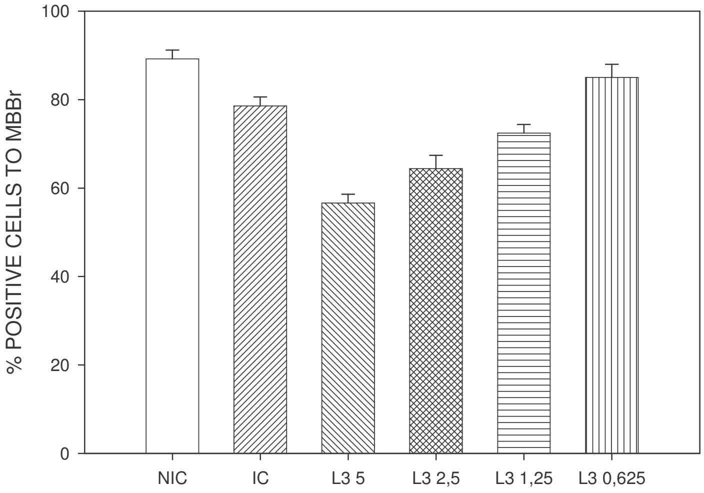

FIG 5: *Decreased levels of intracellular GSH after 24 h from irradiation (2.5 J/cm^2) of Jurkat cells in the presence of* ***L3*** *at the indicated concentrations. NIC = non irradiated control; IC= irradiated control. Data are represented as mean S.E.M. of three experiments.*

The intracellular content of GSH was observed to fall in a concentration-dependent manner after the irradiation in the presence of **L3**. The reduction in GSH content was well correlated with the appearance of HE and DCF positive cells after the treatment with **L3**.

4.6 INVOLVEMENT OF LYSOSOMES IN CELL DEATH

Lysosomes can be involved in apoptotic machinery not only because they participate in the degradation of apoptotic cells contained in the heterophagic vacuole of healthy cells, but also it was proved that in pro-oxidant-induced apoptosis, the release of lysosome enzyme, such as cathepsin D, can precede the release of cytochrome c from mitochondria. Moreover, lysosomotropic photosensitizers resulted to involve these organelles in their photoinduced cell death as they can cause a local ROS-mediated membrane damage [25].

To investigate the integrity of lysosomes after irradiation with **L3**, we performed flow cytometric analysis using the fluorescent dye acridine orange (AO). AO is a lysosomotropic base and a metachromatic fluorochrome exhibiting red fluorescence when highly concentrated, as in the case of intact lysosomes where it is retained in its protonated form. When lysosomes are damaged, AO relocates to the cytosol where it is predominantly in the deprotonated form and it shows green fluorescence [99]. The percentage of cells with intact lysosomes was evaluated by assessing red fluorescence after AO staining.

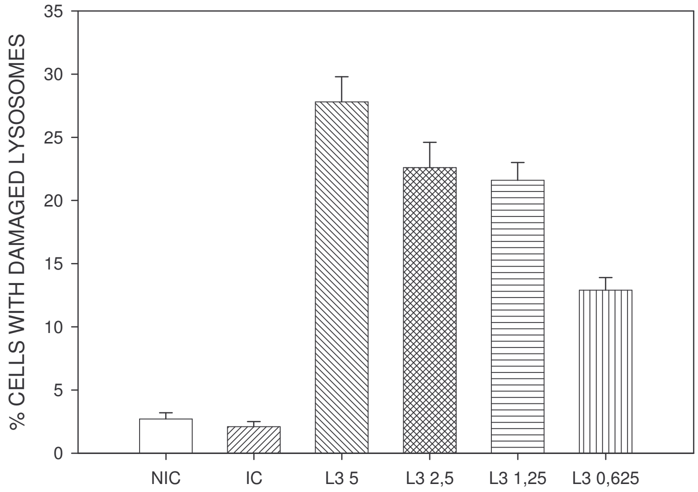

FIG 6: *Percentage of jurkat cells with damaged lysosomes after 24 h from irradiation (2.5 J/cm^2) in the presence of* ***L3*** *at the indicated concentrations. NIC = non irradiated control; IC= irradiated control. Data are represented as mean S.E.M. of three experiments*

A significant extent of lysosomal damage was photoinduced by **L3** after 24 hours from the irradiation, although it was minor than mitochondrial damage. Altogether, these results suggested that lysosomes were not preferential sites of photosensitization for these derivatives.

4.7 CASPASE ACTIVATION ASSAY

A central mechanism in apoptosis is the activation of a family of cysteine proteases, referred to as caspases. Caspases are synthesized as proenzymes that are activated by cleavage. The important role of caspase cascade in PUVA apoptosis was extensively studied by *Martelli et al.* [100].

We decided to examine a potential involvement of this large family of proteases in **L3** apoptosis induction by assessing the activation of caspase-3. Caspase-3 is an executive caspase and is essential for the propagation of apoptotic signals after the exposure to many anticancer drugs and to PUVA therapy.

We prepared lysates from Jurkat cells after 24 hours from the irradiation in the presence of **L3** at different concentrations. Then, they were incubated with the capsase-3 tetrapeptide substrate DEVD (*N*-acetyl-Asp-Glu-Val-Asp). This substrate is conjugated with a chromophore *p*-nitroaniline (*p*NA), which can be cleaved by activated caspase-3. The release of *p*NA into the solution leads to an increase of absorbance in the *p*NA band (405 nm) [30].

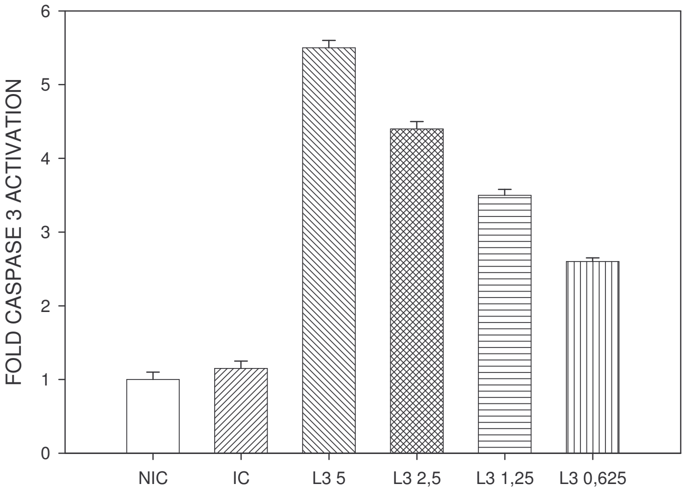

FIG 7: *Caspase-3 activation induced by* ***L3****. Jurkat cells were exposed to 2.5 J/cm^2 of UV-A in the presence of increasing concentrations (μM) of* ***L3****. After 24 h, cells were harvested and the lysates were assayed for caspase-3 activity using the caspase-3 substrate Ac-DEVD-pNA. NIC = non irradiated control; IC= irradiated control. Data were represented as fold increase of activity of the enzyme in comparison to the non-irradiated control*

The results indicated **L3** was able to activate caspase-3 in a dose-dependent manner, after 24 hours from irradiation. Thus, caspase system was involved in **L3** apoptosis induction.

4.8 PHOTOREACTION WITH THE MAIN BIOMOLECULES

In my graduation thesis, I analyzed the photoreaction of **L3** with the main biomolecules to find molecular targets inside the cell: proteins, DNA and lipids. Briefly, I found **L3** was able to react with all these cellular components. Proteins were found to be substrate of phototoxic activity of thiopyrano[2,3-*e*]indol-2-ones after fluorimetric studies and membrane protein cross-links in erythrocyte ghost experiments. Spectroscopic titrations and CD and LD analysis indicated that these compounds did not interact significantly with DNA, but **L3** was found to provoke DNA base modifications after irradiation of pBR322. Furthermore, a lipidic peroxidation was assessed in irradiated cells in presence of **L3** by TBARs test [95, 96].

4.9 CONCLUSIONS

Thiopyrano[2,3-*e*]indol-2-ones were found to show a potent photoantiproliferative activity. The most active compound, **L3**, presented a double bound in 5-6 positions and a methyl group in 7 position. The phototoxicity of these compounds was reduced for the dihidroderivatives but also with an increase of steric hindrance of the substituents in N-position.

To understand the mechanism of cell death photoinduced by thiopyrano[2,3-*e*]indol-2ones, we performed a series of flow cytometric experiments, using the most phototoxic compound, where we looked for some apoptotic characteristics. One typical apoptotic feature is the loss of plasmatic membrane asymmetry due to the exposure of signals for phagocytosis, such as PS outer leaflet translocation. Thanks to Annexin-V/PI analysis, we observed that jurkat cells had exposed PS after 24 hours from the irradiation in the presence of **L3**. Thus, **L3** induced cell death by apoptosis. To further study the apoptotic process, we performed some experiments (mitochondrial membrane potential, ROS production and CL peroxidation tests) to prove the involvement of mitochondria in cell death. In addition to the fundamental role played by mitochondria, we found a certain participation of lysosomes and the activation of caspase cascade in inducing apoptosis.

As thiopyrano[2,3-*e*]indol-2-ones resulted hydrophobic, we investigated a possible photodamage at membrane level, assessing it both in lipid and protein content. We determined an increase of lipid peroxidation with TBARs assay and a photoinduced cross-linking in ghost protein after irradiation in the presence of **L3** [95].

Finally, we decided to investigate the photodamage to DNA, as it represents an important target for PUVA antiproliferative activity. After assessing a low affinity for DNA by LD and spectrofluorimetric techniques, we found **L3** was not able to induce significant frank strand breaks in plasmidic DNA but photooxidations of DNA bases [95].

In conclusion, we thought that thiopyrano[2,3-*e*]indol-2-ones could be interesting for application as potential photochemiotherapics.

5. PYRROLO[3,4-*h*]QUINOLIN-2-ONES

5.1 PHYSICOCHEMICAL PROPERTIES

Pyrrolo[3,4-*h*]quinolin-2-ones were synthesized as analogues of angelicin, which is a tricyclic aromatic system. The absorption and emission spectra of pyrrolo[3,4-*h*]quinolin-2-ones were collected in DMSO or in phosphate buffer (10 mM, pH = 7,2), as described in Materials and methods section .

	λ_{MAX} abs.(A)	**$\varepsilon^{(M^{-1}cm^{-1})}$ (A)**	**λ_{MAX} emiss. (A)**	**λ_{MAX} abs.(B)**	**clogP**
BV1	409 nm	18849,5	432 nm	396 nm	+ 2,01
BV2	353 nm	18641,2	396 nm	394 nm	+ 4,58
BV3	413 nm	24463,2	445 nm	398 nm	+ 2,47
BV4	414 nm	27901,0	440 nm	392 nm	+ 3,88
BV5	277, 351, 401	17322,8	435 nm	251, 385 nm	+ 5,84
BV6	410 nm	26833,3	442 nm	400 nm	+ 4,34
BV7	410 nm	34338,6	436 nm	386 nm	+ 3,88
BV8	355, 405 nm	23928,0	433 nm	392 nm	+ 3,98
BV9	268, 352 nm	29983,3	401 nm	355 nm	+ 4,17
BV10	270, 350 nm	33957,8	401 nm	362 nm	+ 4,93
BV11	261, 370 nm	37263,2	397 nm	361 nm	+ 6,44
BV12	261, 409 nm	36753,2	436 nm	395 nm	+ 3,87
BV13	261, 408 nm	38804,6	434 nm	394 nm	+ 2,36
BV14	262, 413 nm	42799,2	442 nm	400 nm	+ 4,23
BV15	354 nm	15740,5	406 nm	353 nm	+ 3,52
BV16	271, 355 nm	29148,4	411 nm	351 nm	+ 2,01
BV18	262, 406 nm	26281,3	438 nm	396 nm	- 0,28
BV19	261, 355, 404	11084,5	434 nm	399 nm	+ 0,51
BV20	261, 352, 405	19301,0	437 nm	398 nm	+ 2,00
Ang	299 nm	9350,0	401 nm	303 nm	+ 2,08

TAB 1*: Physicochemical properties of pyrrolo[3,4-h]quinolin-2-ones. Absorption and emission maxima, molar extinction coefficient (ε) in DMSO (A) or in phosphate buffer (B) and clogP.*

All compounds absorbed solar radiation spectrum and presented bands in UV-A region and this fact is fundamental for a photosensitizer. All compounds demonstrated higher values of molar extinction coefficients than angelicin thanks to the presence of a sulfonyl group in position 3 and of the substituent in 8. This is probably due to the higher electronic density, to the increased extension of the molecule conjugation but also to the increased structural rigidity for the steric hindrance of this group.

The partition coefficients of the test compounds were calculated using the computational method as described by *Ghose and Crippen* [97]. Most of pyrrolo[3,4-*h*]quinolin-2-ones were highly hydrophobic, reaching clogP values of + 6,44 in the case of **BV11**. But depending on the nature of the substituent in 7 position, some molecules also resulted more hydrophilic than angelicin: in particular, **BV18**, **BV19** and **BV20** presented a carboxylic acid in 7.

5.2 PHOTOSTABILITY

When irradiated in solution, furocoumarins are subjected to photolysis [50]. Thus, absorption spectra of 20 μM pyrrolo[3,4-*h*]quinolin-2-ones in DMSO were recorded after increasing doses of UV-A. These spectra gave information about the photostability of compounds and about the formation of other species as a consequence of irradiation.

All photobleaching spectra were reported in figure 1.

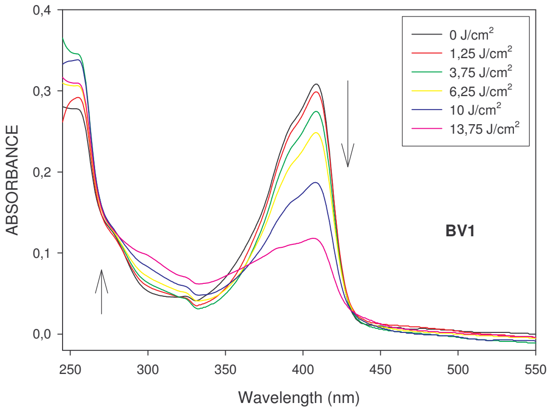

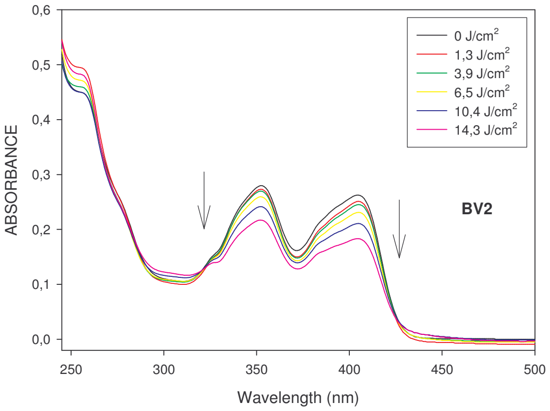

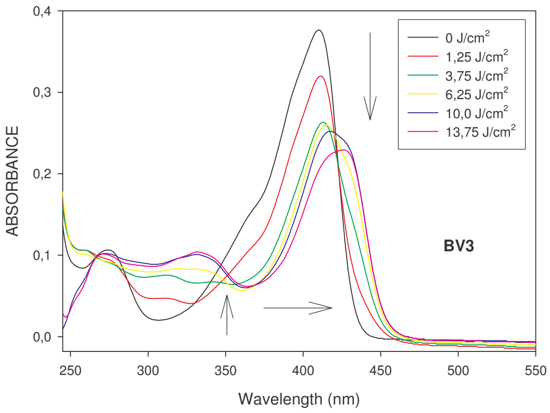
0 J/cm²
1,25 J/cm²
3,75 J/cm²
6,25 J/cm²
10,0 J/cm²
13,75 J/cm²
BV3
ABSORBANCE
0,0
0,1
0,2
0,3
0,4
Wavelength (nm)
250
300
350
400
450
500
550

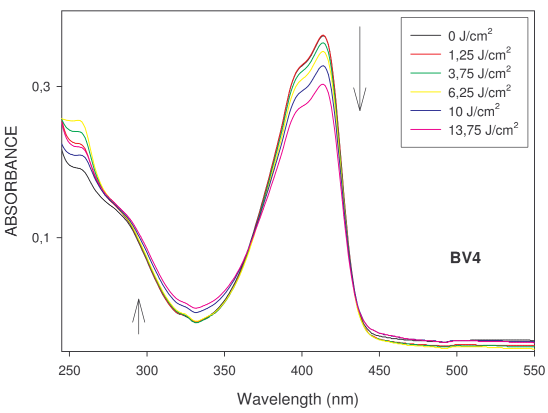
0 J/cm²
1,25 J/cm²
3,75 J/cm²
6,25 J/cm²
10 J/cm²
13,75 J/cm²
BV4
ABSORBANCE
0,1
0,3
Wavelength (nm)
250
300
350
400
450
500
550

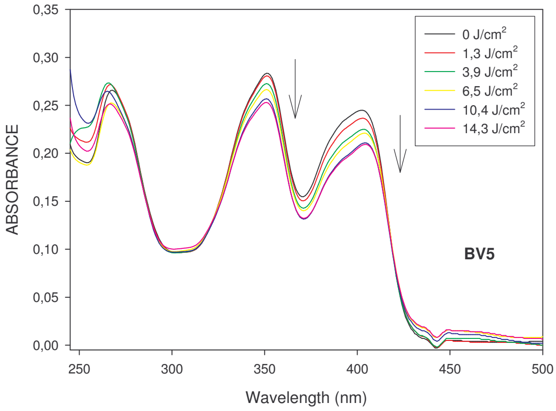
0 J/cm²
1,3 J/cm²
3,9 J/cm²
6,5 J/cm²
10,4 J/cm²
14,3 J/cm²
BV5
ABSORBANCE
0,00
0,05
0,10
0,15
0,20
0,25
0,30
0,35
Wavelength (nm)
250
300
350
400
450
500

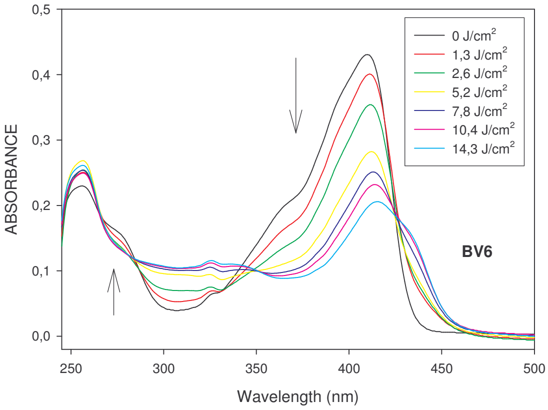
0 J/cm²
1,3 J/cm²
2,6 J/cm²
5,2 J/cm²
7,8 J/cm²
10,4 J/cm²
14,3 J/cm²
BV6
ABSORBANCE
0,0
0,1
0,2
0,3
0,4
0,5
Wavelength (nm)
250
300
350
400
450
500

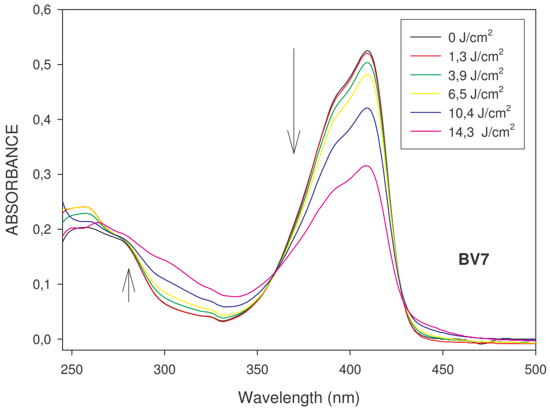
0 J/cm²
1,3 J/cm²
3,9 J/cm²
6,5 J/cm²
10,4 J/cm²
14,3 J/cm²
BV7
ABSORBANCE
0,0
0,1
0,2
0,3
0,4
0,5
0,6
Wavelength (nm)
250
300
350
400
450
500

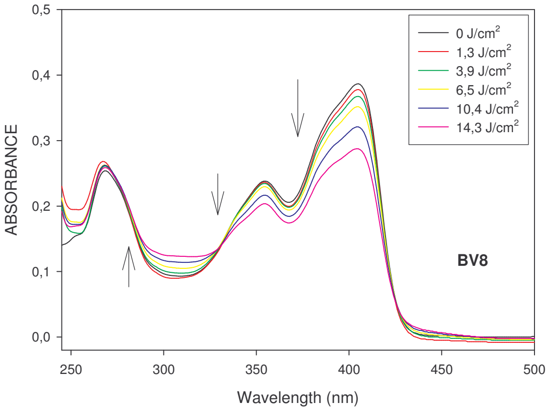
0 J/cm²
1,3 J/cm²
3,9 J/cm²
6,5 J/cm²
10,4 J/cm²
14,3 J/cm²
BV8
ABSORBANCE
0,0
0,1
0,2
0,3
0,4
0,5
Wavelength (nm)
250
300
350
400
450
500

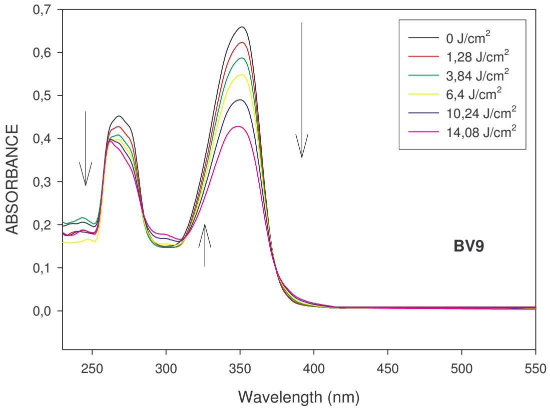
0 J/cm²
1,28 J/cm²
3,84 J/cm²
6,4 J/cm²
10,24 J/cm²
14,08 J/cm²
BV9
ABSORBANCE
0,0
0,1
0,2
0,3
0,4
0,5
0,6
0,7
Wavelength (nm)
250
300
350
400
450
500
550

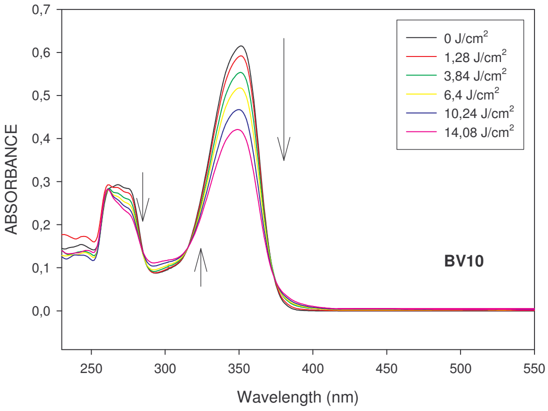
0 J/cm²
1,28 J/cm²
3,84 J/cm²
6,4 J/cm²
10,24 J/cm²
14,08 J/cm²
BV10
ABSORBANCE
0,0
0,1
0,2
0,3
0,4
0,5
0,6
0,7
Wavelength (nm)
250
300
350
400
450
500
550

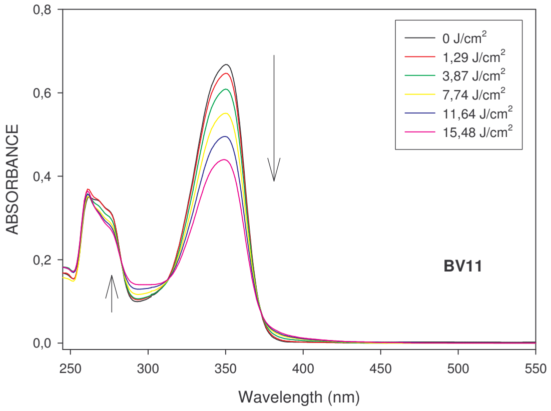
0,8
0,6
0,4
0,2
0,0
ABSORBANCE
250
300
350
400
450
500
550
Wavelength (nm)
0 J/cm2
1,29 J/cm2
3,87 J/cm2
7,74 J/cm2
11,64 J/cm2
15,48 J/cm2
BV11

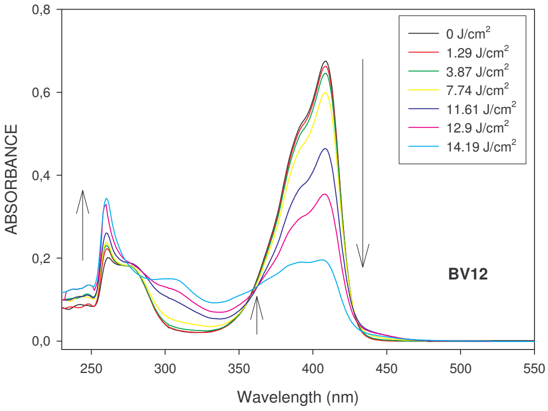
0,8
0,6
0,4
0,2
0,0
ABSORBANCE
250
300
350
400
450
500
550
Wavelength (nm)
0 J/cm2
1.29 J/cm2
3.87 J/cm2
7.74 J/cm2
11.61 J/cm2
12.9 J/cm2
14.19 J/cm2
BV12

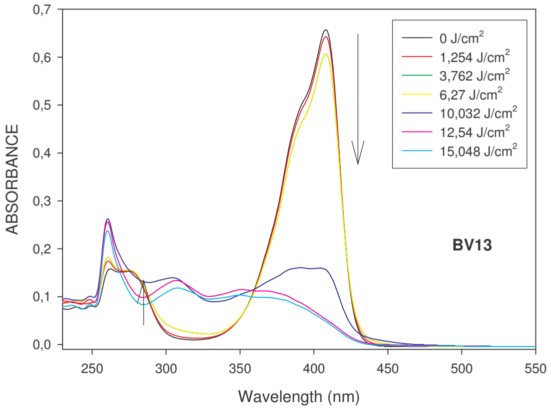
0,7
0,6
0,5
0,4
0,3
0,2
0,1
0,0
ABSORBANCE
250
300
350
400
450
500
550
Wavelength (nm)
0 J/cm2
1,254 J/cm2
3,762 J/cm2
6,27 J/cm2
10,032 J/cm2
12,54 J/cm2
15,048 J/cm2
BV13

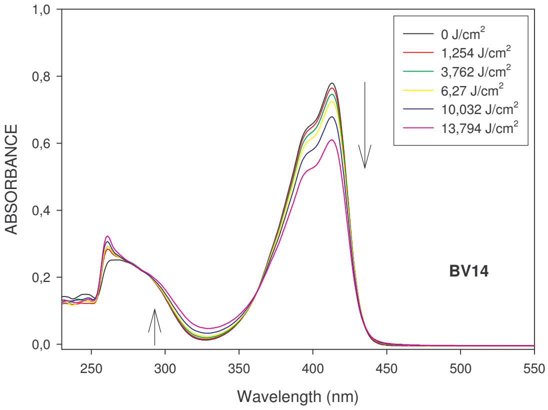
1,0
0,8
0,6
0,4
0,2
0,0
ABSORBANCE
250
300
350
400
450
500
550
Wavelength (nm)
0 J/cm2
1,254 J/cm2
3,762 J/cm2
6,27 J/cm2
10,032 J/cm2
13,794 J/cm2
BV14

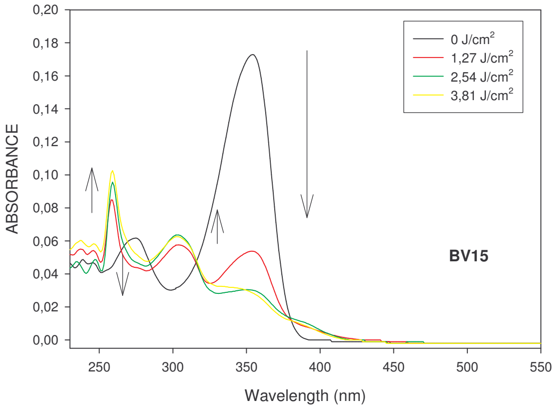
0,20
0,18
0,16
0,14
0,12
0,10
0,08
0,06
0,04
0,02
0,00
ABSORBANCE
250
300
350
400
450
500
550
Wavelength (nm)
0 J/cm2
1,27 J/cm2
2,54 J/cm2
3,81 J/cm2
BV15

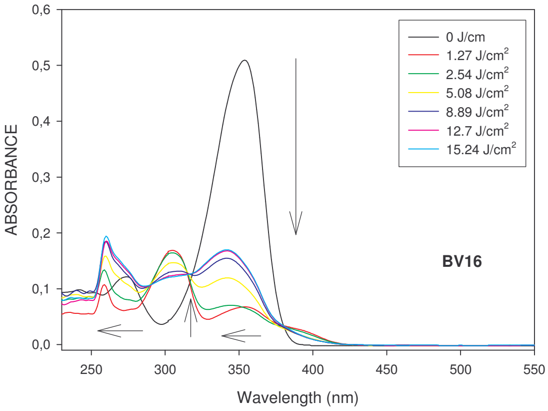
0,6
0,5
0,4
0,3
0,2
0,1
0,0
ABSORBANCE
250
300
350
400
450
500
550
Wavelength (nm)
0 J/cm
1.27 J/cm2
2.54 J/cm2
5.08 J/cm2
8.89 J/cm2
12.7 J/cm2
15.24 J/cm2
BV16

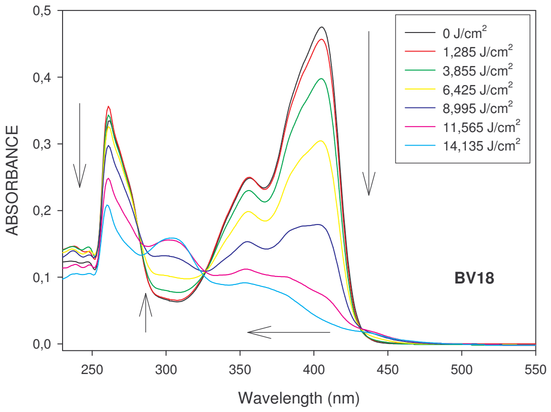
0,5
0,4
0,3
0,2
0,1
0,0
ABSORBANCE
250
300
350
400
450
500
550
Wavelength (nm)
0 J/cm2
1,285 J/cm2
3,855 J/cm2
6,425 J/cm2
8,995 J/cm2
11,565 J/cm2
14,135 J/cm2
BV18

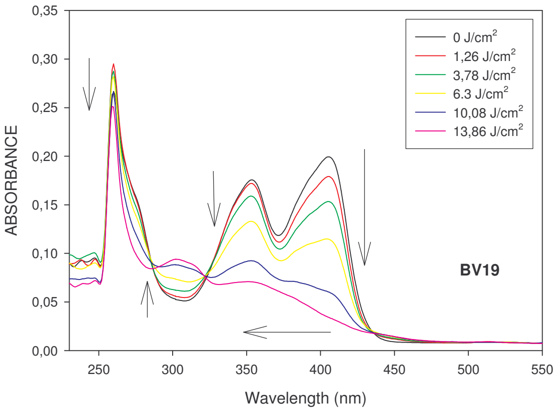
0,35
0,30
0,25
0,20
0,15
0,10
0,05
0,00
ABSORBANCE
250
300
350
400
450
500
550
Wavelength (nm)
0 J/cm2
1,26 J/cm2
3,78 J/cm2
6.3 J/cm2
10,08 J/cm2
13,86 J/cm2
BV19

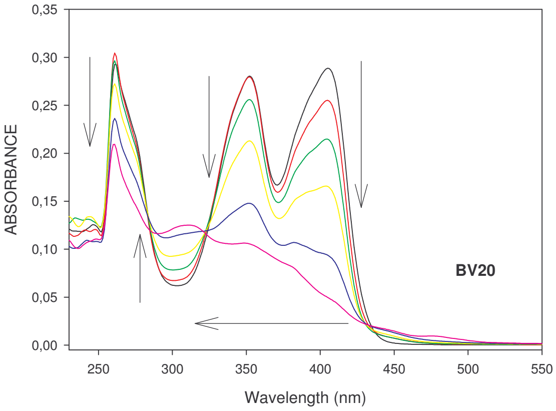

FIG 1: *Photodegradation of pyrrolo[3,4-h]quinolin-2-ones. Absorption spectra of 20 µM* ***BV*** *in DMSO were recorded after increasing UV-A doses.*

As can be observed in fig 1, all spectra were deeply modified by increasing doses of UV-A, indicating that all compounds underwent a certain degree of photodegradation. Among these changes, we can find simple reduction of maxima absorbance (ex: **BV2**, **BV5**), but also the onset of new bands (ex: **BV15** and **BV16**) or the shift in wavelength of peak (ex: **BV3** and **BV18**). In most spectra (**BV1**, **BV2**, **BV4**, **BV5**, **BV6**, **BV7**, **BV8**, **BV9**, **BV10**, **BV11**, **BV14**, **BV19**), the presence of isosbestic points can be detected. An isosbestic point indicates that two species, the non-degradeted compound and a photoproduct, are in equilibrium in solution.

5.3 CELLULAR CYTOTOXICITY AND PHOTOTOXICITY

After having assessing they did not present any antiproliferative activity, the phototoxicity of pyrrolo[3,4-*h*]quinolin-2ones was evaluated on a panel of cultured human cell lines. The phototoxicity tests were conducted in different human tumour cell lines: HL-60 (promyelocytic leukaemia), Jurkat (lymphoblastoid leukaemia), LoVo (intestinal carcinoma) and MCF-7 (breast adenocarcinoma). We performed the same tests in an immortalized cell line of human keratinocytes, NCTC-2544. These experiments were carried out as described in Materials and methods section. Briefly, we incubated cells with the test compounds for 30 min prior to the irradiation. We used two UV-A doses: 2,5 and 3,75 J/cm^2. Then, the irradiated solution was replaced by cellular medium. Table 2 and 3 showed IC$_{50}$ in leukaemic and solid cell lines after 72 hours from irradiation.

	HL-60		JURKAT	
	2,5 J/cm^2	3,75 J/cm^2	2,5 J/cm^2	3,75 J/cm^2
BV1	› 10	5,6±0,6	› 10	› 10
BV2	3,6±0,3	1,8±0,2	2,0±0,2	1,4±0,2
BV3	› 10	› 10	› 20	› 20
BV4	12,2±1,0	8,0±1,0	› 20	7,4±0,7
BV5	1,2±0,2	0,8±0,1	2,9±0,3	1,9±0,2
BV6	4,0±0,4	2,5±0,3	13,0±1,5	3,0±0,5
BV7	› 20	14,5±1,5	› 20	› 20
BV8	13,7±1,0	9,1±0,8	18,0±2,0	10,0±1,0
BV9	› 20	5,8±0,6	› 20	12,5±1,3
BV10	1,2±0,2	0,9±0,1	1,2±0,1	0,8±0,1
BV11	5,4±0,6	2,6±0,3	2,9±0,3	1,3±0,1
BV12	4,4±0,4	2,8±0,3	3,6±0,4	2,5±0,3
BV13	› 20	› 20	› 20	› 20
BV14	› 20	› 20	› 20	› 20
BV15	8,3±0,8	7,3±0,7	8,5±0,9	6,3±0,6
BV16	1,6±0,1	0,9±0,1	0,97±0,08	0,14±0,01
BV18	› 20	› 20	› 20	› 20
BV19	› 20	› 20	› 20	› 20
BV20	› 20	› 20	› 20	› 20
8-MOP	1,4±0,2	1,2±0,4	n.d.	n.d.
ANG	1,2±0,1	0,9±0,2	n.d.	n.d.

TAB 2: *IC$_{50}$ (µM) in some human leukemia cell lines after 72 h from irradiation (2,5 and 3,75 J/cm^2), as determined by MTT assay. Data are expressed as means ± SEM for at least three independent experiments. n.d. not determined.*

	MCF-7		**LoVo**		**NCTC-2544**	
	2,5 J/cm^2	3,75 J/cm^2	2,5 J/cm^2	3,75 J/cm^2	2,5 J/cm^2	3,75 J/cm^2
BV1	› 20	› 20	› 20	› 20	› 20	› 20
BV2	10,0±1.0	5,1±0,6	7,9±0,8	4,0±0,4	10,1±1,0	6,2±0,6
BV3	› 20	› 20	› 20	› 20	› 20	› 20
BV4	› 20	› 20	› 20	› 20	› 20	› 20
BV5	3,3±0,4	1,4±0,1	4,0±0,4	2,3±0,2	4,0±0,5	2,5±0,3
BV6	› 20	7,7±0,8	› 20	› 20	› 20	14,4±0,8
BV7	› 20	› 20	› 20	› 20	› 20	› 20
BV8	› 20	› 20	15,5±1,5	13,6±1,5	› 20	15,0±1,4
BV9	› 20	› 20	› 20	13,2±1,3	› 20	› 20
BV10	1,7±0,1	1,3±0,1	0,7±0,05	0,4±0,03	2,4±0,2	1,3±0,2
BV11	› 20	14,4±1,5	12,1±1,2	8,7±0,8	› 20	14,3±1,5
BV12	6,6±0,7	3,7±0,4	3,9±0,4	2,8±0,3	8,2±0,9	5,8±0,6
BV13	› 20	› 20	› 20	› 20	› 20	› 20
BV14	› 20	› 20	› 20	› 20	› 20	› 20
BV15	10,0±1,2	7,5±0,8	9,9±0,1	8,7±0,9	15,3±2,0	9,6±1,1
BV16	2,5±0,3	2,0±0,2	1,9±0,2	0,9±0,09	4,9±0,5	1,1±0,1
BV18	› 20	› 20	› 20	› 20	› 20	› 20
BV19	› 20	› 20	› 20	› 20	› 20	› 20
BV20	› 20	› 20	› 20	› 20	› 20	› 20
8-MOP	n.d	n.d.	7,8±0,4	2,7±0,1	5,5±0,6	n.d.
ANG	n.d.	n.d.	4,0±0,4	1,1±0,4	4,2±0,5	n.d.

TAB 3: *IC_{50} (µM) in some human solid tumor cell lines after 72 h from irradiation (2,5 and 3,75 J/cm^2), as determined by MTT assay. Data are expressed as means ± SEM for at least three independent experiments. n.d. not determined.*

Among pyrrolo[3,4-*h*]quinolin-2-ones, some compounds were found to be non phototoxic at the employed concentrations (**BV3**, **BV7**, **BV13**, **BV14**, **BV18**, **BV19** and **BV20**), some molecules were active only toward leukeamic cell lines (**BV1**, **BV4**, **BV8** and **BV9**), other demonstrated a moderate (**BV2**, **BV6**, **BV11**, **BV12** and **BV15**) or high phototoxicity (**BV5**,

BV10 and **BV16**). When detected, the antiproliferative activity of pyrrolo[3,4-*h*]quinolin-2-ones resulted dependent on UV-A dose and higher in leukaemias than in solid tumours.

The most phototoxic compounds, **BV5**, **BV10** and **BV16**, presented micromolar-submicromolar IC_{50} values comparable to the ones of the reference molecules both in leukemic and solid cell lines.

A relationship between activity and structure can be hypothesized thanks to the large number of evaluated compounds. We started from the structure of the most phototoxic compounds (**BV5**, **BV10** and **BV16**). In *structure a*, we found the importance of the presence of a substituent in position 8 and the $–COOCH_2CH_3$ group in 7. In fact, compounds that had no substituent or a different one in 7 (ex: a carboxyl acid such as **BV18**, **BV19** and **BV20**) exhibited moderate or no phototoxicity. Among the compounds with the $–COOCH_2CH_3$ group in 7, the presence of a substituent of any nature (Me or Benzyl group) in 8 was fundamental for activity: in fact **BV8** and **BV9** demonstrated a reduced phototoxicity. Despite of the small number of compound with *structure b*, we found a general increase in the phototoxicity. In fact, **BV16** was one of the most active molecule and it is worthy to note that the correspondent compound (**BV1**) with *structure a* was almost inactive.

Caffieri et al. demonstrated the ability of photoirradiation to generate cytotoxic products (POPs) that were likely to play a relevant role in PUVA therapy. They also found mitochondrial permeability transition pore opening emerged as a central mechanism in the sequence of events set in motion by POPs that committed Jurkat cells to apoptosis [51]. Thus, as we detected pyrrolo[3,4-*h*]quinolin-2-ones underwent photolysis when irradiated, we analysed the possible contribution of photoproducts in antiproliferative action. After having irradiated (1,25 and 6,5 J/cm^2) solutions of the most active compounds, we incubated jurkat cells with that mixture for 72 hours. No cytotoxic effect was assessed by MTT test.

Phototoxicity experiments in the presence of some scanvengers can be very useful to identify which reactive species are involved in photosensitization [101]. These tests were performed with the most active compounds using MCF-7 cells. We employed the radical scavengers reduced glutathione (GSH) and 2,6-di-tert-butylhydroxyanisole (BHA); the hydroxyl radical scavengers dimethylthiourea (DMTU) and mannitol (MAN), and the singlet oxygen scavenger 1,4-diazabicyclo[2,2,2]octane (DABCO), sodium azide (NaN_3). MCF-7 were irradiated (2,5 J/cm^2) in the presence of 4 µM **BV5** or 2 µM **BV10** or 3 µM **BV16**: we chose drug concentrations near to IC_{50} values.

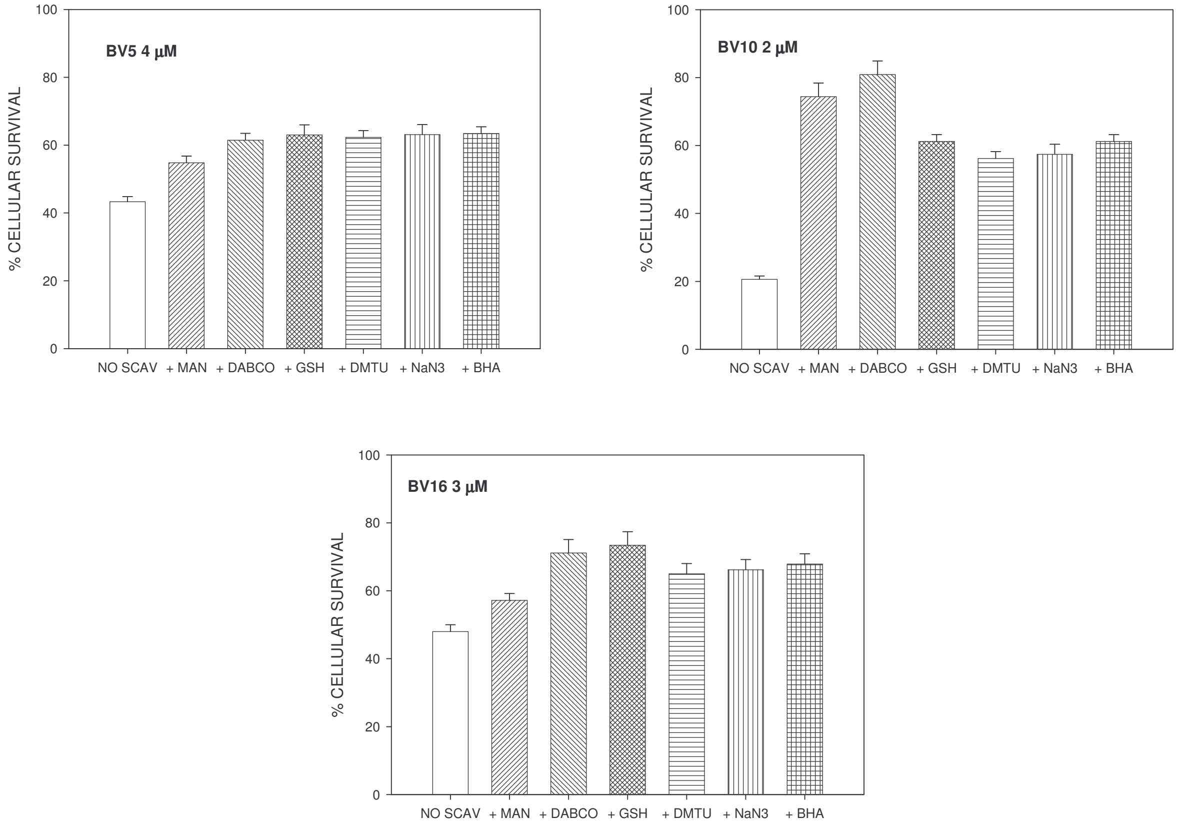

FIG 2: *Effect of different scavengers on the phototoxicity induced by* ***BV5****,* ***BV10*** *and* ***BV16*** *in MCF-7 cells. Cell viability was assayed by MTT test after 72 h from the irradiation (2,5 J/cm^2) in the presence of the compounds and the scavengers. Data were expressed as means ± SEM for at least three independent experiments.*

For **BV5** and **BV16**, the protective effect of scavengers was very slight and non-specific; while a major increase in cellular survival was detected with **BV10**. In particular, all scavengers seemed to demonstrate a protective effect in **BV10** experiments but 80% of cell viability was assessed when the irradiation was conducted in the presence of MAN and DABCO, indicating hydroxyl radical and singlet oxygen may be involved in **BV10** phototoxicity. However, from these data, an univocal mechanism of photosensitization was not distinguished but the complexity of pyrrolo[3,4-*h*]quinolin-2-ones actions was clear.

5.4 INTRACELLULAR LOCALIZATION OF THE PHOTOSENSITIZER

The intracellular localization of the sensitizer coincides with the primary site of photodamage. Hence, the local photodamage to specific subcellular targets critically influences the mode of cell death and the activated regulatory pathways. The subcellular localization of a photosensitizer is due to its physicochemical properties such as hydrophobicity, charge, pKa, etc. For example, lysosomes are preferential sites of two fluoroquinolones such as lomefloxacin and ciprofloxacin [102], whereas mitochondria are the primary targets in PUVA therapy [103]. Moreover, a new class of analogues of the test compounds, pyrrolo[2,3-*h*]quinolinones, was found to accumulate mainly in lysosomes in our laboratory [70].

The analysis of intracellular localization of pyrrolo[3,4-*h*]quinolin-2-ones was performed using confocal and epifluorescence microscopy thanks to the fluorescence of the compounds. **BV5** was chosen as a model for this kind of test thanks to its suitable spectroscopic characteristics. Briefly, NCTC cells were incubated in the presence of 20 μM **BV5** for 1 hour. Moreover, for a co-localization analysis, we made the addition of some organelle-staining probes such as JC-1, which localized in mitochondria, or Acridine Orange (AO), which accumulated mainly in lysosomes. These probes fluoresced at 590 nm when excited at 488 nm while **BV5** fluorescence was recorded at 450 nm after an excitation at 405 nm. The fluorescences were separated using suitable band pass optical filters.

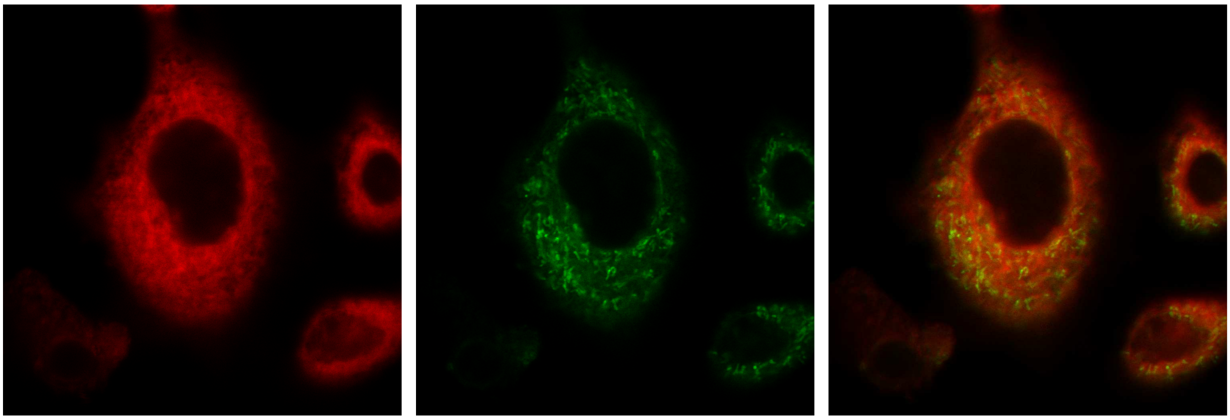

***FIG 3**:Fluorescence image of **BV5** (left panel), JC-1 (middle panel) and co-localization (right panel). These imagines were acquired with a Leica TCS SP5 confocal microscope.*

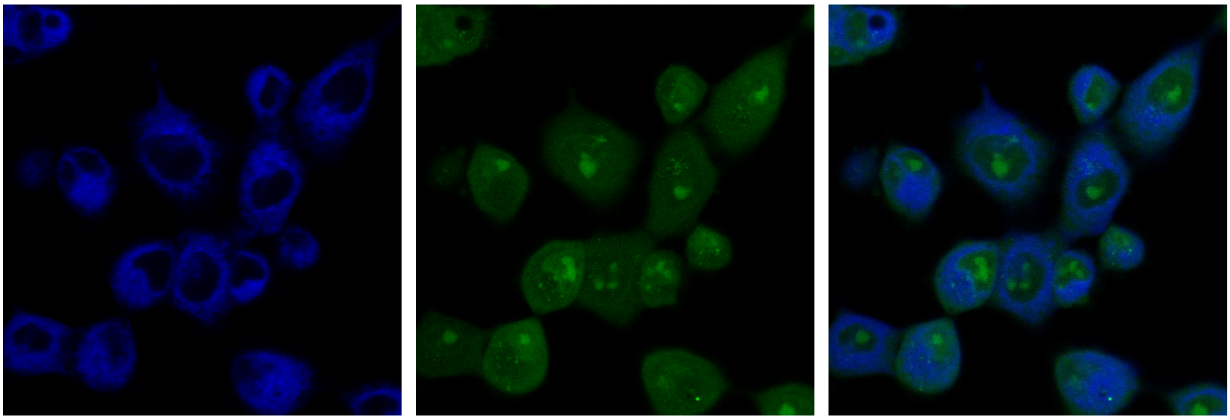

***FIG 4**:Fluorescence image of **BV5** (left panel), AO (middle panel) and co-localization (right panel). These imagines were taken with a Leica TCS SP5 confocal microscope.*

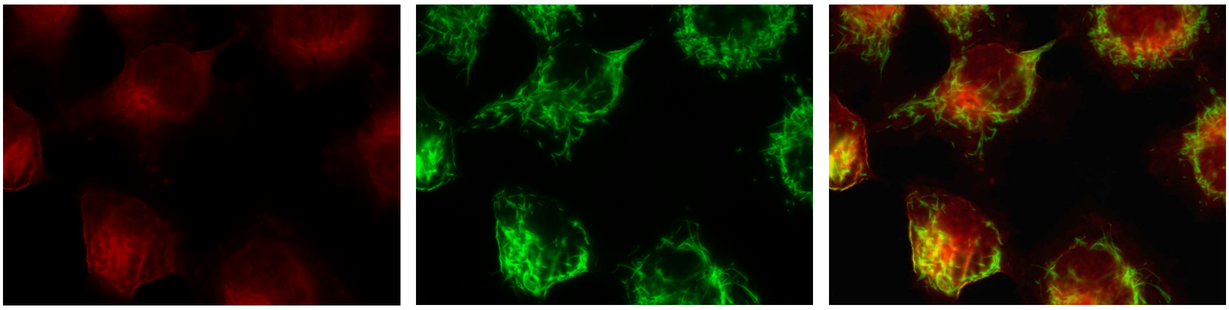

FIG 5*:Fluorescence image of* ***BV5*** *(left panel), JC-1 (middle panel) and co-localization (right panel). These imagines were acquired with Olympus IX81 microscope.*

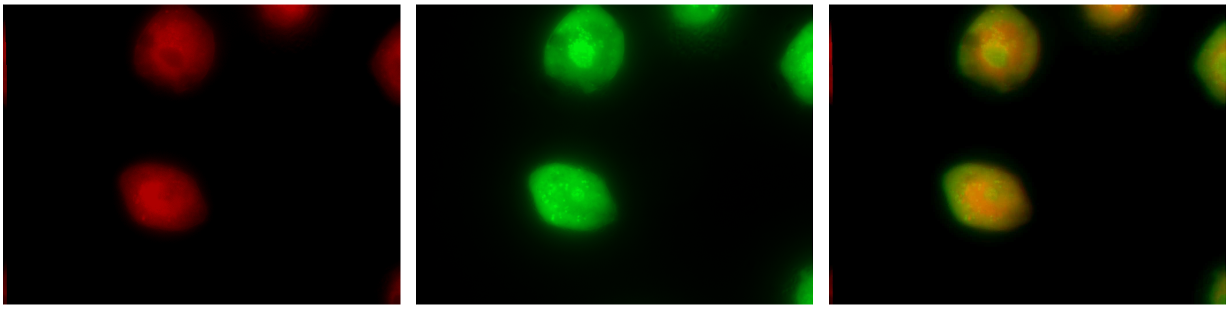

FIG 6*:Fluorescence image of* ***BV5*** *(left panel), AO (middle panel) and co-localization (right panel). These imagines were taken with Olympus IX81 microscope.*

The imagines indicated that **BV5** entered the cell and widely spread into the cytosol. A specific accumulation in a part of the cell can not be observed. As can be noted by the co-localization imagines, there is a good overlay with the fluorescence of JC-1 but a scarce overlay with the AO one. Thus, after entering the cell, **BV5** diffused in all cytosol with an accumulation in mitochondria too.

5.5 DETERMINATION OF MECHANISM OF CELLULAR DEATH

We performed Annexin-V-FITC/PI test to evaluate the mechanism of cellular death, as described in Materials and Methods section. In brief, jurkat cells were irradiated in the presence of 10 and 5 µM **BV5** and **BV10** and the analysis was conducted after 24 hours from the irradiation. Annexin-V-FITC fluorescence was detected after the translocation of PS to the outer leaflet of plasmatic membrane while PI fluorescence was index of plasmatic membrane disruption [73].

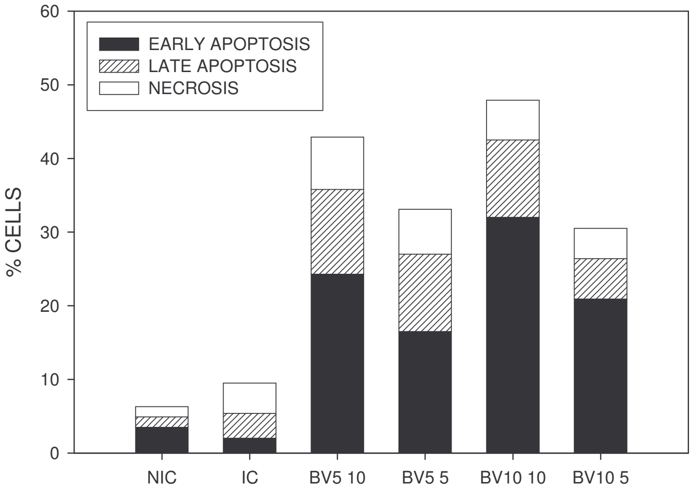

***FIG 7**: Percentage of early apoptotic cells (FITC$^+$/PI$^-$), late apoptotic cells (FITC$^+$/PI$^+$) and necrotic cells (FITC$^-$/PI$^+$) after 24 hours from the irradiation (2,5 J/cm^2) in the presence of **BV5** and **BV10** at indicated concentrations (µM). NIC = non irradiated control; IC= irradiated control. Data were expressed as Mean ± SEM of three independent experiments.*

A significant increase of early apoptotic cells was determined when the irradiation was conducted in the presence of the test compounds. A percentage of cells was positive to both the probes and this was compatible with a later stage of apoptosis. A small part of treated cells (up to 5 %) resulted necrotic but this amount was more over the same in the irradiated control. From these data, a main apoptotic pathway can be associated to the cellular death photoinduced by pyrrolo[3,4-*h*]quinolin-2-ones.

5.6 CELL CYCLE

Cell cycle analysis of cells irradiated in the presence of **BV5**, **BV10** and **BV16** were carried out to obtain more information about the mechanism of cell death. Moreover, many authors reported deep modifications in cell cycle after PUVA treatment. In particular, these changes seemed dependent on the type of cells: for example PUVA treatment induced a G1 phase arrest in NCTC while a G2-S phase block was detected in jurkat cells [103, 54]. As already seen before, this test based on the fact that in each phase of the cell cycle the DNA content is different. Thus, after fixation in ethanol, cells were stained with PI which intercalated in DNA and gave the typical fluorescence in the red region [21].

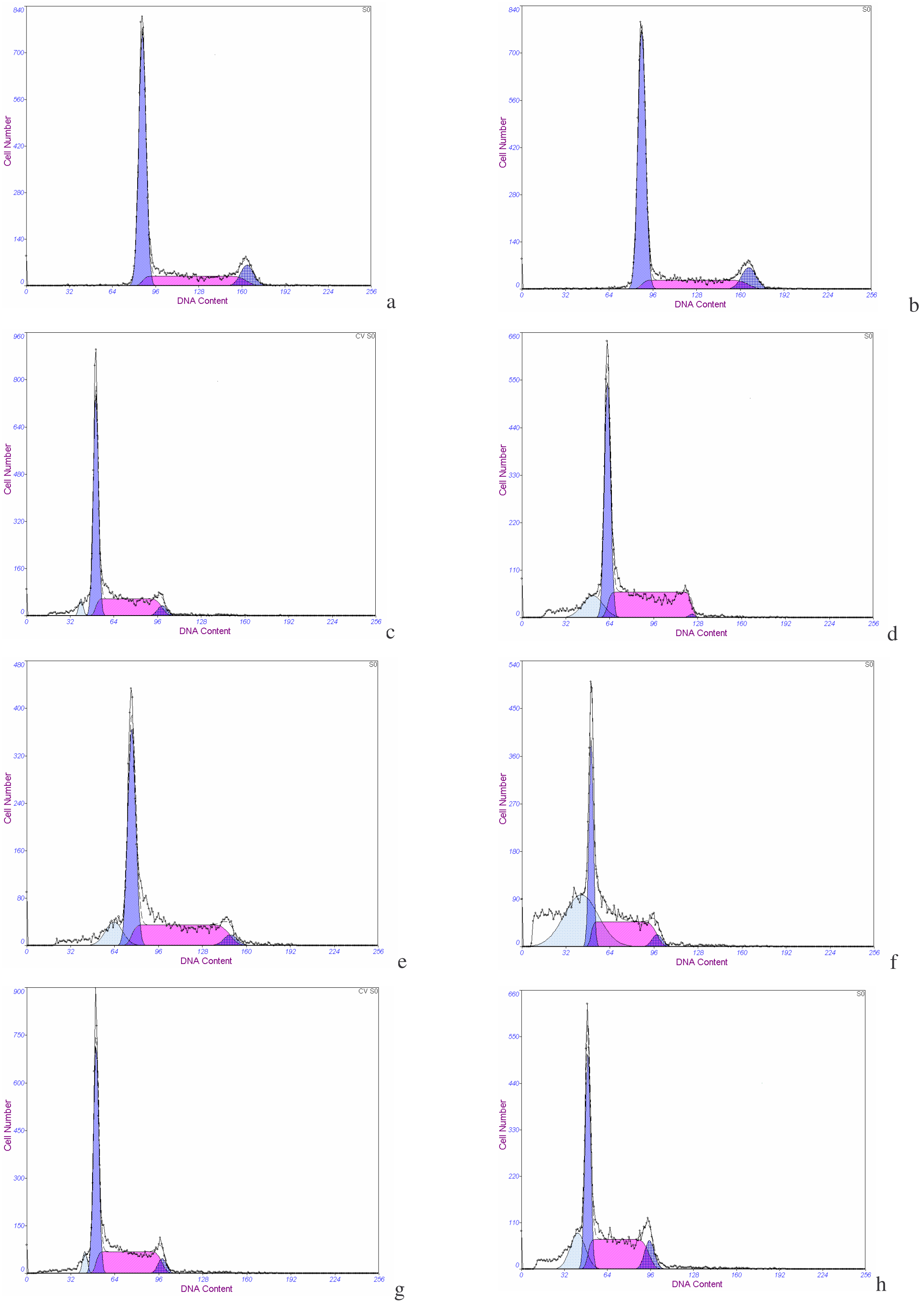

FIG 8: *Histograms of cell cycle of jurkat after 24 hours from the treatment/irradiation (2,5 J/cm^2). a= non irradiated cells; b= irradiated cells; c= 5 µM **BV5**; d= 10 µM **BV5**; e = 5 µM **BV10**; f= 10 µM **BV10**; g= 5 µM **BV16**; h= 10 µM **BV16**.*

The cell cycle modifications were summarized in table 4:

	G1 phase	**S phase**	**G2-M phase**	**subG1**
NIC	63,0	27,6	9,4	/
IC	64,4	25,3	10,3	/
BV5 5 µM	53,8	41,8	4,4	3,8
BV5 10 µM	44,8	54,4	0,8	12,5
BV10 5 µM	48,9	46,9	4,2	10,5
BV10 10 µM	39,1	55,6	5,3	43,0
BV16 5 µM	49,6	45,4	5,0	4,0
BV16 10 µM	40,1	50,4	9,5	15,9

TAB 4: *Percentage of jurkat cells in each cell cycle phase. NIC= non irradiated control; IC= irradiated control. The calculation of cell cycle did not consider subG1 percentage.*

Form these data, a little reduction of G1 cells and a small increase of cells in S-phase were detected. Nevertheless, the most important modification was the concentration-dependent onset of a subG1 peak, which represented apoptotic cells. The subG1 was a consequence of the ordered degradation of DNA which occurred during apoptosis [23]. This phenomenon is considered a later event than PS externalization, thus these data were well in agreement with the ones of the previous experiment.

5.7 DETERMINATION OF MITOCHONDRIAL MEMBRANE POTENTIAL

Continuing the study of apoptotic machinery, the involvement of mitochondria was evaluated through the determination of the mitochondrial membrane potential, as a consequence of the dysfunction of these organelles. This analysis was carried out by JC-1 flow cytometric test 24 hours after having irradiated jurkat cells in the presence of **BV5** and **BV10**. In particular, the green fluorescence was detected after collapse of mitochondrial potential while greenish-orange fluorescence was observed in cells with normal mitochondria [74].

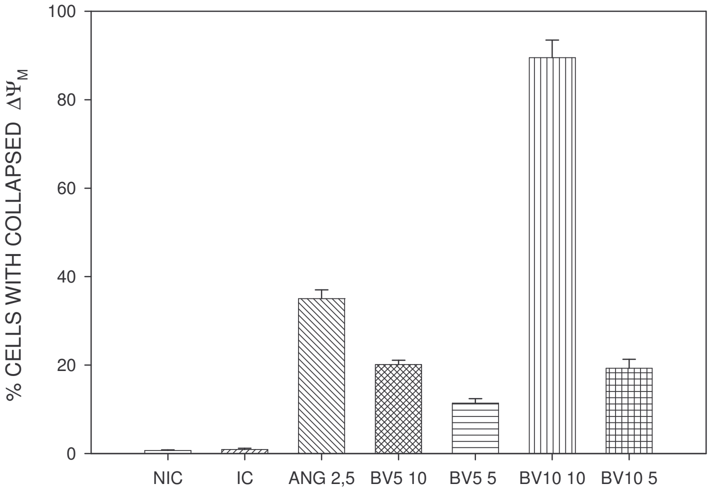

***FIG 9**: Percentage of jurkat with collapsed $\Delta\psi_M$ (fluorescence of the JC-1 monomeric form) after 24 hours from the irradiation (2,5 J/cm^2) with **ANG, BV5** and **BV10** at the indicated concentrations (µM). Data were expressed as Mean ± SEM of three independent experiments.*

A concentration-dependent increase of percentage of cells with collapsed mitochondrial potential was detected after irradiation in the presence of the test compounds. Thus, a mitochondrial involvement in inducing apoptosis can be assess.

5.8 INVOLVEMENT OF LYSOSOMES IN CELL DEATH

The involvement of another organelle such as lysosome in inducing apoptosis was examined. In fact, in addition to necrosis, the lysosomal destabilization can be associated to apoptosis: for example, the release of lysosomal hydrolytic enzymes was found to led the activation of caspase cascade or of other lytic cytosol enzymes [99].

After the irradiation in the presence of **BV5** and **BV10**, jurkat cells were assessed for lysosomal stability using AO uptake method. AO is a lysosomotropic base and a metachromatic fluorochrome exhibiting red fluorescence when highly concentrated (as is the case in intact lysosomes where AO is retained in its charged) and green fluorescence at low concentration (as is the case when some lysosomes have ruptured and AO relocates to the cytosol where it occurs predominantly in the deprotonated form) [99]. The number of cells with intact lysosomes was evaluated by assaying red fluorescence in flow cytometer after staining cells with AO.

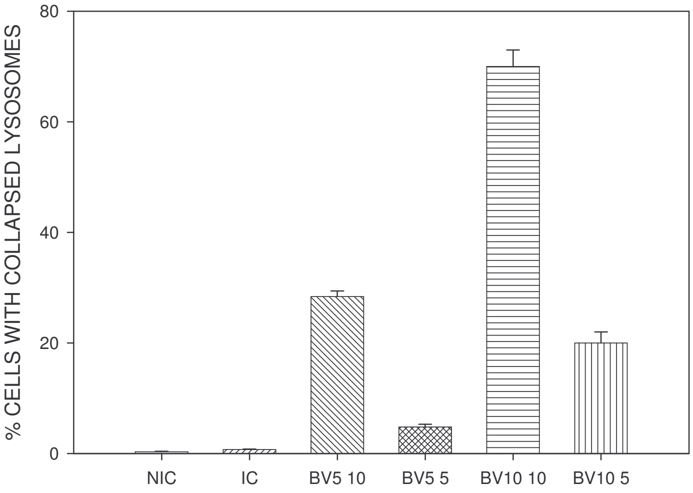

FIG 10: *Percentage of jurkat cells with damaged lysosomes after 24 h from irradiation (2.5 J/cm^2) in the presence of* ***BV5*** *and* ***BV10*** *at the indicated concentrations. NIC = non irradiated control; IC= irradiated control. Data are represented as mean S.E.M. of three experiments*

A concentration-dependent increase of lysosomal disruption was assessed after irradiation in the presence of **BV5** and **BV10**. From these data, the lysosomal dysfunction seemed to be deeply involved in the photoinducted apoptosis, although these compounds did not accumulate in these organelles. Thus, lysosomes could be involved as a consequence of the activation of apoptotic machinery.

5.9 CASPASE ACTIVATION ASSAY

As last experiment for the evaluation of apoptotic machinery, the caspase cascade activation was assessed. Our attention was focused on the participation of an effector caspase such as caspase-3, whose activation was established after PUVA treatment [100]. As described in the materials and methods section, we performed a colorimetric assay: it was based on the cleavage of the peptide substrate *N*-acetyl-Asp-Glu-Val-Asp- *p*-nitroaniline (Ac-DEVD-*p*NA) by caspase-3, resulting in the release of the *p*NA moiety, which presented an absorbance peak at 405 nm. Thus, the concentration of the *p*NA released from the substrate was calculated by the absorbance values [30].

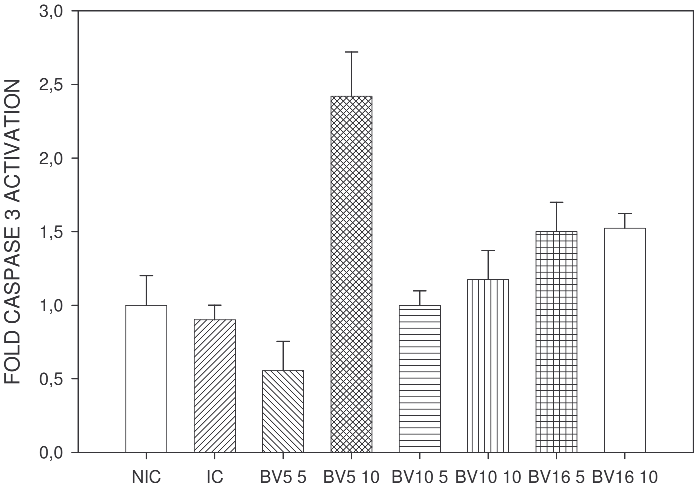

FIG 11: *Caspase-3 activation induced by* ***BV5****,* ***BV10*** *and* ***BV16****. Jurkat cells were exposed to 2.5 J/cm^2 of UV-A in the presence of different concentrations (μM) of* ***BV5****,* ***BV10*** *and* ***BV16****. After 24 h, cells were harvested and the lysates were assayed for caspase-3 activity using the caspase-3 substrate Ac-DEVD-pNA. NIC = non irradiated control; IC= irradiated control. Data were represented as fold increase of activity of the enzyme in comparison to the non-irradiated control*

Caspase-3 was marginally involved in photoinducted apoptosis by pyrrolo[3,4-*h*]quinolin-2-ones. A little activation of caspase-3 was detected and this can be due to the low sensitivity of the method. However, a lot of caspase-independent apoptosis were described in literature [104, 105].

5.10 DNA INTERACTION

DNA is considered the main cellular target for antiproliferative activity of psoralens and angelicins. Furocoumarins are able to intercalate between nucleic acids bases and after UV activation, they can induce photocycloaddition to pyrimidinic bases [38].

5.10.a DNA BINDING

In order to understand the binding nature between the title compounds and DNA, linear dichroism (LD) measurements were performed on solutions with salmon testes DNA (st-DNA) and the title compounds at various molar ratios. This technique allows to obtain interesting information about the nature of the binding between DNA and a compound [89], as already described in 3–methoxy-5H-isoindolo[2,1-*a*]quinoxalin-6-one section.

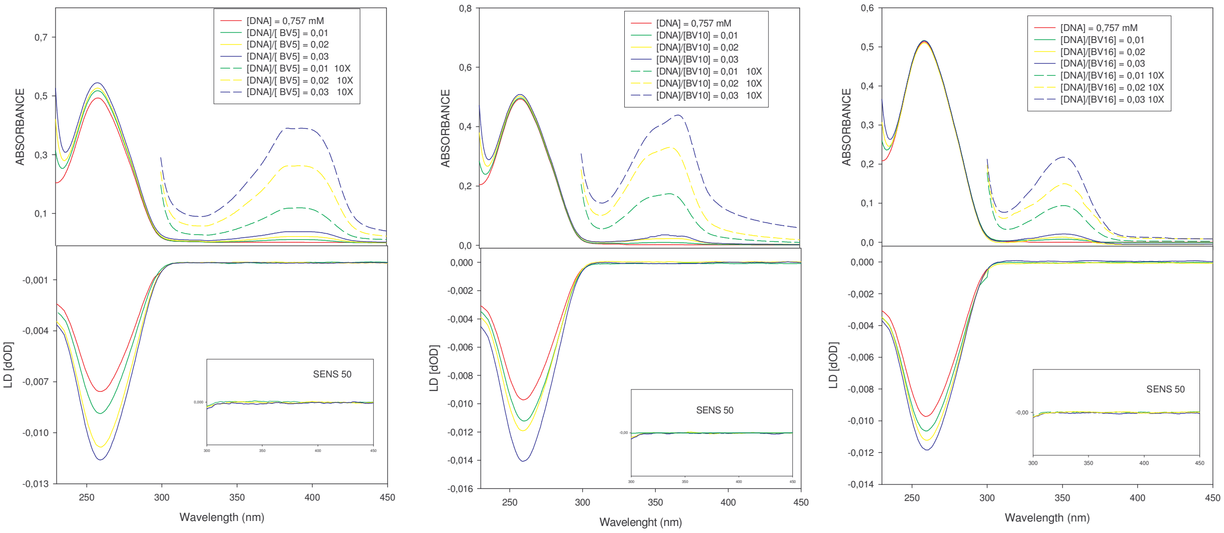

FIG 12: *Absorbance (upper panel), linear dichroism LD (lower panel) of mixtures of st-DNA and* ***BV5*** *(left panel),* ***BV10*** *(medium panel) and* ***BV16*** *(right panel) at different [drug]/[DNA] ratios (0; 0,01; 0,02; 0,03) in phosphate buffer pH = 7,2.*

Investigation of the LD spectra of three derivatives (**BV5**, **BV10** and **BV16**) in the presence of st-DNA revealed that, despite a strong absorption in the 300 450 nm region, they gave no LD bands in this region. These observations strongly suggested that the new derivatives did not interact efficaciously without irradiation with the macromolecule, as indeed demonstrated with natural furocoumarins.

5.10.b DNA PHOTODAMAGE

Even if pyrrolo[3,4-*h*]quinolin-ones did not display a high affinity for DNA, further experiments were carried out in order to determine whether the new derivatives were able to photosensitize DNA strand break activity. Their ability to photodamage DNA was evaluated using supercoiled circular DNA because it allowed the detection of structural alterations such as strand breaks. Double-stranded supercoiled (SC or I form) plasmid is sensitive to damage by a variety of photosensitizers [106]. Cleavage of one strand produces a relaxed, but still double-stranded, open circular (OC or II form) DNA. Further cleavage of the other strand within a short distance of the first site of cleavage generates a linear (L or III form) DNA.
The irradiation of supercoiled plasmid pBR322 was conducted in the presence of various rate [DNA]/[BV]. DNA samples were resolved by an electrophoretic run in agarose 1% gel thanks to the different hydrodynamic properties of the plasmidic forms.

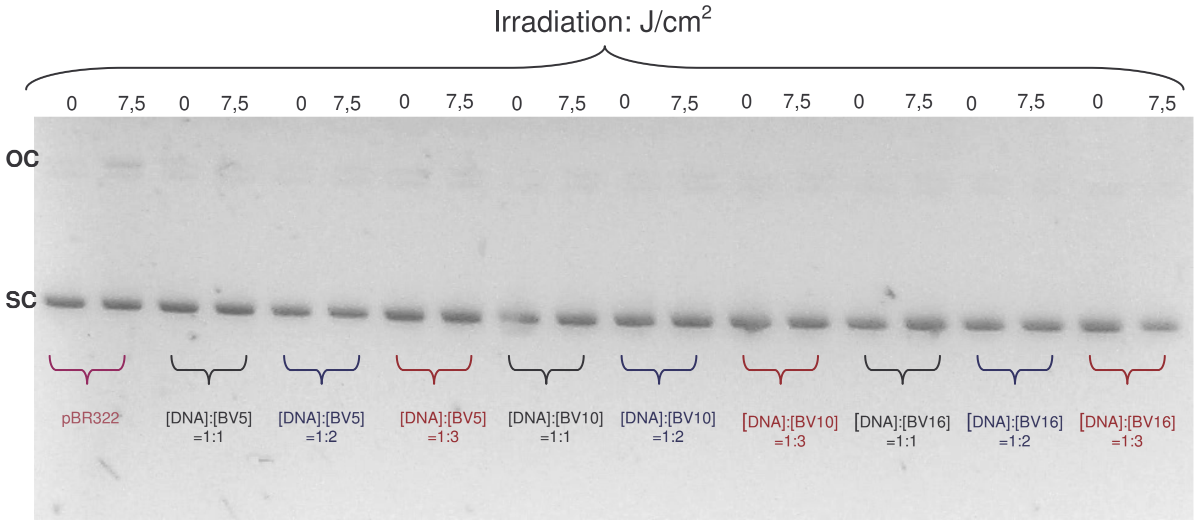
Irradiation: J/cm2
0
7,5
0
7,5
0
7,5
0
7,5
0
7,5
0
7,5
0
7,5
0
7,5
0
7,5
0
7,5
OC
SC
pBR322
[DNA]:[BV5] =1:1
[DNA]:[BV5] =1:2
[DNA]:[BV5] =1:3
[DNA]:[BV10] =1:1
[DNA]:[BV10] =1:2
[DNA]:[BV10] =1:3
[DNA]:[BV16] =1:1
[DNA]:[BV16] =1:2
[DNA]:[BV16] =1:3

FIG 13: *DNA strand breaks photoinduced by pyrrolo[3,4-h]quinolin-2-ones. Supercoiled circular pBR322 was irradiated (7,5 J/cm^2) in the presence of different ratio [DNA]/[BV] and then treated as described in materials and methods.*

The results pointed out that the new compounds did not provoke any formation of open circular or linear bands, indicating they did not sensitize single strand breaks.

In addition to frank strand breaks, the oxidative damage of purine and/or pyrimidine bases was also evaluated using the base excision repair enzymes Formamido pyrimidin glycosilase (Fpg) and Endonuclease III (Endo III), respectively. DNA strand breaks can be induced either directly (frank strand breaks) or indirectly using DNA repair enzymes. Fpg demonstrated to recognize 8-hydroxy guanine, purines whose imidazole ring was open (Fapy residues) and sites of base loss (apurinic sites). Endonuclease III recognized 5,6-dihydropyrimidine derivatives, in addition to apurinic sites. Damaged base recognition was followed by an elimination step, resulting in DNA breakage [106].

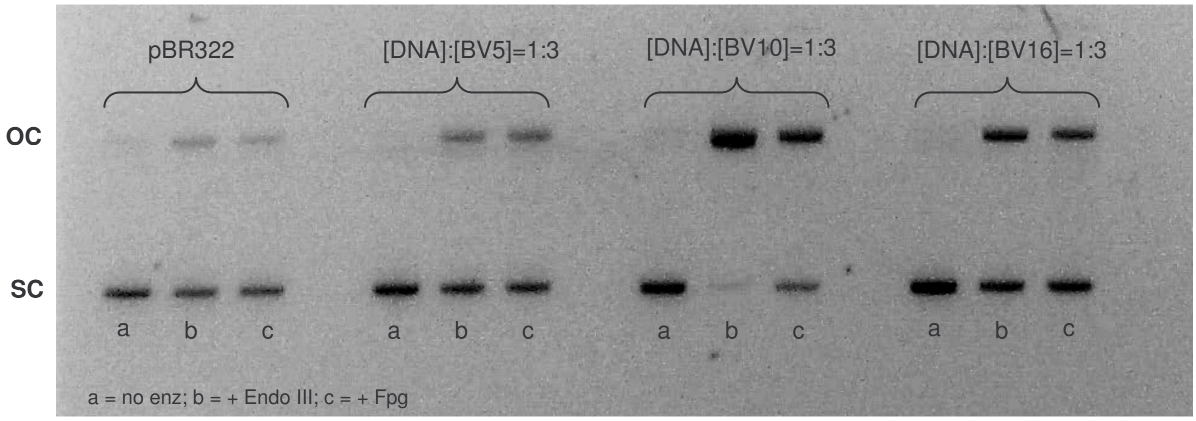
pBR322
[DNA]:[BV5]=1:3
[DNA]:[BV10]=1:3
[DNA]:[BV16]=1:3
OC
SC
a
b
c
a
b
c
a
b
c
a
b
c
a = no enz; b = + Endo III; c = + Fpg

FIG 14: *DNA base modifications photoinduced by pyrrolo[3,4-h]quinolin-2-ones. Supercoiled circular pBR322 was irradiated (3,75 J/cm^2) in the presence of [DNA]/[BV]=1/3 and then treated with base excision enzyme. a = no enzyme; b = + Endo III; c = + Fpg.*

Thus, after the irradiation in the presence of **BV5**, **BV10** and **BV16**, pBR322 was incubated with Fpg or Endo III at 37°C for 30 min. Then, DNA samples were resolved by electrophoretic run as described in Material and Methods section.

The treatment with the two base excision enzymes revealed that they were able to photooxidize DNA bases in a great amount. The percentages of OC form were calculated as suggested by *Ciulla et al.* [107] and were summarized in fig 15:

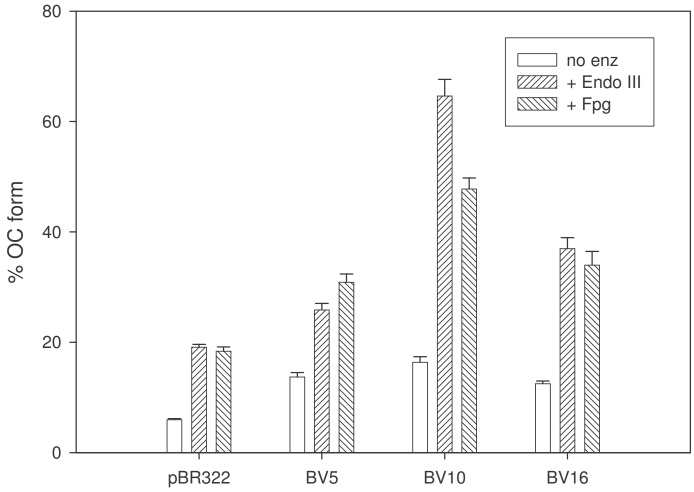

FIG 15: *Percentage of II form after irradiation (3,75 J/cm^2) in the presence of* ***BV5****,* ***BV10*** *and* ***BV16*** *at the ratio [DNA]/[BV]=1/3. Prior to the electrophoretic run , pBR322 was treated with base excision enzymes.*

All compounds were able to photoinduce base oxidation but **BV10** resulted the most active especially in the presence of Endo III, indicating pyrimidinic bases were its preferential targets (in fact the SC band was practically disappeared).

To better understand the mechanism of base photooxidation, the irradiation of pBR322 was conducted in the presence of **BV10** and some reactive species scavengers. We used MAN, a hydroxyl radical scavanger, DABCO, which protected from the generation of singlet oxygen, and GSH, a free radical scavenger.

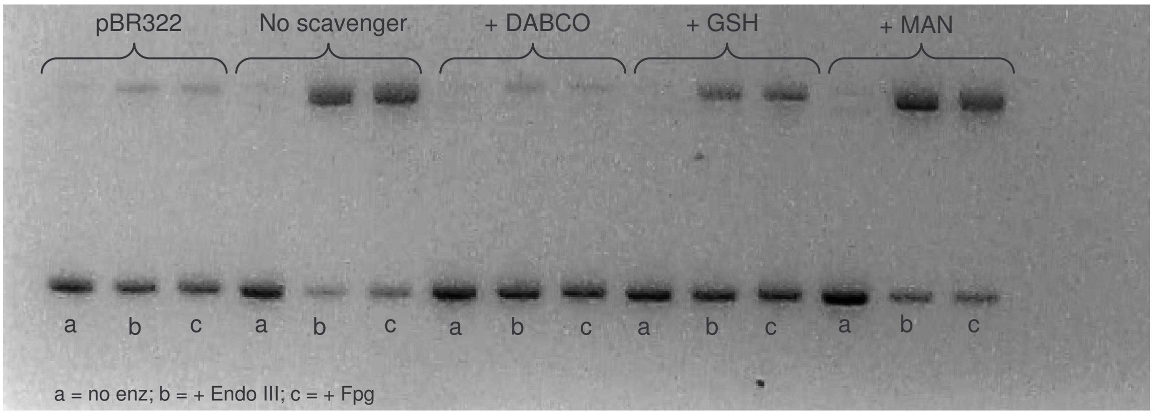
pBR322
No scavenger
+ DABCO
+ GSH
+ MAN
OC
SC
a b c a b c a b c a b c a b c
a = no enz; b = + Endo III; c = + Fpg

FIG 16: *DNA base modifications photoinduced by* ***BV10*** *in the presence of some scavengers: DABCO, GSH and MAN. Supercoiled circular pBR322 was irradiated (3,75 J/cm*^{2}*) in the presence of [DNA]/[****BV10****]=1/3 and then treated with base excision enzyme. a = no enzyme; b = + Endo III; c = + Fpg.*

The percentages of OC form were reported in fig 17:

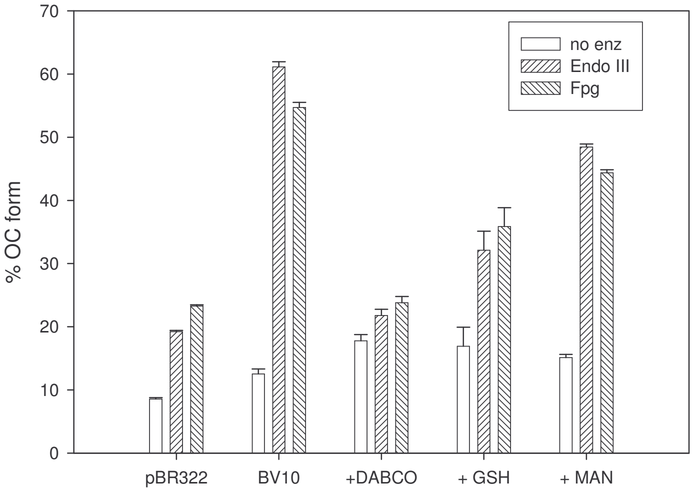

FIG 17: *Percentage of II form after irradiation (3,75 J/cm*^{2}*) in the presence of* ***BV10*** *at the ratio [DNA]/[BV]=1/3 and scavengers. Prior to the electrophoretic run , pBR322 was treated with base excision enzymes.*

A little reduction in the formation of II form was observed when irradiation was conducted with GSH and MAN. While, in the presence of DABCO, the oxidations photoinduced by **BV10** were not detected, suggesting an involvement of singlet oxygen in photosensitization reaction. As DABCO is not absolutely specific toward singlet oxygen, these data were confirmed by irradiation in presence of D_2O buffer (data not shown).

In conclusion, pyrrolo[3,4-*h*]quinolin-2-ones did not sensitize the formation of single strand breaks but after the treatment with the two base excision enzymes they were able to photooxidize DNA bases. **BV10** resulted the most active compound and the photoxidation seemed to be caused by singlet oxygen formation.

5.11 LIPID PEROXIDATION

Like nucleic acids and proteins, unsaturated lipids, glycolipids and cholesterol are important targets of $^1O_2$ or free radical attack in cells subjected to photooxidative stress. That photodamage develops as lipid peroxidation. This phenomenon is initiated by the attack of any chemical species that has sufficient reactivity to abstract a hydrogen atom from a methylene carbon in the side chain. The hydrogen atom is a free radical and its removal leaves behind an unpaired electron on the carbon to which it was originally attached. That new radical can give a peroxyl radical after the reaction with oxygen. Peroxyl radicals can combine each other or they can attack membrane proteins , but also are capable of abstracting hydrogen from adjacent fatty acid side chains in a membrane and so propagating the chain reaction of lipid peroxidation [108].

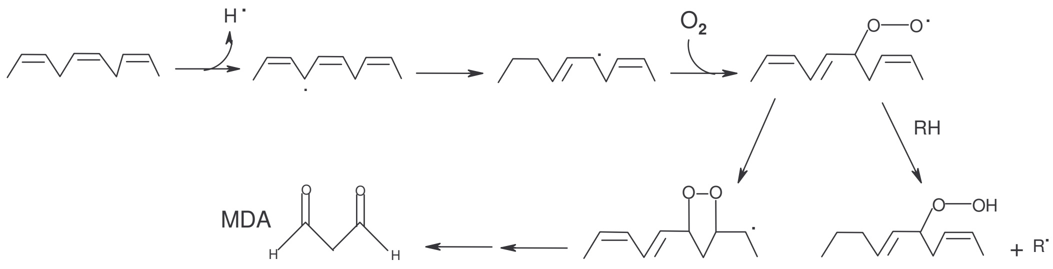

FIG 18: *Schematic representation of lipidic peroxidation*

Membrane lipids may be a central site of photodamage if sensitizing agents localize in the membrane bilayer. Being hydrophobic, as their partition coefficients indicated (see Table 1), pyrrolo[3,4-*h*]quinolin-2-ones may be expected to be localized mainly in plasmatic and/or in subcellular membranes, making these structures particularly sensitive to photodamage.

The thiobarbituric assay (TBA test) was used in order to determine a potential lipid peroxidation after irradiation of jurkat cells in the presence of test compounds. The TBA test was performed as described in the experimental section. In brief, this assay used the reaction of one molecule of malondialdehyde (MDA), which is a secondary product of lipid peroxidation, with two molecules of TBA, forming a pink chromogen. Thus, the resulting chromogen was monitored by fluorescence at 553 nm [109].

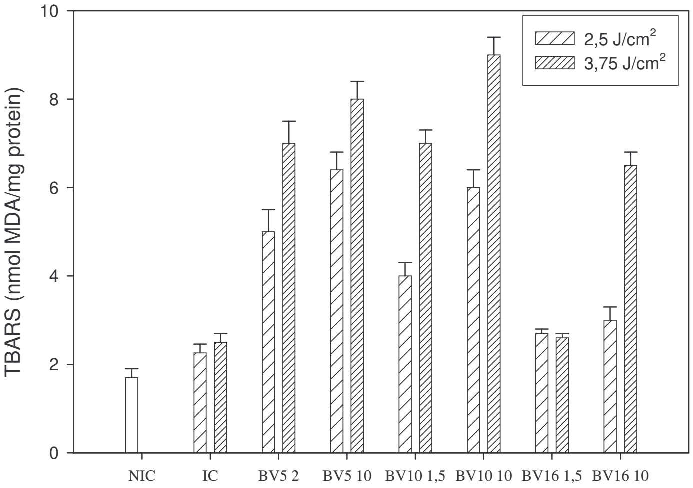

FIG 19: *Lipid peroxidation in jurkat cells after 24 hours from the irradiation (2,5 and 3,75 J/cm^2) in the presence of* ***BV5****,* ***BV10*** *and* ***BV16*** *at the indicated concentrations (μM). NIC = non irradiated control; IC= irradiated control. Data are represented as mean S.E.M. of three experiments*

Figure 19 showed the results obtained for compounds **BV5**, **BV10** and **BV16** as a function of light doses. Thiobarbituric reactive substances (TBARS) were significantly produced in a concentration-dependent manner when the cells were exposed to the compounds and UV-A. A good correlation was observed between the extent of lipid peroxidation and the hydrophobic character of pyrrolo[3,4-*h*]quinolin-2-ones.

5.12 CONCLUSIONS

Pyrrolo[3,4-*h*]quinolin-2-ones were synthesized in Palermo University as new potential photochemiotherapics with minor side effects than psoralens. In fact, they are analogues of angular furocoumarins whose oxygens were substituted with nitrogen atoms.

After assessing their non-cytotoxicity, several pyrrolo[3,4-*h*]quinolin-2-ones demonstrated to be phototoxic in many human tumour cell lines, after UV-A irradiation (2,5 and 3,75 J/cm^2). Three compounds, **BV5**, **BV10** and **BV16**, resulted the most active after UV irradiation, reaching submicromolar IC$_{50}$ in most cell lines. Starting from these three molecules, a relationship between structure and activity was hypothesised. In brief, for compounds with the carbonyl in 2, –COOEt group in 7 and the presence of a substituent in 8 seemed important for phototoxicity; while the molecules with a methoxyl group in 2 demonstrated an interesting activity.

Through confocal and epifluorescence microscopy, the cellular localization of pyrrolo[3,4-*h*]quinolin-2-ones was determined to observe where the first photodamages occurred. Thanks to their high hydrophobic character, they easily entered the cell and diffused in the cytosol but they did not accumulate into a specific organelle.

An evaluation of the kind of photoinduced cell death was performed using flow cytometry. We found that pyrrolo[3,4-*h*]quinolin-2-ones induced cell death by apoptosis through Annexin-V-FITC/PI test, which allowed to verify an early apoptotic event such as the exposure of a phagocytosis signal. These data were confirmed by the analysis of cell cycle in irradiated cells, where a subG1 peak, index of apoptotic DNA degradation, was observed in the presence of these compounds. The involvement of mitochondria and lysosomes in inducing cell death was assessed through a series of cytofluorimetric analysis (determination of mitochondrial membrane potential and AO-uptake method).

A potential interaction with DNA was investigated, as this biomolecule represents an important target for antiproliferative activity of PUVA. Pyrrolo[3,4-*h*]quinolin-2-ones did not demonstrate high affinity for DNA. Moreover, through a series of plasmidic DNA photocleavage experiments, the formation of frank strand breaks was not assessed but a large number of base oxidation was observed probably because of the production of singlet oxygen.

Pyrrolo[3,4-*h*]quinolin-2-ones were found to provoke membrane lipid peroxidation and the degree of this oxidation depended on the UV-A dose but also on the concentration and the hydrophobic degree of compounds.

The high antiproliferative activity after UV irradiation was similar to that of 8-MOP while the lack of affinity of the new compounds with DNA could be of great relevance in modulating the long-term toxic effect such as skin cancer or mutagenesis exhibited by psoralen.

6. MATERIALS AND METHODS

6.1 MATERIALS

- **Compounds**: the following compounds, synthesized by Cirrincione's group in "Dipartimento Farmacochimico, Tossicologico e Biologico" of University of Palermo, were analyzed:
    - **L1**: 8-methyl-7-phenyl-5,6-dihydro-2H-thiopyrano[2,3-*e*]indol-2-one.
    - **L2**: 8-methyl-7-phenyl-2H-thiopyrano[2,3-*e*]indol-2-one.
    - **L3**: 7,8-dimethyl-2H-thiopyrano[2,3-*e*]indol-2-one.
    - **L4**: 7-benzyl-8-methyl-5,6-dihydro-2H-thiopyrano[2,3-*e*]indol-2-one.
    - **L5**: 7-Benzenesulfonyl-8-methyl-5,6-dihydro-2H-thiopyrano[2,3-*e*]indol-2-one.
    - **L6**: 7,8-dimethyl-5,6-dihydro-2H-thiopyrano[2,3-*e*]indol-2-one.
    - **BV1**:3-Benzenesulfonyl-8-methyl-5,8-dihydro-1H,6H-pyrrolo[3,4-*h*]quinolin-2-one.
    - **BV2**: 3 -Benzenesulfonyl-8,9 -dimethyl-2 -oxo-2,5,6,8 -tetrahydro-1H-pyrrolo[3,4-*h*] quinoline-7-carboxylic acid ethyl ester.
    - **BV3**: 3-Benzenesulfonyl-8,9-dimethyl-5,8-dihydro-1H,6H-pyrrolo[3,4-*h*]quinolin-2-one.
    - **BV4**: 3-Benzenesulfonyl-8-phenyl-5,8-dihydro-1H,6H-pyrrolo[3,4-*h*]quinolin-2-one
    - **BV5**: 3 -Benzenesulfonyl-8 -benzyl-9 -methyl-2 -oxo-2,5,6,8 -tetrahydro-1H-pyrrolo [3,4-*h*] quinoline-7-carboxylic acid ethyl ester.
    - **BV6**: 3 -Benzenesulfonyl-8 -benzyl-9 -methyl-5,8 -dihydro-1H,6H -pyrrolo[3,4-*h*] quinolin-2-one.
    - **BV7**: 3-Benzenesulfonyl-8-benzyl-5,8-dihydro-1H,6H-pyrrolo[3,4-*h*]quinolin-2-one.
    - **BV8**: 3 -Benzenesulfonyl-9 -methyl-2 -oxo- 2,5,6,8 -tetrahydro-1H -pyrrolo[3,4-*h*] quinoline-7-carboxylic acid ethyl ester.
    - **BV9**: 3 -Benzenesulfonyl-1,9 -dimethyl-2 -oxo-2,5,6,8 -tetrahydro-1H-pyrrolo[3,4-*h*] quinoline-7-carboxylic acid ethyl ester.
    - **BV10**: 3- Benzenesulfonyl- 1,8,9 -trimethyl- 2 – oxo - 2,5,6,8 – tetrahydro - 1H-pyrrolo[3,4-*h*] quinoline-7-carboxylic acid ethyl ester.
    - **BV11**: 3 -Benzenesulfonyl-8 -benzyl-1,9 -dimethyl-2 -oxo-2,5,6,8 -tetrahydro-1H-pyrrolo[3,4-*h*] quinoline-7-carboxylic acid ethyl ester.

  - **BV12**: 3 -Benzenesulfonyl-8 -benzyl-1 -methyl-5,8 -dihydro-1H,6H -pyrrolo[3,4-*h*] quinolin-2-one.
  - **BV13**: 3 – Benzenesulfonyl -1,8- dimethyl -5,8 – dihydro -1H,6H- pyrrolo[3,4-*h*] quinolin -2-one.
  - **BV14**: 3-Benzenesulfonyl- 1-methyl- 8-phenyl- 5,8-dihydro- 1H,6H- pyrrolo[3,4-*h*] quinolin-2-one.
  - **BV15**: 3 –Benzenesulfonyl –8– benzyl -2- methoxyl -2,5,6,8- tetrahydro -1H-pyrrolo[3,4-*h*] quinoline.
  - **BV16**:3-Benzenesulfonyl-8-methyl-2-methoxyl-2,5,6,8-tetrahydro-1H-pyrrolo[3,4-*h*] quinoline.
  - **BV18**: 3 -Benzenesulfonyl- 8- methyl- 2- oxo- 2,5,6,8- tetrahydro- 1H-pyrrolo[3,4-*h*] quinoline-7-carboxylic acid.
  - **BV19**: 3 -Benzenesulfonyl-8,9 -dimethyl-2 -oxo-2,5,6,8 -tetrahydro-1H -pyrrolo[3,4-*h*]quinoline-7-carboxylic acid.
  - **BV20**: 3-Benzenesulfonyl-8 -benzyl-9 -methyl-2 -oxo-2,5,6,8-tetrahydro-1H-pyrrolo [3,4-*h*]quinoline-7-carboxylic acid.
  - **ISQ3**: 3-Methoxy-5H-isoindolo[2,1-*a*]quinoxalin-6-one.

- UV-Vis double beam instrument Lambda 12 and LS50B fluorimeter, Perkin Elmer (MA,USA); J810A and J500A spectropolarimeter, Jasco (Cremella, IT); microtiter plate reader, BIO RAD (Milano Italy); fluorescence microplate reader Fluoroskan Ascent FL Labsystems (Milano, Italy).
- HPW 125 lamps, Philips (Eindhoven, The Netherlands) and Cole-Parmer Instrument Company radiometer (IL, USA), equipped with a 365-CX sensor.
- RPMI 1640 medium, HAM'S (Nutrient Mixture F-12 HAM), DMEM (Dulbecco's Modified Eagle's Medium) and Penicillin-Streptomycin solution, Sigma Aldrich (Milano, Italy); foetal bovine serum, Invitrogen (Milano, Italy).
- MTT (3-[4,5-dimetiltiazol-2yl]-2,5-difenil tetrazolium bromide), Sigma Aldrich (IT).
- DABCO (1,4 diazabicyclo [2,2,2] octane), Acros Organics (N.J., USA); BHA (2,6-di-tert-butylhydroxyanisole), DMTU (N-N' dimethyl thiourea), GSH (reduced glutathione) and NaN_3 (sodium azide), MAN (mannitol), Sigma Aldrich (IT).
- Confocal microscope Leica TCS SP5 (Mannheim, Germany), Olympus IX81 fluorescent microscope (USA).
- Epics XL-MCL flow cytometer, Cytomics FC500 cytofluorimeter and FACS Vintage, Becton Dickinson (NY,USA).

- Annexin-V-FLUOS Staining Kit, Roche (Penzberg, Germany), JC-1 (5,5’,6,6’tetrachlo-1,1’,3,3’-tetraethylbenzimidazol-carbocyanine), HE (hydroethidine) DCFDA (dihydrochlorofluorescein-diacetate), NAO (10-N-nonyl-acridine orange) and mBBr (monobromobimane), Molecular Probes Eugene (OR, USA); AO (acridine orange), Sigma Aldrich (IT).
- FITC-DEVD-fmk, FITC-IETD-fmk and FITC-LEDH-fmk, Bender Medsystem (USA); Caspase-3 colorimetric assay kit, Sigma Aldrich (IT).
- Microtubule polymerization assay kit Cytoskeleton (Denver, USA), DAPI (4',6-diamidino-2-phenylindole), Sigma Aldrich (IT).
- Ethidium bromide, agarose, tris(hydroxymethyl)aminomethane, EDTA, dithiothreitol, bromophenol blue, sodium dodecyl sulfate, proteinase K, BSA (bovine serum albumin) and human topoisomerase II, Sigma Aldrich (IT); glycerol, Carlo Erba (Milano, ITALY); human topoisomerase I, Calbiochem (Nottingham, UK); plasmid pBR322, Fermentas (Burlington, Canada).
- Image analyser software Quantity One, BIO RAD (IT).
- Digital photocamera Kodak DC256.

6.2 METHODS

6.2.a SPECTROPHOTOMETRIC DETERMINATIONS

All spectrophotometric measures were performed using UV-Vis Perkin Elmer instrument (Lambda12, double beam). For all the compounds, absorption spectra, molar extinction coefficients (ε) and determination of maxima peaks (λ_{max}) were carried out both in DMSO and phosphate buffer (10 mM and pH=7,2).

Solubility of all molecules in aqueous medium was determined through the construction of a calibration curve by spectrophotometer method in the range of concentration used for experiments.

6.2.b SPECTROFLUORIMETRIC DETERMINATIONS

Fluorimetric spectra were recorded in phosphate buffer or in DMSO by a Perkin Elmer LS50B fluorimeter.

6.2.c IRRADIATION PROCEDURES

HPW 125 Philips lamps, mainly emitting at 365 nm, were used for irradiation experiments. The spectral irradiance of the source was 4,0 mW cm^{-2} as measured, at the sample level, by a Cole-Parmer Instrument Company radiometer (Niles, IL), equipped with a 365-CX sensor.

6.2.d CELL CULTURES

For experiments of cellular viability, various human cell lines were used: HL-60, Jurkat, K-562, CEM, CEM^{vin100}, LoVo, LoVo^{doxo}, NCTC-2544, MCF-7, MCF-7^{MDR}, A-549, HT-1080.
HL-60 were promyelocytic leukaemia cells taken in a woman of 35 years in 1976. They were grown in RPMI 1640 medium supplemented with 115 units/ml of penicillin G, 115 µg/ml streptomycin and 10% heat-inactivated foetal bovine serum (complete RPMI 1640 medium). Cells were kept at 37°C in 5% CO_2 humidified atmosphere and re-seeded into fresh medium three times a week.
Jurkat were human lymphoblastoid cells taken in 14 years old boy in 1976. They were grown in complete RPMI 1640 medium. Cells were kept at 37°C in 5% CO_2 humidified atmosphere and re-seeded into fresh medium three times a week.
K-562 were obtained by a 53 year old woman with chronic myelogenous leukemia in terminal blast crisis. Cells were kept at 37°C in 5% CO_2 humidified atmosphere and re-seeded into fresh medium (complete RPMI) three times a week.
CEM were human lymphocyte T leukaemia cells taken in a 4-years old child. Cells were kept at 37°C in 5% CO_2 humidified atmosphere and re-seeded into fresh medium (complete RPMI) three times a week.
CEM^{vin100} were a multidrug-resistant line selected against vinblastine and expressing the 170-kD-P-glycoprotein [93]. Cells were kept at 37°C in 5% CO_2 humidified atmosphere and re-seeded into fresh medium (complete RPMI), supplemented with vinblastine (0,1 µg/ml), three times a week.
LoVo were human intestinal adenocarcinoma taken in a 56 years old man in 1971. LoVo were grown in HAM'S F12 medium, supplemented with 115 units/ml of penicillin G, 115 µg/ml streptomycin and 10% heat-inactivated foetal bovine serum (complete HAM'S medium). Cells were kept at 37°C in 5% CO_2 humidified atmosphere, trypsinized and re-seeded into fresh medium twice a week.

LoVo^{doxo} were doxorubicin resistant subclone of LoVo cells [94]. They were grown in complete HAM'S F12 medium supplemented with doxorubicin (0,1 µg/ml).

NCTC-2544 were human immortalized keratinocytes, they were grown in DMEM medium supplemented with 115 units/ml of penicillin G, 115 µg/ml streptomycin and 10% heat-inactivated foetal bovine serum (complete DMEM medium). Cells were kept at 37°C in 5% CO_2 humidified atmosphere, trypsinized and re-seeded into fresh medium twice a week.

MCF-7 were human breast adenocarcinoma cells. They were grown in complete DMEM medium. Cells were kept at 37°C in 5% CO_2 humidified atmosphere, trypsinized and re-seeded into fresh medium once a week.

MCF-7^{MDR} were human mammary carcinoma exhibiting multi-drug resistance for Pgp expression [94]. They were grown in complete DMEM medium supplemented with doxorubicin (0,1 µg/ml).Cells were kept at 37°C in 5% CO_2 humidified atmosphere, trypsinized and re-seeded into fresh medium once a week.

A-549 derived from a non-small cell lung cancer. They were grown in complete DMEM medium. Cells were kept at 37°C in 5% CO_2 humidified atmosphere, trypsinized and re-seeded into fresh medium twice a week.

HT-1080 derived from a human fibrosarcoma. They were grown in complete DMEM medium. Cells were kept at 37°C in 5% CO_2 humidified atmosphere, trypsinized and re-seeded into fresh medium twice a week.

6.2.e CELLULAR CYTOTOXICITY AND PHOTOTOXICITY

Individual wells of a 96-well tissue culture microtiter plate were inoculated with 100 µl of complete medium containing $5x10^3$ cells. Plates were harvested at 37 °C in a humidified 5% CO_2 incubator for 24 hours prior to the cell viability experiments. Drugs were dissolved in DMSO and then were diluted with Hank's Balanced Salt Solution (HBSS pH=7,2) for phototoxicity experiments or in the appropriated complete medium for the cytotoxicity ones.

In cytotoxicity tests after medium removal, 100 µl of the drug solution at different concentration were added to each well and incubated at 37 °C for 72 hours.

In phototoxicity experiments after medium removal, 100 µl of the drug solution were put into each well and incubated at 37 °C for 30 minutes and then irradiated (2,5 and 3,75 J/cm^2). After irradiation, drug solution was replaced by cellular medium and plates were incubated for 72 hours.

After the period of incubation, in both cases cell viability was assayed by the MTT [(3-(4,5-dimethylthiazol-2-yl)-2,5 diphenyl tetrazolium bromide)] test [72, 110]. In each well, 10 µl of MTT (5 mg/ml in PBS[1]) were added and plates were put in incubator for 3 or 4 hours. MTT is a yellow dye that can be absorbed by viable cell and reduced by mitochondrial dehydrogenases, producing insoluble blue crystals. After incubation, crystals were solubilized adding 100 µl of 0,08 N HCl in isopropanol and plates were detected through microplate Biorad reader at 570 nm. The absorbance of each sample was corrected by instrument which subtracted the mean value of blanks, i.e. wells in which there were all the reactives except cells.

The absorbance is proportional to cellular viability, so the cellular survival was calculated by this equation:

$$\% \text{ cell survival} = \frac{A_{100\%} - A_{\text{sample}}}{A_{100\%}}$$

$A_{100\%}$ = mean of controls, i.e. cells without drug nor irradiation exposure, which represents 100% of survival.

A_{sample} = absorbance of various samples in which cells were in contact with drug or irradiated in presence of drug.

For every cellular line, GI_{50}[2] was measured through SigmaPlot software.

In phototoxicity experiments, the protective effect of some scavengers was also evaluated: reduced glutathione (GSH, 1mM in PBS), 2,6-di-tert-butylhydroxyanisole (BHA, 10 µM in ethanol), N-N’ dimethyl thiourea (DMTU, 1 mM in ethanol), mannitol (MAN, 10 mM in PBS), 1,4 diazabicyclo[2,2,2]octane (DABCO, 1 mM in PBS), sodium azide (NaN_3, 1 mM in PBS). Each experiment was repeated at least three times.

6.2.f INTRACELLULAR LOCALIZATION OF THE PHOTOSENSITIZER

Intracellular localization of the photosensitizer was performed through microscopy, when possible, using the compound natural fluorescence. NCTC-2544 were grown on sterile 24mm cover slips and incubated with the test compound for one hour. Then, slips were washed in HBSS three times and analysed by confocal and epifluorescence microscopy. For subcellular co-localization studies 5,5’,6,6’ tetrachlo-1,1’,3,3’-tetraethylbenzimidazol-carbocyanine (JC-

---

[1] PBS = phosphate buffer 10 mM, NaCl 9g/L, pH=7,2.

[2] GI_{50} is the drug concentration at which 50% of treated cells are dead.

1) and acridine orange (AO) were used as fluorescent probes which stained mitochondria and lysosomes, respectively. JC-1 (final concentration: 1 µg/ml) or AO (final concentration: 1 µM) were added to cells incubated with the compound 30 minutes before the analysis.

6.2.f.1 CONFOCAL MICROSCOPY

Images were acquired with a Leica TCS SP5 confocal microscope coupled with a optical system DMI 6000 CS. The instrument was equipped with a 63X oil immersion objective (Leica HCX PL APO) of numerical aperture NA = 1,4. Each image was represented with 512x512 pixels.

Compound excitation was performed with DIODO laser (405 nm) and emission was read at 450 nm. Probes excitation was realised with argon laser LASOS 80 (488nm) and emission was taken at 590 nm. Long pass emission filter settings were used to separate the emission of the probes from that of the test compounds. Data were acquired using Leica FW4000 software and analyzed with Leica Deblur and ImageJ version 1.35.

6.2.f.2 EPIFLUORESCENCE MICROSCOPY

Images were taken using an Olympus IX81 microscope with optical cell^R olympus system. It was equipped with a 100X/1,4 oil immersion objective (Olympus Uplansapo). Each image was taken with a F-view camera and consisted of 1376x1038 pixels. Excitation was performed with a fluorescence xenon lamp (Olympus MT20). The excitation and emission wavelengths of compounds and probes were the same employed for confocal microscopy. Long pass emission filter settings were used to separate the emission of the probes from that of the test compounds. Data were acquired and analysed using the MATLAB^{TM} (The Math-Works, USA) and ImageJ version 1.35.

6.2.g FLOW CYTOMETER

Flow cytometry is a very important technique to obtain cellular characteristics: from the presence of membrane antigens with immunofluorescence methods to cellular volume, from cellular granularity to cellular membrane permeability.

Flow cytometer is an instrument that makes statistical analysis in samples of microscopic dispersed particles in liquid suspension, through light diffusion and fluorescence phenomena. Flow cytometer is formed by five components: fluidic system, optical system, electronic system, mechanic system and finally data SW-analysis system. Fluidic system consists of a flow cell, a special capillary , usually in quartz, where an hydrodynamic apparatus permits to obtain the so called “ hydrodynamic focalization”. In this system, single particles are forced to flow at the centre of this capillary, where ideally they can perform laminar flow. Inside this flow cell, particles are in single line, so the instrument has the possibility to take single measures sequentially.

The light source can be a laser or mercury vapour lamp. The optical system lets the light beam arrives in the capillary core where it is focalized to each single cell flowing. Signals from cells are sent to respective photomultipliers. There is also an optical group parallel and orthogonal to light beam to check side scattering (SS) and forward scattering (FS), respectively. SS gives information about cellular morphology (shape, cytoplasmatic granularity and nucleus/cell rate), while FS about the size of objects [21]. In the SS, there are also fluorescent phenomena if fluorochromes are utilized for analysis (FITC, PE,etc). The emitted light is checked for spectral analysis (separation of wavelength through dichroic spectra) and is sent to photomultiplier to amplify signals.

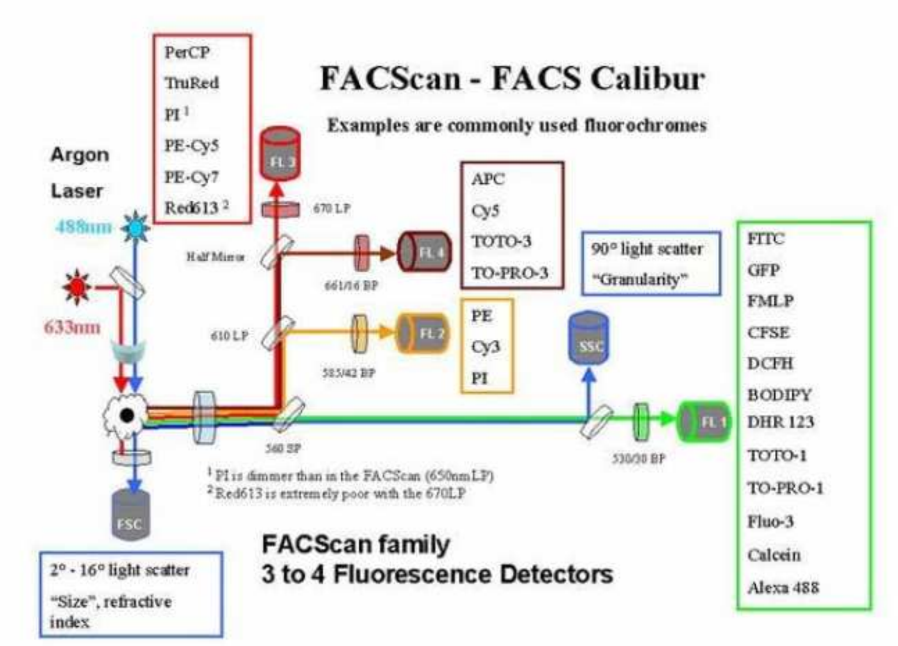
FACScan - FACS Calibur
Examples are commonly used fluorochromes
Argon
Laser
488nm
633nm
PerCP
TruRed
PI 1
PE-Cy5
PE-Cy7
Red613 2
FL 3
670 LP
Half Mirror
661/16 BP
FL 4
APC
Cy5
TOTO-3
TO-PRO-3
90° light scatter
"Granularity"
610 LP
585/42 BP
FL 2
PE
Cy3
PI
SSC
560 SP
530/30 BP
FL 1
FITC
GFP
FMLP
CFSE
DCFH
BODIPY
DHR 123
TOTO-1
TO-PRO-1
Fluo-3
Calcein
Alexa 488
1 PI is dimmer than in the FACScan (650nmLP)
2 Red613 is extremely poor with the 670LP
FSC
2° - 16° light scatter
"Size", refractive index
FACScan family
3 to 4 Fluorescence Detectors

FIG 1*: Schematic rappresentation of a flow cytofluorimeter.*

Signals are transformed to electric impulses and digitalised. A computer analyses the data and helps their visualization.

It is possible to isolate single populations of cell (for example living cells) and analyse only in this subpopulation parameters (gating).

Flow cytometry presents numerous advantages: the possibility of multiparametric analysis, the reproducibility, the high number of analysed cells (100000 events), the speed of analysis (seconds) and the simplicity of the preparation of samples.

6.2.h ANALYSIS OF CELL CYCLE

The analysis of cell cycle was conducted through flow cytometry; this test is based on the fact that each phase presents a different content of DNA.

For flow cytometric analysis of DNA content, $5x10^5$ Jurkat cells in exponentially growth were treated with different concentrations of **ISQ3** for 24, 48 and 72 hours. In the case of the phototoxic compounds, Jurkat cells were irradiated in the presence of them at various concentrations and after the removal of drug solution they were incubated for 24, 48 or 72 hours in RPMI medium.

In both experiments, after the incubation period, cells were centrifuged and fixed with ice-cold ethanol (70%), then treated overnight with PBS buffer containing RNAse (10 Kunit/ml) and propidium iodide (PI, 10 µg/ml). When intercalated in DNA, PI fluoresces in the red (620 nm, FL3), if it is excited at 488 nm [21]. Each experiment was repeated three times.

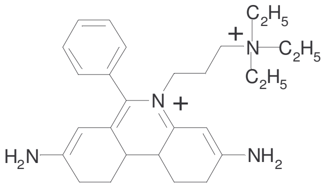

FIG 2: *Propidium Iodide*

Samples were analyzed on a Becton Coulter Epics XL-MCL flow cytometer. For cell cycle analysis, results were examined using MultiCycle for Windows (Phoenix Flow Systems, San Diego, CA). Data were expressed as fractions of cells in the different cycle phases.

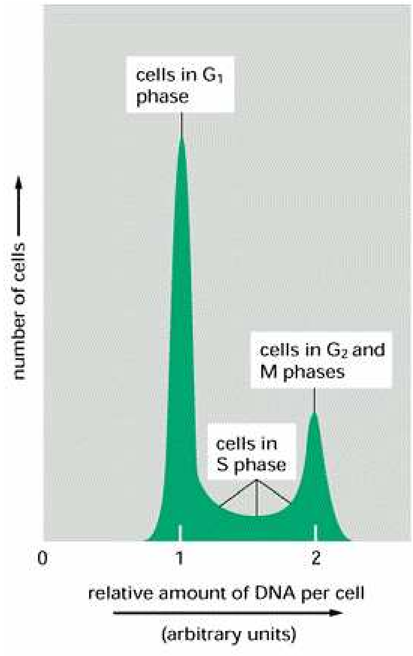

FIG 3*: Representation of cell cycle distribution.*

Diagrams of growing cultures display the characteristic x-axis distribution according to the DNA content, the first peak corresponding to cells in the G1 phase, and the second peak to cells in G2/M phase. Cells with an intermediate DNA content are in the S phase. When DNA is fragmented, as in apoptotic cells, the affinity with the intercalating PI dye is decreased and a so-called hypodiploid peak (or area) becomes apparent to the left of the G1 peak.

6.2.i DETERMINATION OF MECHANISM OF CELLULAR DEATH

In the early stages of apoptosis, changes occur at the cell surface: one of these modifications is the loss of plasmatic membrane asymmetry, with the translocation of phosphatidylserine (PS) from the inner side of the plasma membrane to the outer layer, by which PS becomes exposed at the external surface of the cell. Annexin-V binds PS selectively and, when conjugated with the fluorophore fluorescein isothiocyanate (FITC), it can be used as a sensitive probe for PS exposure upon cell membrane. The measurement of Annexin V binding to the cell surface as indicative for apoptosis was performed in conjunction with a dye exclusion test to establish integrity of the cell membrane. This dye was PI [73, 110].

100.000 Jurkat cells were treated with different concentrations of **ISQ3** or irradiated in presence of **L3**, **BV5** and **BV10**. After 24 of incubation, samples were centrifuged and 100 µl of Annexin V-FITC/PI solution were added, according to the kit instructions. Samples were incubated for 15 minutes in the dark and then were analysed by Coulter Cytomics FC500

(Beckman–Coulter) cytofluorimeter by which the fluorescence of FITC (green, FL1) and of PI (red, FL3) were measured.

In conclusion, living cells do not show any fluorescence, late apoptosis cells demonstrate both fluorescence, early apoptotic cells present only the FITC one as their plasmatic membrane is still integer, necrotic cells demonstrate PI one.

6.2.j INVOLVEMENT OF MITOCHONDRIA IN CELL DEATH

6.2.j.1 DETERMINATION OF MITOCHONDRIAL MEMBRANE POTENTIAL

One parameter of mitochondrial dysfunction is the loss of mitochondrial membrane potential. The mitochondrial membrane potential was measured with the lipophilic cation 5,5',6,6' tetrachlo-1,1',3,3'-tetraethylbenzimidazol-carbocyanine (JC-1).

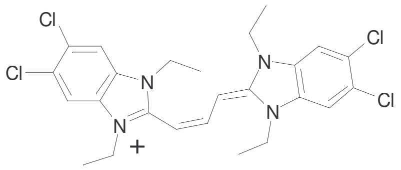

***FIG 4**: 5,5',6,6' tetrachlo-1,1',3,3'-tetraethylbenzimidazol-carbocyanine (JC-1).*

The method is based on the ability of this fluorescent probe to enter selectively mitochondria and to change reversibly its colour from green to orange as membrane potential increases. This property is due to the reversible formation of JC-1 aggregates upon membrane polarization that causes shift in the emitted light from 530 nm (i.e. emission of JC-1 monomeric form) to 590 nm (emission of J-aggregate) when excited at 490 nm [74]. Briefly, after 6, 15 or 24 hours from the irradiation in the presence of **L3**, **BV5** and **BV10** or the incubation with **ISQ3**, Jurkat were collected by centrifugation and resuspended in HBSS containing the JC-1 at the concentration of 1 μg/ml. Cells were then incubated at 37 °C for 10 min, centrifuged and resuspended again in HBSS. The cytofluorimetric analysis (Coulter Cytomics FC500) was performed collecting green (FL1) and orange (FL2) fluorescence in at least 10000 events for each sample.

6.2.j.2 DETERMINATION OF ROS PRODUCTION

ROS production was assessed by flow cytometry using three different probes: hydroethidine (HE), which reveals superoxide anion, and dihydrochlorofluorescin-diacetate (DCFDA), which reveals the presence of hydrogen peroxide, and 10-N-nonyl-acridine orange (NAO), which indicates the oxidation of cardiolipin [77, 79].

In the presence of superoxide anion, hydroethidine is oxidized to ethidium, which intercalates into DNA and can give the characteristic red fluorescence.

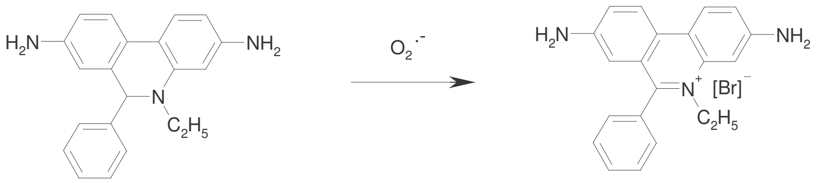

***FIG 5**: Oxidation of hydroethidine into ethidium by superoxide anion.*

Dihydrochlorofluorescin-diacetate penetrates very slowly the cell, then inside it is deacetilated by endogenous esterases, so it is trapped in the cytosol. It can be oxidised to dichlorofluorescein in the presence of peroxides and can give the characteristic fluorescence in the green region.

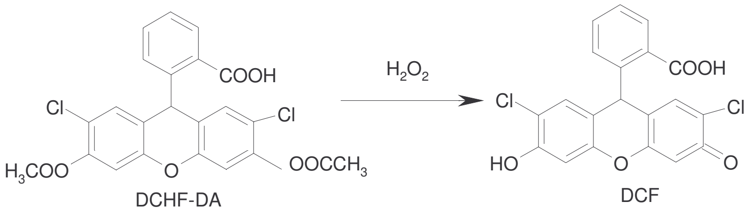

***FIG 6**: Oxidation of dichlorofluorescin-diacetate by hydrogen peroxide, after deacetilation by endogenous esterases.*

NAO is able to bind selectively to cardiolipin, a phospholipid inside the mitochondrial inner membrane, and this complex fluoresces at 530 nm when excited at 488 nm. Yet, if cardiolipin is oxidised by the formation of ROS, NAO looses its affinity for this phospholipid and its fluorescence at 530 nm.

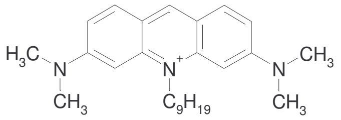

***FIG 7**: 10-N-nonyl-acridine orange (NAO).*

After 24 hours from the irradiation in the presence of **L3**, **BV5** and **BV10** or the treatment with **ISQ3**, cells were collected by centrifugation and resuspended in HBSS containing the fluorescence probes HE, DCFDA or NAO at the concentration of 2,5 μM, 5,0 μM and 0,1 μM respectively. Cells were then incubated at 37 °C for 15 or 30 min, centrifuged and resuspended again in HBSS. The fluorescence was directly recorded with the flow cytometer (Coulter Cytomics FC500) using the 488 nm wavelength as excitation and the emission at 620 nm for HE and at 530 nm for NAO and DCFDA. At least 10000 events for each sample were acquired.

6.2.k INVOLVEMENT OF LYSOSOMES IN CELL DEATH

To investigate the integrity of lysosomes after irradiation with **L3**, **BV5** and **BV10**, we performed flow cytometric analysis using the fluorescent dye acridine orange (AO). AO is a lysosomotropic base and a metachromatic fluorochrome exhibiting red fluorescence when highly concentrated, as in the case of intact lysosomes where AO is retained in its charged protonated form, and green fluorescence at low concentration as in damaged lysosomes. In this case, AO relocates to the cytosol where it is predominantly in the deprotonated form [99].

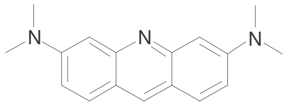

FIG 8: *acridine orange (AO).*

After 24 hours from the irradiation in the presence of **L3**, **BV5** and **BV10**, jurkat cells were collected by centrifugation and resuspended in RPMI containing AO at the concentration of 1 μM. Cells were then incubated at 37 °C for 15 min, centrifuged and resuspended again in RPMI. The fluorescence was directly recorded with the flow cytometer (Coulter Cytomics FC500) using the 488 nm wavelength as excitation and the emission in FL3 channel.

6.2.l DETERMINATION OF REDUCED GLUTATHIONE CONTENT

The oxidative stress was measured by the determination of the reduced glutathione content. This analysis was performed by flow cytometry using Monobromobimane (mBBr), which binds selectively to the sulphidric group of GSH [98].

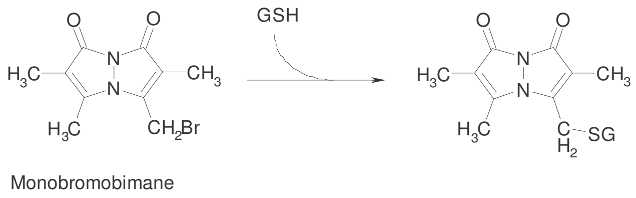

FIG 9*: Monobromobimane and the formation of the bound with GSH.*

After 24 hours from the irradiation in the presence of **L3**, jurkat cells were collected by centrifugation and resuspended in 50 μM Monobromobimane (mBBr) in HBSS. After an incubation at 37°C for 10 min, cells were centrifuged and resuspended in HBSS. Analysis was performed by FACS Vintage Becton Dickinson using as λ_{ex} 354 nm and collecting fluorescence at 450 nm.

6.2.m CASPASE ACTIVATION ASSAY

Caspases are Cistein-Aspartic acid proteases and participate in a cascade that is triggered in response to proapoptotic signals and culminates in cleavage of a set of proteins, resulting in disassembly of the cell [29].

The activation of caspase-3, an executioner caspase, was tested by a colorimetric assay using a caspase-3 assay kit and following the recommended protocol [30]. We irradiated 2000000 jurkat cells in the presence of **L3**, **BV5** and **BV10** and after 24 h the cells were harvested, washed and resuspended in a lysis buffer. Lysates were put in contact with the caspase-3-substate tetrapeptide conjugated with *p*-nitroaniline (*N*-acetyl-Asp-Glu-Val-Asp-pNA, DEVD-*p*NA).

The formation of *p*NA was measured at 405 nm using a microtiter plate reader. Values were normalized to the protein content in cell lysates, obtained by Bradford method [111]. Data were expressed as fold of enzymatic activity in comparison to the non irradiated control.

In the case of **ISQ3**, we tested caspase activation through flow cytometry [30].

Jurkat cells were treated in the presence of 500 nM **ISQ3** and after 24 h, cells were harvested, washed and resuspended in HBSS buffer containing the cell-permeable substrates for caspase-3 (FITC-DEVD-fmk), caspase-8 (FITC-IETD-fmk) and caspase-9 (FITC-LEDH-fmk), respectively. After 1 h of incubation at 37 °C, cells were washed and analyzed by flow cytometer (Coulter Cytomics FC500) using the FL-1 channel. Cells showed FITC fluorescence only after caspase activation.

6.2.n MITOTIC INDEX DETERMINATION

Exponentially growing Jurkat cells were incubated with **ISQ3** or with colchicine, as control compound, for 24 h prior to centrifugation at 400g for 5 min and resuspension of the resultant cell pellet in 1 ml of KCl 75 mM at 4 °C (ipotonic treatment). After 20 min, 1 ml of methanol-acetic acid (3:l) as fixative was slowly added during constant mild agitation. Slides were prepared after cells were repelleted and washed twice with 1 ml of fixative, and resuspended in fixative. After drying, samples were stained with 4% Giemsa solution. Four hundred cells/treatment were scored for the presence of mitotic figures by optical microscopy with a 40X objective and the mitotic index was calculated as the proportion of cells with mitotic figures.

6.2.o IMMUNOFLUORESCENCE DETECTION OF MICROTUBULE PERTURBATION

Immunofluorescence experiments were performed to evaluate a perturbation in microtubule network after the treatment with **ISQ3**.

A549 cells were seeded on sterile microscope coverslips. After 24 h, **ISQ3** (5 and 2,5 μM) or vinblastine (1 μM), as reference compound, were added to the culture medium, and cells were then incubated for 18 h. After, cells were fixed with 4% formaldehyde in PBS at room temperature for 10 min, washed three times with PBS, permeabilized in 0.2% Triton X-100 in PBS at room temperature for 10 min, and placed in methanol at -20 °C for 30 min. They were then washed with PBS, incubated at 37 °C with 2% bovine serum albumin (BSA) to block nonspecific sites for 1 h, and subsequently, with a mouse monoclonal anti-β-tubulin antibody (diluted 1:400 in PBS) at 37 °C for 1 h. Slides were washed three times with PBS and incubated with a Tetramethyl Rhodamine Isothiocyanate (TRITC)-conjugated rat antimouse IgG antibody (diluted 1:200 in 2% BSA) at 37 °C for a further 1 h. Slides were then washed repeatedly with PBS, mounted with mounting medium and analyzed by confocal microscopy (SP-2, Leica) under green light.

6.2.p TUBULIN POLYMERIZATION

The effects of test compound on the polymerization of microtubule protein isolated from porcine brain were analyzed using a microtubule polymerization assay kit (Cytoskeleton, USA) and following the recommended protocol. Polymerization was monitored by fluorescent enhancement due to the incorporation of a fluorescent reporter, DAPI 4',6-diamidino-2-phenylindole, into microtubules as polymerization occurs [80].

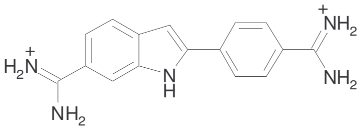

FIG 10: 4',6-diamidino-2.phenylindole (DAPI)

The assay was carried out in 96-well microtiter plates and the reaction was initiated with the addition of tubulin. The plate was incubated at 37 °C in a fluorescence microplate reader (Fluoroskan Ascent FL Labsystems) and the fluorescence measurement (λ_{ex} 355 nm; λ_{em} 450 nm) was determined every minute for 60 min. As references compounds, Taxol and Colchicine were used.

6.2.q INTERACTION WITH DNA

As complexation between a ligand molecule and a nucleic acid leads to optical changes, absorption and emission spectroscopy are useful tools for monitoring DNA-binding process.

6.2.q.1 SPECTROPHOTOMETRIC AND SPECTROFLUORIMETRIC TITRATIONS

UV-absorption spectra of compounds were recorded after the addition of serial aliquots of salmon testes DNA solution. The same titrations were performed recording emission spectra of the molecules. To avoid dilution of the analyte solutions, the titrant solutions contained DNA as well as the ligand at the same concentration as in the titrated solution.

Measurements were carried out in phosphate buffer (10 mM, pH=7,2) and 25 °C. DNA concentration was determined using an extinction coefficient of 6600 M^{-1} cm^{-1} at 260 nm. Titrations were finished after no changes were observed in absorption/fluorescence spectra upon addition of at least three two-equivalent portions of the titrant. All spectrophotometric titrations were performed at least three times to ensure the reproducibility.

To obtain the intrinsic binding constant and the binding site size as well, spectra of solutions with different [Drug]/[DNA] ratios and constant drug concentration were recorded. The binding isotherms obtained were represented as Scatchard plots [87] and evaluated according to the McGhee and von Hippel model [86].

EVALUATION OF BINDING COSTANTS (K_i) AND BINDING SITE SIZE (n):

Absorption A measured at any wavelength reflects both the free and DNA-bound drug species:

$$A = A_f + A_b = \varepsilon_f C_f + \varepsilon_b C_b$$

where A_f is the absorbance at a given wavelength in the absence of DNA (usually absorption maximum of the unbound ligand), A_b is the absorbance of the fully bound ligand, ε_f and Cf are the extinction coefficient and concentration of the free drug and ε_b and C_b represent the extinction coefficient and concentration of the bound drug.

Thus, the drug binding fraction α (on a 0-1 scale) and hence the equilibrium distribution at each titration position is calculated from:

$$\alpha = \frac{C_b}{C} = \frac{1 - C_f}{C} = \frac{A_f - A}{A_f - A_b}$$

The ratio of bound ligand molecules per DNA unit (*r*):

$$r = \frac{\alpha C}{C_{DNA}}$$

where C_{DNA} is the total concentration of DNA at that point.

The data can be presented as Scatchard plots, i.e. r/C_f versus. r values to determine the values of the binding constant (K_i) and the binding site size (n).

$$\frac{r}{C_f} = K_i (n - r)$$

However, such a linear relationship is rare for nucleic acid system and it is more usual to use the "neighbour exclusion" model developed by McGhee and von Hippel, which considers occupancy of multiple binding sites. The numerical fitting was performed using the Levenberg–Marquardt non-linear curve fitting algorithm implemented into the Sigma-Plot ® software.

$$\frac{r}{C_f} = K_i (n - r) \left(\frac{1 - nr}{1 - (n - 1) r} \right)^{n-1}$$

Fluorescence-based procedures are often preferred to absorption titrations due to the greater sensitivity and selectivity.

6.2.q.2 CIRCULAR DICHROISM SPECTROSCOPY

Another spectrometric analysis of DNA binding was performed using circular dichroism (CD) [89, 112] Circular dichroism is defined as the differential absorption of right (A_R) and left (A_L) circularly polarized light. At a given wavelength:

$$CD (\lambda) = A_R (\lambda) - A_L (\lambda)$$

Since circularly polarized light itself is "chiral", it interacts differently with chiral molecules. In a CD experiment, equal amounts of left and right circularly polarized light are radiated into a compound solution. One of the two types is absorbed more than the other one and this wavelength dependent difference of absorption is measured, yielding the CD spectrum of the sample. Due to the interaction with the molecule, the electric field vector of the light traces out an elliptical path while propagating. Generally, the circular dichroism effect is small so the ellipticity values usually are on the order of mdeg. The ellipticity becomes, in radians:

$$\theta_r = \frac{2{,}303}{4} \ (A_L - A_R) \ [\ rad\ ]$$

and it could be easily converted into mdeg:

$$\theta_d = \frac{2{,}303}{4} \ (A_L - A_R) \ \frac{180}{\pi} \ [\ deg\ ]$$

Circular dichroism spectra were recorded in 10 mM phosphate buffer, pH=7,2, in a quartz sample cuvette (pathlength ℓ = 1 cm) at 25°C on a Jasco J810A spectropolarimeter. In these experiments, compound solution aliquots were added to 2,72 mM salmon testes DNA. So spectra at different [DNA]/[dye] ratios were recorded using 50 nm/min scan speed and 20 mdeg sensibility.

6.2.q.3 LINEAR DICHROISM SPECTROSCOPY

Finally, DNA binding was checked by linear dichroism (LD), since it is possible to elucidate the binding geometry with this technique. Linearly polarized light is polarized in a certain direction (i.e. the magnitude of its electric field vector oscillates only in one plane, similar to a sine wave). Linear dichroism is defined as the differential absorption of linearly polarized light:

$$LD = A_{//} - A_{\perp}$$

where $A_{//}$ is the absorbance of the sample when the light is polarized parallel to a reference axis, and $A_{\perp}$ is the absorbance of the light which is polarized perpendicular to this axis. By dividing the LD value by the absorbance of the unoriented sample under isotropic conditions (A_{iso}), the "reduced" linear dichroism (LD_r), i.e. the wavelength-dependent LD, is obtained:

$$LD_r = LD / A_{iso} = 3/2\ S\ (3 \cos^2 \alpha - 1)$$

where S is orientation factor and α is the angle which quantified the orientation of the transition moment of the compound relative to the reference axis [82].
LD measurements were performed with a Jasco J500A circular dichroism spectropolarimeter, converted for LD and equipped with an IBM PC and Jasco J interface. For these analysis, the sample orientation was obtained using a flow device designed by *Wada and Kozawa* [113], which presents a cylindrical rotating couette, a 0,14 cm optical path and a constant flow of 800 rpm. LD spectra were performed using different [Drug]/[DNA] ratios, dissolved in phosphate buffer (10 mM, pH=7,2).

6.2.r DNA PHOTOCLEAVAGE

To evaluate the capability of provoking DNA photodamage by pyrrolo[3,4-*h*]quinolin-2-ones, we used supercoiled pBR322 plasmid, dissolved in phosphate buffer 10 mM. Plasmid solutions were irradiated (3,75 and 7,5 J/cm^2) in the presence of the most active compounds (**BV5**, **BV10** and **BV16**) in a 96-wells microplate. We used growing [compound]/[DNA] rates.
Irradiation with a photosensitezer can induce cleavage of one or both DNA strands and so the formation of a open circular plasmid (OC, II form) or of a linear one (L, III form), respectively.

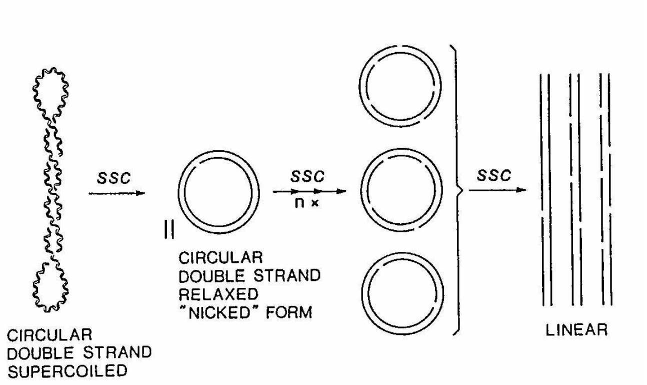

FIG 11*: Presentation of the three possible plasmidic DNA forms: supercoiled (SC, form I), open circular (OC, form II) and linear (L, form III).*

It is possible to separate the three different forms with horizontal electrophoresis thanks to their different hydrodynamic properties.

In addition to frank strand break, we also evaluated if purine and/or pyrimidine bases were involved in the oxidative damage to DNA using base excision repair enzymes Formamido pyrimidin glycosilase (Fpg) and Endonuclease III (Endo III), respectively.

Each pBR322 DNA sample (100 ng) dissolved in TAE buffer (40 mM Tris-acetate, 1 mM EDTA, pH=8,0) was irradiated with UV in the presence of the compounds. After irradiation, two aliquots of sample were incubated at 37 °C with Fpg (Formamydo pyrimidin glycosilase) and Endo III (Endonuclease III) respectively as described by Epe *et al.* [106]. Prior to the run, samples were added of loading buffer (0,25% bromophenol blue, 0,25% xilene cianol, 30% glycerol in water). Samples were loaded on 1% agarose gel and the run was carried out in TAE buffer at 80 V for 2 hrs. After staining with ethidium bromide solution, gel was washed with water and the DNA bands were detected under UV radiation with a UV transilluminator. Photographs were taken by a digital photocamera Kodak DC256 and the quantification of the bands was achieved by image analyzer software Quantity One. The fractions of supercoiled DNA (Form I) were calculated:

$$\text{sc-DNA} = \frac{\text{Area}_{sc}}{\text{Area}_{sc} + \text{Area}_{rel}/1.66}$$

Where Area_{sc} is the area of supercoiled DNA and Area_{rel} is the area of relaxed DNA (form II and III) obtained by the densitometric analysis of gels. The presence of the coefficient 1,66 in the formula is due to the fact that ethidium bromide bound to the supercolied pBR322 is 1,66 times less than that bound to the relaxed form [107].

Analogue experiments were conducted in the presence of some reactive species scavengers.

6.2.s TOPOISOMERASE I ASSAY

6.2.s.1 TOPOISOMERASE I RELAXATION ASSAY

Topoisomease I assay was adapted from *Bridewell et al.* [91]. Assay buffer was composed of 50 mM Tris-HCl (pH=7,5), 50 mM KCl, 0,5 mM dithiothreitol (DTT), 10 mM $MgCl_2$,0,1 mM EDTA, 30 μg/ml of BSA. Incubation mixtures (20μl) contained assay buffer, drug at various concentrations, 0,250 μg pBR322 supercoiled plasmid and 10 unit of human topoisomerase I. Reactions were assembled on ice, adding topoisomerase I last, and incubated at 37°C for 30 min. Reactions were stopped by the addition of pre-warmed SDS (final concentration 1%) followed by proteinase K treatment (final concentration 50μg/ml) for an additional digestion at 37°C for 30 min. Before the run, 2 μl of loading buffer (0,25% bromophenol blue, 50% glycerol) were added to each sample. The samples contained the compound were successively extracted with chloroform and isoamyl alcohol (24:1) prior to load. Relaxation assay samples were analysed by electrophoresis on 0,8% agarose gel in TAE buffer at 20 V overnight and then stained with a solution containing 0,5μg/ml of ethidium bromide. DNA bands were visualized by UV light and photographed through a digital photocamera Kodak DC256.

6.2.s.2 TOPOISOMERASE I CLEAVABLE-COMPLEX ASSAY

The samples from cleavable complex formation assay were prepared as the relaxation assay but were loaded into a 0,8% agarose gel containing 0,5μg/mL of ethidium bromide in order to resolve the more slowly migrating nicked product from the relaxed molecules. The gel was run as previously described and then destained in deionized water. DNA bands were visualized by UV light and photographed through a digital photocamera Kodak DC256.

6.2.t TOPOISOMERASE II ASSAY:

6.2.t.1 TOPOISOMERASE II RELAXATION ASSAY

Assay mixtures (20 μl) were prepared using 125 ng of supercoiled plasmid pBR322, 2 units of human topoisomerase IIα and 0-50 μM of selected compound in aqueous solution (50 mM Tris-HCl, pH=8,0, 10 mM $MgCl_2$, 120 mM KCl, 0,5 mM DTT and 30 μg of BSA). The reactions were carried out as described in Meth. Topo I.

6.2.t.2 TOPOISOMERASE II CLEAVABLE COMPLEX ASSAY

Incubation mixtures (20 µl) contained 100 ng of supercoiled plasmid pBR322, 6 units of human topoisomerase IIα and 0-50 µM of selected compound in aqueous solution (50 mM Tris-HCl, pH=8,0, 120 mM KCl, 10 mM $MgCl_2$, 0,5 mM DTT and 30 µg of BSA). Reactions were assembled on ice with drug and topoisomerase IIα being added at last, incubated at 37°C for 30 min and enzyme-DNA cleavage intermediates were trapped by the addition of pre-warmed SDS (final concentration 0,5%) followed by proteinase K treatment (final concentration 50 µg/ml) for 1h at 45°C to digest topoisomerase IIα. Samples were mixed with 2 µl of loading buffer (0,25% bromophenol blue, 50% glycerol) and then subjected to electrophoresis in 1% agarose gel, containing 0.5 µg/ml of ethidium bromide, in TAE buffer [40 mM Tris-acetate (pH=8.0), 1 mM EDTA] at 20 V overnight and then washed with distilled water. DNA bands were visualized by UV light and photographed through a digital photocamera Kodak DC256.

6.2.u EVALUATION OF LIPIDIC PEROXIDATION

Lipidic peroxidation was monitored by Morlière method or TBARS assay [109], which checks the formation of malondialdehyde, one of the final product of this oxidation process, as it reacts with thiobarbituric acid.

500.000 jurkat cells were irradiated (2,5 and 3,75 J/cm^2) in the presence of the most active compounds, dissolved in HBSS. Then, the drug solution was replaced by RPMI medium and cells were incubated for 24 hours. To verify lipidic peroxidation, after cell centrifugation, 900 µl of surnatant were collected and put at 253 K after having added 90 µl of 2,6-di-tert-butyl-*p*-cresol (BHT, 2% in absolute ethanol). Cells were washed, resuspended in 500 µl of water.400 µl of cells were lysed with 400 µl of SDS (1% in water) and vortexed. This suspension was divided into two aliquots: in 500 µl were added 50 µl of BHT; 300 µl were used for protein quantification with Peterson method [114]. Lipid peroxidation was measured using a thiobarbituric acid assay as described by Morliere *et al.* [109]. A standard curve of 1,1,3,3 tetraethoxypropane was used to quantify the amount of produced malondialdehyde. Data were expressed in terms of nanomoles of TBARS normalized to the total protein content in an aliquot of the cell extract.

7. REFERENCES

1. D Hanahan, R.A. Weinberg, The hallmarks of cancer, *Cell, 100* (**2000**), pp.57-70.

2. Cancer, Fact Sheet N°297 (**2006**), World Health Organization, Geneva, Switzerland (http: //www.who.int/mediacentre/fatcsheets/fs297/en/print.html).

3. S.L. Wolfe, Biologia molecolare e cellulare, (**1994**) ed. EdiSES Napoli Italy, pp. 1006-1048.

4. L.A. Mitscher, Antibiotics and antimicrobial agents, in "Foye's principle of medicinal chemistry" (**2002**) D.A. Williams, T.L. Lemke, ed. Lippincott Williams & Wilkins, pp. 819-864.

5. V Spataro, G Bonadonna, Principi di distruzione e resistenza cellulare, in "Medicina Oncologica" (**2003**), ed. Masson Milano Italy, pp. 429-448 .

6. S Drukman, M Kavallaris, Microtubule alterations and resistance to tubulin-binding agents, *Intern. J. Oncol., 21* (**2002**), pp. 621-628.

7. D.S. Lawrence, J.E. Copper, C.D. Smith, Structure-activity studies of substituted quinoxalinones as multiple-drug-resistance antagonists, *J. Med. Chem., 44* (**2001**), pp. 594-601.

8. E.D. Israels, L.G. Israels, The cell cycle, *Oncologist, 5* (**2000**), pp. 510-513.

9. M Dorée, S Galas, The cyclin-dependent protein kinases and the control of cell division, *FASEB J., 8* (**1994**), pp. 1114-1121.

10. L Gianni, C Sessa, G Capri, G Grasselli, G Bianchi, G Vitali, Farmaci chemioterapici, in Medicina Oncologica (**2003**), Ed. Masson Milano Italy, pp. 583-676.

11. P Callery, P Gannet, Cancer and cancer chemotherapy, in "Foye's principles of medicinal chemistry"(**2002**), D.A. Williams, T.L. Lemke, ed. Lippincott Williams & Wilkins, pp. 924-951.

12. M.R. Middleton, G.P. Margison, Improvement of chemotherapy efficacy by inactivation of a DNA-repair pathway, *Lancet Oncol., 4* (**2003**), pp. 37-44.

13. J.M. Berger, Structure of DNA topoisomerases, *Biochim. Biophys. Acta, 1400* (**1998**), pp. 3-18.

14. A.K McClendon, N Osheroff, DNA topoisomerase II, genotoxicity, and cancer, *Mut. Res., 623* (**2007**), pp. 83-97.

15. N Galjard, F Perez, A plus-end raft to control microtubule dynamics and function, *Curr. Opin. Cell Biol., 15* (**2003**), pp. 48-53.

16. A Jordan, J.A. Hadfield, N.J. Lawrence, A.T. McGown, Tubulin as a target for anticancer drugs: agents which interact with the mitotic spindle, *Inc. Med. Res. Rev., 18* (**1998**), pp. 259-296.

17. J Zhou, P Giannakakou, Targeting microtubules for cancer chemotherapy, *Curr. Med. Chem – Anti-Cancer Agents, 5* (**2005**), pp. 65-71.

18. C Sawyers, Targeted cancer therapy, *Nature, 432* (**2004**), pp. 294-297.

19. P Cohen, Protein kinases- the major drug target of the twenty-first century? *Nat. Rev., 1* (**2002**), pp. 309-316.

20. U Ziegler, P Groscurth, Morphological features of cell death, *News Physiol. Sci., 19* (**2004**), pp. 124-128.

21. Z Darzynkiewicz, G Juan, X Li, W Gorczyca, T Murakami, F Traganos, Cytometry in cell necrobiology: analysis of apoptosis and accidental cell death (necrosis), *Cytometry, 21* (**1997**), pp. 1-20.

22. L.G. Israels, E.D. Israels, Apoptosis, *Oncologist, 4* (**1999**), pp. 332-339.

23. F Oberhammer, J.W Wilson, C Dive, I Morris, J.A. Hickman, A.E. Wakeling, R.P. Walker, M Sikorska, Apoptotic death in epithelial cells: cleavage of DNA to 300 and/or 50 kb fragments prior to or in the absence of internucleosomal fragmentation, *EMBO J., 12* (**1993**), pp. 3679-3684.

24. K Vermeulen, D.R. Van Bockstaele, Z.N. Berneman, Apoptosis: mechanism and relevance in cancer, *Ann. Hematol., 84* (**2005**), pp. 627-639.

25. K.F. Ferri, G Kroemer, Organelle-specific initiation of cell death pathways, *Nat. Cell Biol., 3* (**2001**), pp. E255-E263.

26. N Demaurex, C Distelhorst, Apoptosis -the calcium connection, *Science, 300* (**2003**), pp. 65-67.

27. B Verhoven, R.A. Schlegel, P Williamson, Mechanisms of phosphatidylserine exposure, a phagocyte recognition signal, on apoptotic T lymphocytes, *J. Exp. Med., 182* (**1995**), pp. 1597-1601.

28. J Savill, V Fadok, Corpse clearance defines the meaning of cell death, *Nature, 407* (**2000**), pp. 784-789.

29. N.A. Thornberry, Y Lazebnik, Caspase: enemies within, *Science, 281* (**1998**), pp. 1312-1316.

30. C Köhler, S Orrenius, B Zhivotovsky, Evaluation of caspase activity in apoptotic cells, *J. Immunol. Meth., 265* (**2002**), pp. 97-110.

31. K.M. Boatright, G.S. Salvesen, Mechanisms of caspase activation, *Curr. Opin. Cell Biol., 15* (**2003**), pp. 725-731.

32. G Denecker, D Vercammen, W Declercq, P Vandenabeele, Apoptotic and necrotic cell death domain receptors, *Cell. Mol. Life Sci., 58* (**2001**), pp. 356-370.

33. J.A. Parrish, T.B. Fitzpatrick, M.A. Pathak, L. Tanenbaum, Photochemotherapy of psoriasis with oral methoxsalen and longwave ultraviolet light, *N. Engl. J. Med., 291* (**1974**), pp. 1207-1211.

34. T.P. Coohill, Action spectroscopy: ultraviolet radiation, in "CRC Handbook of organic photochemistry and photobiology" (**1995**) ed. Horspool-Song, pp 1267-1275.

35. M. Weichenthal, T. Schwarz, Phototherapy: how does UV work?, *Photodermatol. photoimmunol. photomed., 21* (**2005**), pp. 260-266.

36. J.C. Simon, D. Pfieger, E. Schöpf, Recent advances in phototherapy, Eur. *J. Dermatol. 10* (**2000**), pp. 642-645.

37. D Dolmans, D Fukumura, R.K. Jain, Photodynamic therapy for cancer*, Nat. Rev. Cancer, 3* (**2003**), pp. 380-387.

38. F Dall'Acqua, G Viola, D Vedaldi, Cellular and molecular target of psoralen, in "CRC Handbook of Organic Photochemistry and Photobiology" (**2004**) W. M. Hoorspool, F Lenci, ed. CRC Press, pp. 1–17.

39. A. Madhukar, M.A. Pathak, T.B. Fitzpatrick, The evolution of photochemotherapy with psoralens and UV-A (PUVA): 2000 BC to 1992 AD, *J. Photochem. Photobiol. B:Biol., 14* (**1992**), pp. 3-22.

40. D Bethea, B Fullmer, S Syed, G Seltzer, J Tiano, C Rischko, L Gillespie, D Brown, F.P. Gasparro, Psoralen photobiology and photochemoterapy: 50 years of science and medicine, *J.Dermatol. Sci., 19* (**1999**), pp. 78-88.

41. R. Edelson, C Berger, F Gasparro, C.B. Jegasothy, P Heald, B Wintroub, E Vonderheid, R Knobler, K Wolff, G Plewig, G McKiernan, I Christiansen, M Oster, H Honigsmann, H Wilford, E Koroska, T Rehle, G Stingl, L Laroche, Treatment of T-cell lymphoma by extracorporeal photochemotherapy. Preliminary results, *N. Engl. J. Med., 316* (**1987**), pp. 297-303.

42. A Oliven, Y Shechter, Extracorporeal photopheresis: a review, *Blood Rev., 15* (**2001**), pp. 103-108.

43. J Bladon, P.C. Taylor, Extracorporeal photopheresis: A focus on apoptosis and cytokines, *J. Dermatol. Sci., 43* (**2006**), pp. 85-94.

44. L Lin, G.P. Wiesehahn, P. A. Morel, L Corash, Use of 8-methoxypsoralen and long-wavelength ultraviolet radiation for decontamination of platelet concentrates, *Blood, 74* (**1989**), pp. 517-525.

45. J Llano, J Raber, J.A. Eriksson, Theoretical study of phototoxic reactions of psoralens, *J. Photochem Photobiol A:chem 154* (**2003**), pp. 235–243.

46. SC Shim, Photochemistry of skin-sensitizing psoralens, in "CRC Handbook of organic photochemistry and photobiology" (**1995**) ed. Horspool-Song, pp. 1347–1356.

47. W.W. Mantulin, P.S. Song, Excited states of skin-sensitizing coumarins and psoralens. Spectroscopic studies, *J. Am. Chem. Soc. 95* (**1973**), pp. 5122–5129.

48. F Dall'Acqua, P Martelli, Photosensitizing action of furocoumarins on membrane components and consequent intracellular events, *J. Photochem. Photobiol. B:biol., 8* (**1991**), pp. 235-254.

49. N Kitamura, S Kohtani, R Nakagaki, Molecular aspects of furocoumarin reactions: Photophysics, Photochemistry, Photobiology and structural Analysis, *J .Photochem. Photobiol. C: photochem. rev., 6* (**2005**), pp, 168-185.

50. S Caffieri, Furocoumarin photolysis: chemical and biological aspects, *Photochem. photobiol. Sci., 1* (**2002**), pp. 149-157.

51. S Caffieri, F Di Lisa, F Bolesani, M Facco, G Semenzato, F Dall'Acqua, M Canton, The mitochondrial effects of novel apoptogenic molecules generated by psoralen photolysis as crucial mechanism in PUVA therapy, *Blood, 109* (**2007**), pp.4988-4994.

52. A.B. Santamaria, D.W. Davis, D.X. Nghiem, D.J. McConkey, S.E. Ullrich, M Kapoor, G Lozano, H.N. Ananthaswamy, p53 and Fas ligand are required for psoralen and UVA-induced apoptosis in mouse epidermal cells, *Cell Death Differ., 9* (**2002**), pp. 549-560.

53. M Canton, S Caffieri, F Dall'Acqua, F Di Lisa, PUVA-induced apoptosis involves mitochondrial dysfunction caused by the opening of the permeability transition pore, *FEBS Lett. 522* (**2002**), pp. 168-172.

54. G Viola, E Fortunato, L Cecconet, S Disarò, G Basso, Induction of apoptosis in Jurkat cells by photoexcited psoralen derivatives: Implication of mitochondrial dysfunction and caspase activation, *Toxicol in Vitro 21* (**2007**), pp. 211-216.

55. M Patel, R.J. McHugh, B.C. Cordova, R.M. Klabe, S Erickson-Viitanen, G.L. Trainor, J.D. Rodgers, Synthesis and evaluation of quinoxalinones as HIV-1 reverse transcriptase inhibitors, *Bioorg. & Med. Chem. Lett., 10* (**2000**), pp. 1729-1731.

56. A Carta, P Sanna, L Gherardini, D Usai, S Zanetti, Novel functionalized pyrido[2,3-*g*]quinoxalinones as antibacterial, antifungal and anticancer agents, *Il Farmaco, 56* (**2001**), pp. 933-998.

57. J Guillon, P Grellier, M Labaied, P Sonnet, J Léger, R Déprez-Poulain, I Forfar-Bares, P Dallemagne, N Lemaître, F Péhourcq, J Rochette, C Sergheraert, C Jarry, Synthesis, antimalarial activity, and molecular modeling of new pyrrolo[1,2-*a*]quinoxalines, bispyrrolo[1,2-*a*]quinoxalines, Bispyrido[3,2-*e*]pyrrolo[1,2-*a*]pyrazines, and Bispyrrolo [1,2-*a*]thieno[3,2-*e*]pyrazines, *J. Med. Chem., 47* (**2004**), pp. 1997-2009.

58. S.A.M. El-Hawash, N.S. Habib, M.A. Kassem, Synthesis of some new quinoxalines and 1,2,4-triazolo[4,3-*a*]quinoxalines for evaluation of in vitro antitumor and antimicrobial activities, *Arch. Pharm. Chem. Life Sci., 339* (**2006**), pp. 564-571.

59. S Alleca, P Corona, M Loriga, G Palgietti, R Loddo, V Mascia, B Busonera, P La Colla, Quinoxaline chemistry. Part 16. 4-Substituted anilino and 4-substituted phenoxymethyl pyrrolo[1,2-*a*]quinoxalines and *N*-[4-(pyrrolo[1,2-*a*]quinoxalin-4yl-amino and hydroxymethyl]bezoyl glutamates. Synthesis and evalutaion of in vitro biological activity, *Il Farmaco, 58* (**2003**), pp. 639-650.

60. N Kawanishi, T Sugimoto, J Shibata, K Nakamura, K Masutani, M Ikuta, H Hirai, Structure-based drug design of a highly potent CDK1,2,4,6 inhibitor with novel macrocyclic quinoxalin-2-one structure, *Bioorg.& Med. Chem. Lett.*, *16* (**2006**), pp. 5122-5126.

61. C.H. Nguyen, E Fan, J Riou, M Bissery, P Vrignaud, F Lavelle, E Bisagni, Synthesis and biological evaluation of amino-substituted benzo[*f*]pyrido[4,3-*b*] and pyrido[3,4-*b*]quinoxalines: a new class of antineoplastic agents, *Anti-Cancer Drug Design, 10* (**1995**), pp. 277-297.

62. A.H. Abadi, 5-Substituted 2-Bromoindolo[3,2-*b*]quinoxalines. A class of potential antitumor agents with cdc25 phosphatase inhibitory properties, *Arch. Pharm. Pharm. Med. Chem.*, *331* (**1998**), pp. 352-358.

63. M.R. Boyd, K.D. Paull, Some practical considerations and applications of the National Cancer Institute in vitro anticancer drug discovery screen, *Drug Dev. Res., 34* (**1995**), pp. 91-110.

64. L.H. Hurley, DNA and its associated processes as targets for cancer therapy, *Nat. Rev. Cancer, 2* (**2002**), pp. 188-200.

65. M.T. Khosrow, T.B. Fitzpatrick, The benefits and risks of long-term PUVA photochemotherapy, *Dermatol. Clinics, 16* (**1998**), pp. 227-234.

66. F Dall'Acqua, D Vedaldi, S Caffieri, A Guiotto, P Rodighiero, F Baccichetti, F Carlassare, F Bordin, New monofunctional reagents for DNA as possible agents for the photochemotherapy of psoriasis: derivatives of 4,5'-dimethylangelicin, *J. Med. Chem., 24* (**1981**), pp. 178-184.

67. D Averbeck, E Moustacchi, E Bisagni, Biological effects and repair of damage photoinduced by a derivative of psoralen substituted at the 3,4 reaction site. Photoreactivity of this compound and lethal effect in yeast, *Biochim. Biophys. Acta, 518* (**1978**), pp. 464-481.

68. N.K. Gibbs, E Quanten, S Baydoun, C.N. Knox, R Roelandts, F De Schryver, T.G. Truscott, R Young, Photophysical, photochemical and photobiological properties of pyrrolocoumarins; a new class of photoactive compounds, *J. Photochem. Photobiol, B: Biol., 2* (**1988**), pp. 109-122.

69. G Miolo, S Caffieri, D Vedaldi, F Baccichetti, C Marzano, V Lucchini, P Rodighiero, F Dall'Acqua, Photochemical and photobiological studies on methylthioangelicins, *Il farmaco, 54* (**1999**), pp. 134-144.

70. P Barraja, P Diana, A Montalbano, G Dattolo, G Cirrincione, G Viola, D Vedaldi, F Dall'Acqua, Pyrrolo[2,3-*h*]quinolin-2-ones: A new ring system with potent photoantiproliferative activity, *Bioorg. & Med. Chem., 14* (**2006**), pp. 8712-8728.

71. O Gia, S Mobilio, M Palumbo, M.A. Pathak, Benzo- and tetrehydrobenzo-psoralen congeners: DNA binding and photobiological properties, *Photochem. Photobiol., 57* (**1993**), pp. 497-503.

72. T Mosmann, Rapid colorimetric assay for cellular growth and survival: application to proliferation and citotoxic assay, *J. Immunol. Meth., 65* (**1983**), pp. 55-63.

73. I Vermes, C Haanen, H Steffens-Nakken, C Reutelingsperger, A novel assay for apoptosis: Flow cytometric detection of phosphatidylserine expression on early apoptotic cells using fluorescein labelled Annexin V, *J. Immunol. Meths., 184* (**1995**), pp. 39-51.

74. S Salvioli, A Ardizzoni, C Franceschi, A Cossarizza, JC-1 but not DiOC6(3) or rhodamine 123 is a reliable fluorescent probe to asses ΨΔ changes in intact cells: implications for studies on mitochondrial functionality during apoptosis, *FEBS Lett. 411* (**1997**), pp. 77-82.

75. X Wang, The expanding role of mitochondria in apoptosis, *Genes & Dev., 15* (**2001**), pp. 2922-2933.

76. G Kroemer, J.C. Reed, Mitochondrial control of cell death, *Nat. Med., 6* (**2000**), pp. 513-519.

77. G Rothe, G Valet, Flow cytometric analysis of respiratory burst activity in phagocytes with hydroethidine and 2',7'-dichlorofluorescin, *J. Leukoc. Biol., 47* (**1990**), pp. 440-448.

78. M Garcia Fernandez, L Troiano, L Moretti, M Nasi, M Pinti, S Salvioli, J Dobrucki, A Cossarizza, Early changes in intramitochondrial cardiolipin distribution during apoptosis, *Cell Growth & Diff., 13* (**2002**), pp. 499-455.

79. J.M. Petit, A Maftah, M.H. Ratinaud R Julien 10-N-nonyl acridine orange interacts with cardiolipin and allows the quantification of this phospholipid in isolated mitochondria, *Eur. J. Biochem., 209* (**1992**),pp. 267-273.

80. D Bonne, C Heusèle, C Simon, D Pantaloni, 4',6-diamidino-2-phenylindole, a fluorescent probe for tubulin and microtubules, *J. Biol. Chem., 260* (**1985**), pp. 2819-2825.

81. S.K. Sengupta, in "Cancer Chemotherapeutic Agents" (**1995**), ed American Chemical Society – Washington, Vol 5 pp. 205-217.

82. H Ihmels, K Faulhaber, G Viola, Evaluation of the DNA-binding properties of cationic dyes by absorption and emission spectroscopy, in "Highlights in bioorganic chemistry: methods and applications" (**2004**), ed. C Schmuck H Wennemers Copyright, pp. 172-190.

83. H Li, J Aubrecht, A.J. Fornace J, Toxogenomics: Overview and potential applications for the study of non-covalent DNA interacting chemicals, *Mut. Res., 623* (**2007**), pp. 98-108.

84. M.F. Braña, M Cacho, A Gradillas, B de Pascual-Teresa, A Ramos, Intercalators as anticancer drugs, *Curr. Pharma. Des., 7* (**2001**), pp. 1745-1780.

85. T.C. Jenkins, in: “Methods in Molecular Biology”, (**1997**), ed K.R. Fox , Humana Press, Totowa, New Jersey, vol. 90, pp. 195–218.

86. J.D. McGhee, P.H. Von Hippel, Theoretical aspects of DNA-protein interactions: cooperative and non-cooperative binding of large ligands to a one-dimensional heterogeneous lattice, *J. Mol. Biol., 86* (**1974**), pp. 469-489.

87. G Schatchard, The attraction of proteins for small molecules and ions, *Ann. N.Y. Acad. Sci.*, *51* (**1949**), pp. 660–672.

88. D Suh, J.B. Chaires, Criteria for the mode of binding of DNA binding agents, *Bioorg. & Med. Chem, 6* (**1995**), pp. 723-728.

89. B Nordén, T Kurucsev, Analyzing DNA complexes by circular and linear dichroism, *J. Mol. Recogn., 7* (**1994**), pp. 141-156.

90. Y Pommier, P Pourquier, Y Fan, D Strumberg, Mechanism of action of eukaryotic DNA topoisomerase I and drugs targeted to the enzyme, *Biochim. Biophys. Acta, 1400* (**1998**), pp. 83-106.

91. D.J.A. Bridewell, G.J. Finlay, B.C. Baguley, Mechanism of cytotoxicity of N-[2-(dimethylamino)ethyl]acridine-4-carboxamide and its 7-chloro derivative: the roles of topoisomerase I and II, *Cancer Chemother. Pharmacol. 43* (**1999**), pp. 302-308.

92. M Facompre, C Carrasco, P Colson, C Houssier, J.D. Chisholm, D.L. Van Vranken, C Bailly, DNA binding and topoisomerase I poisoning activities of novel disaccharide indolocarbazoles, *Mol. Pharmacol., 62* (**2002**), pp. 1215-1227.

93. F Luciani, A Molinari, F Lozupone, A Calcabrini, L Lugini, A Stringaro, P Puddu, G Arancia, M Cianfriglia, S Fais, P-Glycoprotein-actin association through ERM family proteins: a role in P-glycoprotein function in human cells of lymphoid origin, *Blood, 99* (**2002**), pp. 641-648.

94. M.T. Santini, R Romano, G Rainaldi, P Filippini, E Bravo, L Porcu, A Motta, A Calcabrini, S Mescini, P.L. Indovina, G Arancia, the relationship between ^{1}H-NMR mobile lipid intensity and cholesterol in two human multidrug resistant cell lines (MCF-7 and LoVo), *Biochim. Biophys. Acta, 1531* (**2001**), pp. 111-131.

95. A Salvador, Nuovi tiopiano[2,3,e]indol-2-oni angolari quali potenziali agenti fotochemioterapici: studio del meccanismo d’azione, master thesis.

96. P Barraja, L Sciabica, P Diana, A Lauria, A Montalbano, A Almerico, G Dattolo, G Cirrincione, S Disarò, G Basso, G Viola, F Dall’Acqua, Synthesis and

photochemotherapeutic activity of thiopyrano[2,3-*e*]indol-2-ones, *Bioorg. & Med. Chem. Lett., 15* (**2005**), pp. 2291-2294.

97. A.K. Ghose, G.M. Crippen, Atomic physicochemical parameter for three-dimensional structure-directed quantitative structrure-activity relationship I. Partition coefficents as measure of hydrophobicity, *J. Comp. Chem., 7* (**1986**), pp. 565-577.

98. D.W. Hedley, S Chow, Evaluation of methods for measuring cellular glutathione content using flow cytometry, *Cytometry 15* (**1994**), pp. 349-358.

99. M Zhao, J.W. Eaton, U.T. Brunk, Protection against oxidant-mediated lysosomal rupture: a new anti-apoptotic activity of Bcl-2? *FEBS Lett., 485* (**2000**), pp. 104-108.

100. A.M. Martelli, A Cappellini, P Tazzari, A Billi, C Tassi, F Ricci, F Falà, R Conte, Caspase-9 is the upsteam caspase activated by 8-methoxypsoralen and ultraviolet-A radiation treatement of Jurkat T leukemia cells and normal T lymphocytes, *Haematol., 89* (**2004**), pp. 471-479.

101. G Viola, A Salvador, L Cecconet, G Basso, D Vedaldi, F Dall'Acqua, GG Aloisi, M Amelia , A Barbafina, L Latterini, F Elisei, Photophysical properties and photobiological behaviour of amiodaquine, chloroquine and primaquine, *Photochem. Photobiol., 83* (**2007**), pp. 1415-1427.

102. G Ouédraogo, P Morlière, R Santus, M.A. Miranda, J.V. Castell, Damage to mitochondria of cultured human skin fibroblasts photosensitized by fluoroquinolones, *J. Photochem. Photobiol. B: Biol., 58* (**2000**), pp. 20-25.

103. G Viola, E Fortunato, L Cecconet, L Del Giudice, F Dall'Acqua, G Basso, Central role of mitochondria and p53 in PUVA-induced apoptosis in human keratinocytes cell line NCTC-2544, *Toxicol. Appl. Pharmacol.* (**2007**), doi:10.1016/j.taap.2007.10.004.

104. M Parreño, J.P. Vaqué, I Casanova, P Frade, M.V. Céspedes, M.A. Pavón, A Molins, M Camacho, L Vila, J.F. Nomdedeu, R Mangues, J León, Novel triiodophenol derivatives induce caspase-independent mitochondrial cell death in leukemia cells inhibited by Myc, *Mol. Cancer Ther., 5* (**2006**), pp. 1166-1175.

105. A.R. Santiago, A.J. cristóvão, P.F. Santos, C.M. Carvalho, A.F. Ambrósio, High glucose induces caspase-independent cell death in retinal neural cells, *Neurobiol. Disease, 25* (**2007**), pp. 464-472.

106. B Epe, M Pflaum, S Boiteux, DNA damage induced by photosensitizers in cellular and cell-free systems, *Mut. Res., 299* (**1993**), pp. 135-145.

107. T.A. Ciulla, J.R. Van Camp, E Rosenfeld, I Kochevar, Photosensitization of single-strand breaks in pBR322 DNA by Rose Bengal, *Photochem. Photobiol. 49* (**1989**), pp. 293-298.

108. A. W. Girotti, Photodynamic lipid peroxidation in biological systems, *Photochem. Photobiol., 53* (**1990**), pp. 497-509.

109. P Morlière, A Moysan, R Santus, G Hüppe, J Mazière, L Dubertret, UVA-induced lipid peroxidation in cultured human fibroblasts, *Biochem. Biophys. Acta, 1084,* (**1991**), pp. 261-268.

110. G Viola, A Salvador, D Vedaldi, E Fortunato, S Disarò, G Basso, M.J. Queiroz, Induction of apoptosis by photoexcited tetracyclic compounds derivatives of benzo[b]thiophenes and pyridines, *J. Photochem. Photobiol. B: Biol. 82* (**2006**), pp. 105–116.

111. M.M. Bradford, A rapid and sensitive method for the quantification of microgram quantities of protein-dye binding, *Anal. Biochem., 72* (**1976**), pp. 248-254.

112. R Lyng, T Härd, B Nordén, Induced circular dichroism of DNA intercalators: electric dipole allowed transitions. *Biopolymers 26* (**1987**), pp. 1327-1345

113. A Wada, S Kozawa, Instrument for the studies of differential flow dichroism of polymer solutions, *J. Polim. Sci. A 2* (**1964**), pp. 853-864.

114. G.L. Peterson, A simplification of the protein assay method of Lowry *et al*. which is more generally applicable, *Analyt. Biochem. 83*, (**1977**), pp. 346-356

UNIVERSITA’ DEGLI STUDI DI PADOVA, DIPARTIMENTO DI SCIENZE FARMACEUTICHE:
Professor Daniela Vedaldi, Professor Francesco Dall’Acqua, Professor Sergio Caffieri, Assistant Professor Giorgia Miolo, Assistant Professor Stefano Moro, Assistant Professor Adriana Chilin, Anita Faccio, Sara Loat, Giampietro Viola, Andrea Bortolato.

UNIVERSITA’ DEGLI STUDI DI PADOVA, DIPARTIMENTO DI SCIENZE CHIMICHE
Professor Maurizio Casarin.

UNIVERSITA’ DEGLI STUDI DI PADOVA, DIPARTIMENTO DI PEDIATRIA
Professor Giuseppe Basso, Elena Fortunato, Laura Cecconet, Silvia Disarò.

UNIVERSITA’ DEGLI STUDI DI PALERMO, DIPARTIMENTO FARMACO-CHIMICO, TOSSICOLOGICO E BIOLOGICO
Professor Girolamo Cirrincione, Assistant Professor Patrizia Diana, Assistant Professor Paola Barraja.